# Investigating the Performance of Wood Portal Frames as Alternative Bracing Systems in Light-Frame Wood Buildings

By

Abdullah Al Mamun

July 2012

Ottawa-Carleton Institute for Civil Engineering
Department of Civil Engineering
University of Ottawa
Ottawa, Ontario
Canada, K1N 6N5

A thesis submitted to the Faculty of Graduate and Post Doctoral Studies in partial fulfillment of the requirements for the degree of Master of Applied Science in Civil Engineering

# Abstract

Light-frame shearwall assemblies have been successfully used to resist gravity and lateral loads, such as earthquake and wind, for many decades. However, there is a need for maintaining the structural integrity of such buildings even when large openings in walls are introduced. Wood portal frame systems have been identified as a potential alternative to meet some aspects of this construction demand.

The overarching goal of the research is to develop wood portal frame bracing systems, which can be used as an alternative or in combination with light-frame wood shearwalls. This is done through investigating the behavior of wood portal frames using the MIDPLY shearwall framing technique. A total of 21 MIDPLY corner joint tests were conducted with varying bracing details. Also, a finite element model was developed and compared with test results from the current study as well as studies by others.

It was concluded from the corner joint tests that the maximum moment resistance increased with the addition of metal straps or exterior sheathings. The test results also showed a significant increase in the moment capacity and rotational stiffness by replacing the Spruce-Pine Fir (SPF), header with the Laminated Veneer Lumber (LVL) header. The addition of the FRP to the standard wall configuration also resulted in a significant increase in the moment capacity. However, no significant effect was observed on the stiffness properties of the corner joint.

The FE model was capable of predicting the behavior of the corner joints and the full-scale portal frames with realistic end-conditions. The model closely predicted the ultimate lateral capacity for all the configurations but more uncertainty was found in predicting the initial stiffness.

The FE model used to estimate the behavior of the full-scale portal frames constructed using the MIDPLY framing techniques showed a significant increase in the lateral load carrying capacity when compared with the traditional portal frame. It was also predicted using the full-scale FE model that the lateral load carrying capacity of the MIDPLY portal frame would increase with the addition of the metal straps on exterior faces.

A parametric study showed that using a Laminated Strand Lumber (LSL) header increased the lateral load carrying capacity and the initial stiffness of the frames relative to the SPF header. The study also showed that there was an increase in the capacity if high strength metal straps were used. Doubling of the nail spacing at header and braced wall segment had a considerable effect on the lateral capacity of portal frame. Also, the initial stiffness was reduced for all the configurations with the doubling of the nail spacing at the header and braced wall segment in comparison with the reference frame.

# Acknowledgement

I would like to thank the Natural Sciences and Engineering Research Council of Canada and FPInnovations for their contributions to this project. It is also my great pleasure to express my appreciation to my supervisor Dr. Ghasan Doudak for his guidance, encouragement and continuous support throughout my research work.

Special thanks to Dr. Mohammad Mohammad and Dr. Chun Ni from the Wood Products Division at FPInnovations for their valuable advice, and allowing me to visit their lab and interact with their scientists and technicians. I would especially like to thank Dr. Williams Munoz for his help and support while I was at the FPInnovations lab facilities.

Special thanks to Dr. Muslim Majid, from the University of Ottawa Structural Lab, and Philippe Ranger, an undergraduate co-op student, for their help in building the test set-up and performing the tests.

Finally, it is my pleasure to acknowledge the moral support of my friends and family that allowed me to finish my research study in a timely manner.

# Table of Contents

# List of Figures

## 1 Introduction



## 2 Literature Review



## 3 Experimental Study

## 4 Results and Discussion

## 5 Numerical Modeling

## Appendix A



## Appendix B

# List of Tables

## 3 Experimental Study



## 4 Results and Discussion



## 5 Numerical Modeling

# CHAPTER 1

# Introduction

## 1.1 Problem Definition

Light-frame wood construction is the predominant method of building low-rise buildings (mostly residential) in Canada and the U.S. Wood frame buildings are economical, sustainable due to the material use and can be easily constructed and erected. The architectural possibilities of wood frame buildings are limitless.

Light-frame shearwall assemblies have been successfully used to resist gravity loads as well as lateral loads such as earthquake and wind for many decades. Figure 1.1 shows an example of such assembly, which typically consists of framing members (studs) and sheathing panels (OSB or Plywood) attached to the framing members via mechanical fasteners such as nails. The success of such systems is attributed to their light weight, redundancy and ductile behavior.

Figure 1.1: Typical light-frame wood shearwall (interior view)

Traditionally, light-frame wood structures were characterized by a relatively smaller area, rectangular shape and the presence of several interior partitions (Figure 1.2 a). In recent years, there has been a demand for relatively larger surface areas with trends that deviate from the “box-like” traditional housing type. There is also more demand for open-concept design with fewer interior walls and large openings.

a) Residential house from the 1960’s b) Modern single family house

Figure 1.2: Typical light frame residential buildings.

Such fundamental shift in construction practices raises questions about the reliability and safety of modern light-frame wood buildings. If the longstanding performance record for low-rise light frame wood structures is to be maintained, then the substitution of wall bracings with openings (i.e. windows, doors or garage opening) must not compromise the structural integrity of the building.

There is evidently a need for alternative bracing systems to respond to the demand of modern-day construction while meeting the performance attribute of the structural system. Wood portal frame systems have been identified by engineers and builders as a potential alternative to meet some aspects of the construction demand, especially but not limited to, garage openings. Work has been done to develop such system by APA - The Engineered Wood Association in 2000s [1.1, 1.2] with the consequence that the portal frame bracing systems have been introduced to the International Residential Code (IRC) [1.3]. Figure 1.3 shows typical construction details of the portal frame system developed by APA.

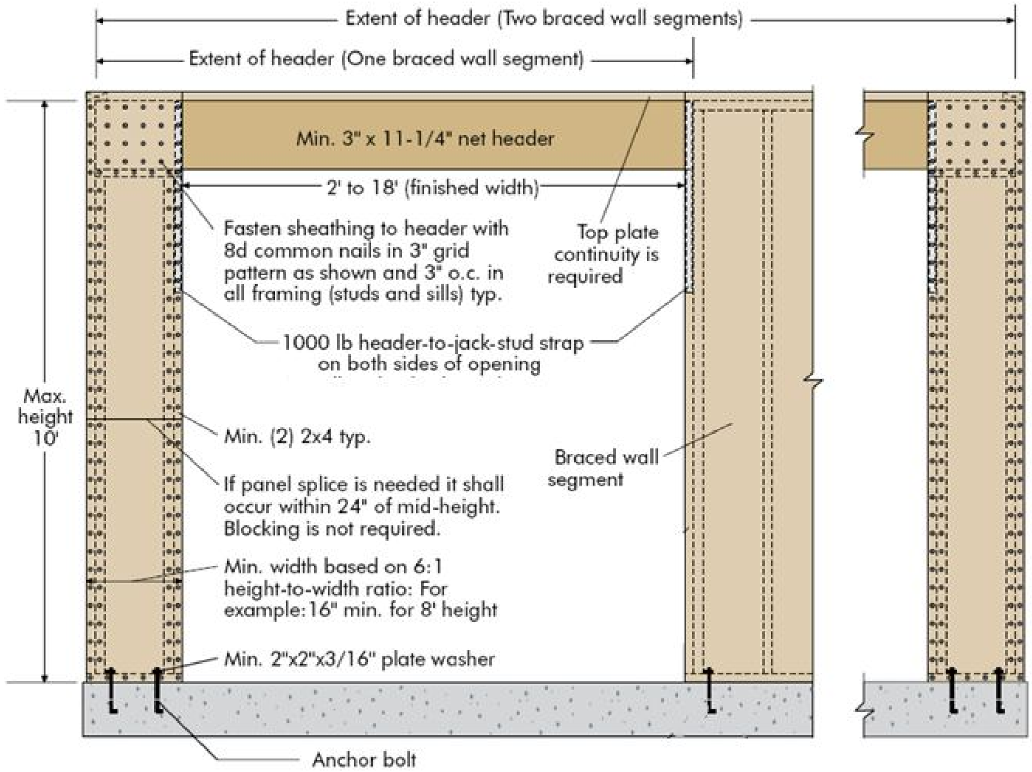


Figure 1.3: Construction details for the APA portal frame over concrete or masonry foundation [1.3]

It is noteworthy to mention that since the developed provisions were intended to be limited to residential construction, the provisions were prescriptive in nature providing details such as maximum height limits and nailing patterns. In order to develop construction details for portal frames that go beyond the prescriptive requirements and that ensures integration with other bracing elements, there is a need to better understand the behavior of such systems. The current research project aims at identifying methods to develop higher capacity wood portal frames. In an attempt to enhance the lateral capacity of portal frames, the focus of the work was on utilizing a different construction system than the typical light-frame wood shearwalls, namely the MIDPLY shear wall [1.4] and reinforcing critical regions with high stress concentrations by using metal straps and or fiber reinforced polymer (FRP).

## 1. 2 Research Objectives

The overarching goal of the research is to develop wood portal frame bracing systems, which can be used as an alternative or in combination with light-frame wood shearwalls. More specifically, the objectives of the current research work are to:

- Investigate the behavior of wood portal frame bracing systems using the mid-ply shearwall framing technique.

- Develop detailed numerical finite element models that are capable of capturing the behavior of portal frame systems

- Investigate the use of fiber reinforced polymer (FRP) on the exterior surface of corner joints as means of constructing or retrofitting portal frame bracing systems.

## 1.3 Research Strategy

### 1.3.1 Why Corner Joint Testing?

Laboratory tests conducted on full-scale portal frame bracing systems with standard construction, have shown that the corner joint connecting the portal frame header and narrow braced wall segment is the critical link that limits the strength in such systems [1.4]. Since one of the main goals of this research is to enhance the performance of portal frame bracing systems, focusing the laboratory testing on the corner joints was deemed a logical and economically efficient way to balance the need for such tests with the cost associated with full-scale tests. This approach allowed the undertaking of more tests with a variety of joint details. In fact, corner tests provide an essential input to create and verify the full-scale finite element model. Once a suitable model is developed and verified, the modeling techniques used in the corner tests can then be expanded to cover a variety of full-scale configurations.

### 1.3.2 Why Use MIDPLY Shearwall Framing Technique?

The MIDPLY shearwall system provides improved performance by rearranging the wall framing components and sheathing allowing load-carrying capacity and stiffness that is at least twice that of comparable standard shear walls [1.5,1.6]. The nails connecting the sheathing with the studs exhibit higher lateral load carrying capacity due to engagement of double or triple shear [1.5]. Figure 1.3 shows the cross section of the standard shearwall and the MIDPLY shearwall.

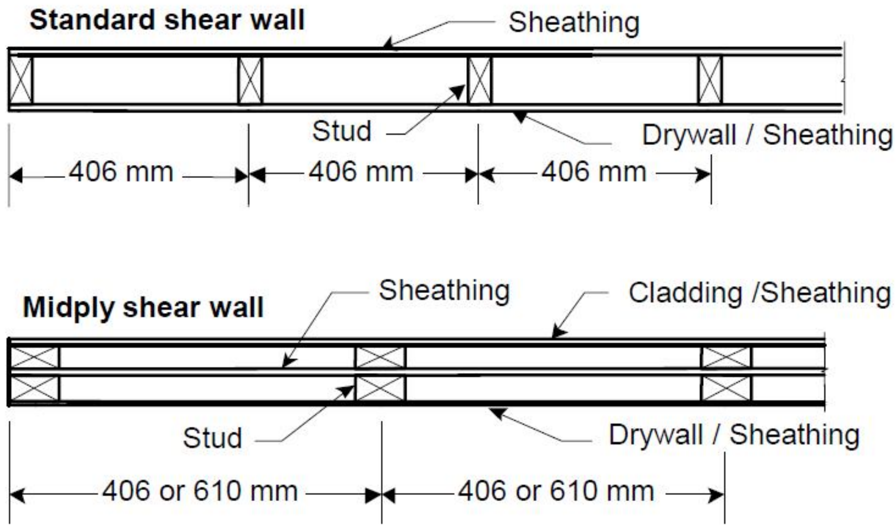


Figure 1.4: Cross section of a standard shear wall (top) and a MIDPLY wall (bottom) with two exterior panels [1.5].

Since the studs are rotated 90-degree about the longitudinal axis relative to standard stud wall, failure modes such as panel chip-out and nail pull-through failures that are commonly observed in standard shear walls are reduced or prevented [1.7].

Portal frame bracings such as the ones approved in the International Residential Code (IRC) [1.3] are limited to construction details for the narrow braced wall segment similar to those shown in Figure 1.4 (top).

Since the corner joint plays the most significant role in determining the lateral load carrying capacity of the portal frame, introducing the MIDPLY framing techniques is not expected to lead to a doubling in the capacity of the portal frame. The goal here is to improve the overall strength, enhance the ductility, and control the failure such that it is in fact limited to the corner joint. Having a controlled and consistent failure mode will make it easier to develop mechanics-based expressions for predicting the portal frame capacity. The latter is outside the scope of the current research work.

Due to its high tensile capacity, fiber reinforced polymer (FRP) has been used to increase the strength of concrete [1.8, 1.9] as well as timber elements [1.10]. In the current research study, FRP is used as a tension membrane to replace or use in conjunction with metal straps to increase the lateral load carrying capacity of the corner joint in portal frame bracing systems.

### 1.3.3 Research Methodology

The methodology followed in this research project involves the following:

- Observation and analysis of existing data: This information will be utilized to develop suitable configurations that would have the potential to enhance the performance of portal frames;
- Conducting material as well as corner joint tests: This will confirm experimentally the suitability of the configurations being considered;
- Develop a detailed finite element model: The model will be verified by experimental tests conducted under the current research program as well as published experimental data. Using the same analytical techniques, the model will be verified against existing test data of full- scale portal frame systems, including boundary conditions.

- Once the model has been verified at the element, subsystem and system levels, it will be used to predict the performance of portal frame systems using corner construction details that were tested and deemed suitable.

- The FE model will then be used to investigate variability in the selected corner details, and propose other, more efficient variation of the construction details tested.

A total of 21 corner joint tests constructed with the MIDPLY shear wall system were conducted at the University of Ottawa Structural Laboratory. The displacement of the narrow wall segment was monitored by linear variable differential transducer (LVDT) and the load was monitored using load cell which was attached to the actuator.

The test results were used to validate a finite element model developed using the SAP2000 software package [1.11]. Figure 4 shows the flowchart of the research methodology.

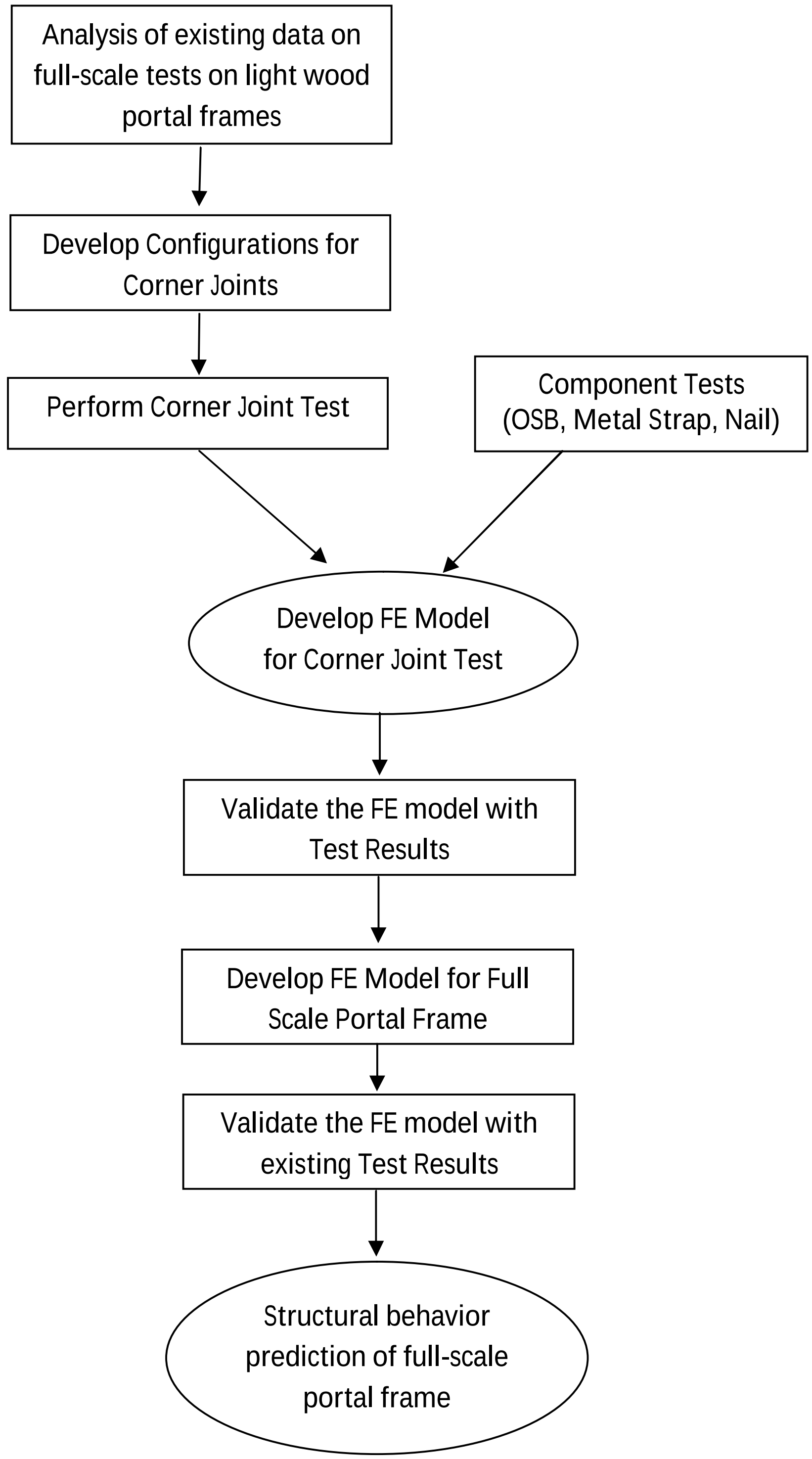


Figure 1.5: Methodology of the research project

## 1.4 Structure of the Thesis

Chapter 1 contains an introduction including the problem definition, research strategy, methodology and structures of the thesis.

Chapter 2 contains a detailed literature review on relevant full-scale portal frame tests. As the MIDPLY shear wall system has been used in the current research, relevant studies are also discussed. Research on the development technique of Finite Element model in SAP 2000 is also presented.

Chapter 3 contains the experimental research work and describes the test set-up, load protocol, test matrix, and the configurations of test specimens.

Chapter 4 contains the test results as well as comparisons of lateral load capacity and rotational stiffness among the various test configurations.

Chapter 5 describes the numerical modeling technique used to model the corner joints as well as the full scale portal frames. Input parameters based on material testing are also described in this chapter. This chapter also contains parametric studies using the full-scale MIDPLY portal frame model.

Chapter 6 contains the key findings, conclusions and recommendations for future research work.

# CHAPTER 2

# Literature Review

## 2.1 Background on Full-Scale Portal Frame Studies

Work on portal frame systems has been limited to developing a frame system with equivalent capacity and stiffness so that they can substitute a given length of a prescriptively designed light-frame braced wall panel. This has lead to the adoption of the portal frame provisions in the International Residential Code in the US [2.1]. In general, developing moment capacity in wood is very difficult due to its weak tensile strength in the perpendicular to grain direction. It is therefore not surprising that the number of studies dealing with wood moment resisting frames has been very scares. The following primarily describes the work undertaken by APA in the US and FPInnovations in Canada, as these studies laid the groundwork for the development of portal frame bracing systems.

### 2.1.1 Full-Scale Portal Frame Test - APA

In the early 2000’s, The Engineered Wood Association (APA) started work on developing portal frames for residential applications [2.1,2.2,2.3,2.4]. The goal of the testing program was to provide prescriptive solutions to be used in low-rise light-frame residential wood buildings. The APA research allowed the introduction of openings with heights extending up to the header, even though provisions in the 2006 IRC restricted the opening height adjacent to the braced wall segment to 65% of the total height [2.2]. The provision change was mainly due to the acceptance that portal frames are capable of transferring shear by means of a semi-rigid moment connection in the corner joint [2.3]. The key observation made by APA was that the capacity of portal frames highly depended on the capacity of the metal straps and opening width [2.1]. These observations were considered when the current testing program was developed.

APA conducted close to 100 cyclic tests on portal frames, where the main concept of force transfer was through the nail connections between the sheathing and the header as well as through metal straps to reinforce the corner joint. Figure 2.1 shows the corner joint details.

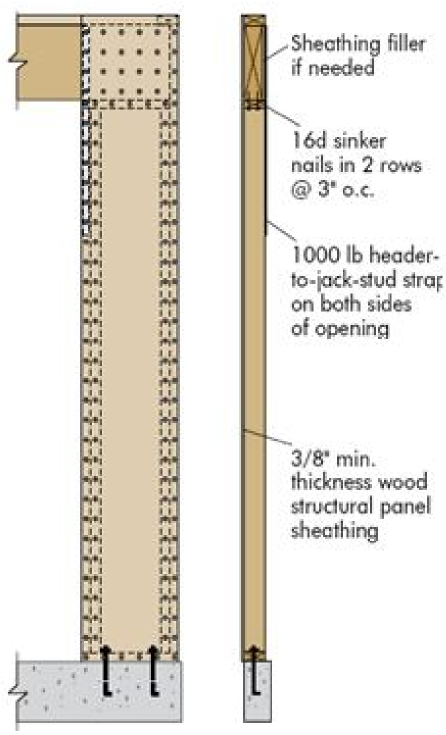


Figure 2.1: Construction details of the APA portal frame [2.3]

The main goal of this study was to establish the behavior of this portal frame configuration with a 6:1 aspect ratio (height to width on the narrow wall segment) and compare it to segments of fully sheathed wood bracing wall elements with structural sheathing panels [2.5]. The braced walls consisted of segments with minimum length using continuous wood structural panel sheathing as described in 2006 IRC R602.10.5. [2.2].

The tests were performed for a wide variety of boundary conditions which included rigid foundation, raised wood floor assembly, and with and without gypsum panel. The study found that there was a significantly higher peak lateral capacity per linear feet for the APA portal frames compared to the IRC bracing systems permitted in high seismic areas in U.S. for all of the boundary conditions.

In 2007, APA conducted a test on a full-scale house structure with dimensions of 25 X 37 feet. The goal of the testing was to compare the performance of the APA portal frame systems, with 6:1 aspect ratio of the narrow wall segment, with braced walls consisting of braced wall segments with 2:1 height-to-width aspect ratio. Only one braced wall line was used in the comparison. The other three braced wall lines were kept consistent with regard to the total length of the braced wall segments. The study looked at the 6:1 aspect ratio portal frames alone as well as in combinations with 4:1 and 3:1 aspect ratios of fully sheathed structural sheathing panels. The total length of the braced wall segments in the braced wall line that was compared was kept constant for all test cases. The test showed that the braced wall line constructed with only 6:1 aspect ratio portal frames had 65 to 127% higher lateral load carrying capacity than the braced wall line constructed with 2:1 aspect ratio of structural sheathing panels. The test also showed that in the case where the braced wall line consisted of a combination of 6:1 aspect ratio portal frame bracings system and one 3:1 and two 4:1 aspect ratio braced wall segment there was an additional increase of 66 to 89% of the lateral load carrying capacity compared to the braced wall line consisted with only 2:1 aspect ratio braced wall segment.

### 2.1.2 Full-Scale Portal Frame Test - FPInnovations

Nine full-scale portal frames were tested monotonically and cyclically at the FPInnnovations laboratories [2.6]. All the portal frames were 3.66 m in length and 2.44 m in height, with 406 mm narrow wall segment at each end of the portal frame. The narrow wall segment was constructed with 38 mm x 89 mm NLGA No.2 and better Spruce-Pine-Fir lumber. The header was built-up with either 45 mm x 302 mm (1.75 inch x 11.875 inch) 1.5E laminated strand lumber (LSL) or 38 mm x 286 mm No.2 and better Spruce-Pine-Fir lumber. Oriented strand board (OSB), with a thickness of 12.5 mm and a span rating of 2R32, was used as sheathing panels. 8d common nails (3.3 mm in diameter and 63.5 mm in length) were used to attach sheathings to framing members.

For the wall segments without hold-downs, 12.7 mm diameter anchor bolts were used to fasten the bottom plate to the test frame. Two types of hold-down devices were used: Simpson Strong Tie HTT16's or 12.7 mm diameter continuous steel rods. The use of hold-downs was intended to simulate the upper bound of end restraint due to fully sheathed return wall, header and dead weight from above. A Simpson

Strong Tie LSTA 21 (1000 lb capacity) was used to connect the header and end studs to provide vertical continuity and moment resistance at the corner of the portal frame.

Observations showed that the failure of portal frame started with OSB tearing at corners of portal frame walls, followed by metal straps fracture. The study found that for portal frame walls without hold-downs, the lateral load carrying capacities were approximately 75% the capacities of identical walls with hold-downs.

Based on the test results and results from the numerical modeling, the study concluded that the wall height had a significant impact on the performance of portal frame walls. It was also found that the tensile strength of metal straps had the highest impact on the lateral load capacities of portal frame walls. Finally, the walls with sheathings attached on both sides of the framing had approximately 30% higher lateral load carrying capacity and stiffness than those with sheathings attached on one side of the framing.

### 2.1.3 Comparative Study with Shearwall - NAHB

The National Association of Home Builders (NAHB) undertook a testing program to develop and optimize a design process for exterior shear walls containing openings (windows and doors) so that both safety and economy could be achieved through more accurate design approaches [2.7]. In the experimental work, a 20-feet long fully sheathed shearwall and a 16-feet long portal frame were investigated. It is noteworthy to mention that the construction details for these portal frames deviated significantly from those described in the APA study. The main differences are the nailing pattern and boundary condition fixities. The shearwalls and portal frames in the tests consisted of 7/16 inch OSB sheathing on one side and ½ inch Gypsum Wall Board (GWB) on the other side. 8d nail @ 6" edge spacing was used to attach the wood sheathing to the framing and #6 screws @ 7" spacing was used to attach the GWB panels. Two Simpson HTT 22 hold-down anchors were used to anchor the end of the shearwall to the foundation, whereas no hold-downs were used for the portal frame. Furthermore, two 1000 pound capacity metal straps were used, one on each end of the portal frame, to connect the header to the framing. The test showed that the lateral load carrying capacity of the shearwall and portal frame tested were comparable but the stiffness of the portal frame was relatively lower than that of the shearwall.

## 2.2 MIDPLY Shear Wall Background

As described in Chapter 1, the MIDPLY shearwall system provides improved performance by rearranging the wall framing components and sheathing allowing load-carrying capacity and stiffness that is at least twice that of comparable standard shear walls. This is primarily due to the nails connecting the wood based panel with framing member being in double-shear as shown in Figure 2.2.

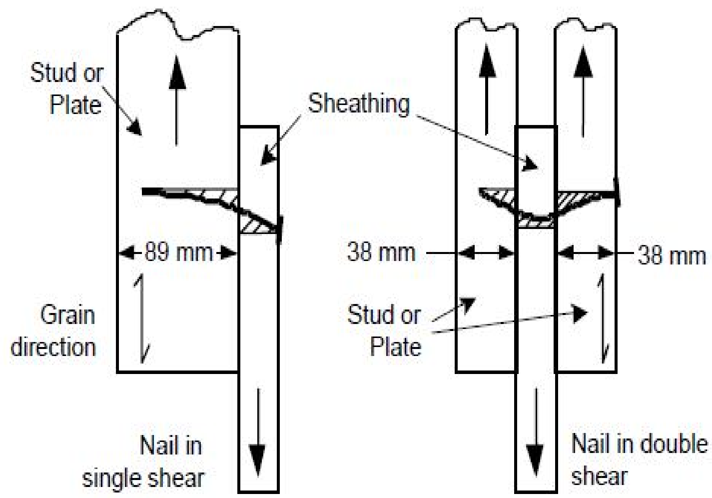


Figure 2.2: Nail acting in single shear in traditional shear wall (left) and nail acting in double shear in MIDPLY shear wall (right) [2.6].

Varoglu and Karacabeyli [2.9] evaluated the performance of MIDPLY shearwalls and compared the results with standard light frame shearwalls. 16 MIDPLY shearwalls were tested and compared with 9 standard shearwalls. All the dimensions of the MIDPLY shearwalls were 2.44 X 2.44 m. Framing members of dimension 38 X 89 mm, SPF were used with 406 to 610 mm C/C spacing. To allow the rotation of middle sheathing there was a 12mm gap between bottom edge of middle sheathing and bottom plate as well as top edge of middle sheathing and top plate. All the standard shearwalls were 2.44 X 2.44 m in dimension and constructed with 38 X 89 mm No. 2 and better grade SPF lumber with a spacing of 406mm on centre. 9.5 mm thick plywood panels were used as exterior sheathing. The study concluded that the MIDPLY shearwall had between 2.4 to 3.4 times higher lateral carrying capacity and 1.9 to 3.1 times higher stiffness when compared with the standard shearwalls. The tests also confirmed that the MIDPLY shearwall was a highly energy dissipative system with 3 to 5 times higher energy dissipation values than the standard shearwall.

Varoglu and Karacabeyli [2.10] also tested a series of MIDPLY shearwalls in a shake table to determine the behavior of MIDPLY shearwalls subjected to a succession of earthquake ground motions. Two different types of 2.44 X 2.44 m specimen were prepared with 38 X 64 mm lumber with 610 mm spacing on center and 38 X 89 mm lumber with 406 mm spacing on center. Three different types of walls were prepared with two identical specimens of each type to test for the Kobe and Landers earthquake. The selected record earthquake was applied at increasing peak ground acceleration (PGA) levels in each shake table test until the specimen failed. The test result confirmed the superior capacity of the MIDPLY walls under repeated earthquake loading. The test also showed that under both Landers and Kobe earthquake loading, the lateral load carrying capacity of the MIDPLY shear walls were more than 2.5 times that of the standard shearwall.

Ni and Follesa [2.11] analysed a four-storey building using the structural analysis software DRAIN-3D. The building was designed so that traditional shearwalls or MIDPLY shearwalls were the only lateral load resisting systems in the structure. The analysis showed that the MIDPLY walls had at least twice the lateral load capacity and stiffness compared to the standard shearwall with the same framing members, sheathing, nail diameter and spacing. It also showed that the same ductility factor ($R_{d)}$ and over-strength factor ($R_o$) used for regular shearwalls can be used for MIDPLY walls.

## 2.3 Finite Element Modeling

Numerical modeling is a complementary tool to predict the structural behavior and strength characteristics of structures. This tool becomes most powerful when the inputs to the model are well-defined and representative of the behavior of the structure and when the model is validated by test results. For the current study, SAP2000 Non-Linear Version 14.1.0 [2.12] was used to develop finite element (FE) model for the corner joint.

The SAP2000 software has been successfully used by several researchers to develop 3-D model of wood shear walls where the framing were defined as beam elements and the sheathing panels were defined as shell elements [2.13, 2.14, 2.15, 2.16].

The models in these studies also concluded that the behavior of the nails, especially the ones connecting the sheathing to the framing members play a major role in the behavior of the shear wall and determination of their properties for model input is essential to developing a robust FE model. The studies also show that SAP2000 was effective in determining the wall displacement and capacity including configurations containing openings, different sheathing panel configurations and various boundary conditions.

Ni and collaborators developed a 3-D SAP2000 model to predict the structural response of portal frames with different corner joint configurations, height variation and effect of unblocked sheathing on exterior face [2.17]. Similar techniques were also used to develop the MIDPLY shear wall model [2.18]. The model was able to capture the non-linear behavior through spring elements which represented the nails on the MIDPLY shear wall.

## 2.4 Concluding Remarks

Only limited studies have been conducted on wood portal frame bracing systems. Even though an extensive experimental program has been undertaken by APA, the work was limited to configurations that can be used in prescriptively designed structures. The works by APA still lead to important observations that were capitalized on in the current study. Understanding the dependency of the portal frame capacity on the capacity of the metal straps and opening width was useful in designing the experimental program under the current research.

Furthermore, the work by APA, FPInnovations and NAHB showed that it is feasible to create portal frame systems with capacities so that they could be used with light frame braced wall systems. The limitation in the APA program regarding targeting prescriptive design requirements rather than performance-based requirements is addressed in the current research project. The current project is the first step in understanding the behavior of these bracing systems and the development of the FE model will allow future studies to investigate the behavior even further.

# CHAPTER 3

## Experimental Study

### 3.1 MIDPLY Corner Joint Tests with Metal Straps

As already discussed in the Introduction section, the MIDPLY wall system is a special type of stud wall arrangement, where a wood-based structural panel (plywood, OSB) is placed at the center of the stud wall, which allows an increase in the lateral load carrying capacity due to the multiple hinges that are developed in the fasteners [3.1]. Furthermore, since the studs are rotated 90-degree about the longitudinal axis, failure modes such as panel chip-out and nail pull-through, which are commonly observed in standard shear walls, are reduced or prevented [3.2]. An L-shaped test assembly was developed to simulate a typical corner joint in a portal frame. This assembly does not simulate boundary conditions where the portal frame is connected to a foundation or framing members in the storey below. Even though testing the corner in isolation may not be representative of the behavior of the full-scale portal frame, these simple tests provide a base for comparing the performance of the different corner joints and allow the optimization of the corner details before full-scale tests can be undertaken. The corner joint test results can also be used to verify the numerical model and help predict the behavior of the full-scale portal frame.

### 3.1.1 Specimen Details

All MIDPLY corner joints consisted of 1720 mm high and 405 mm wide wall segments connected to a 285 mm deep header. The header was built with a two-ply beam using nominal 2x12 Spruce-Pine-Fir (SPF) or 2x12 laminated veneer lumber (LVL) members. Figure 3.1 shows a typical MIDPLY corner joint configuration.

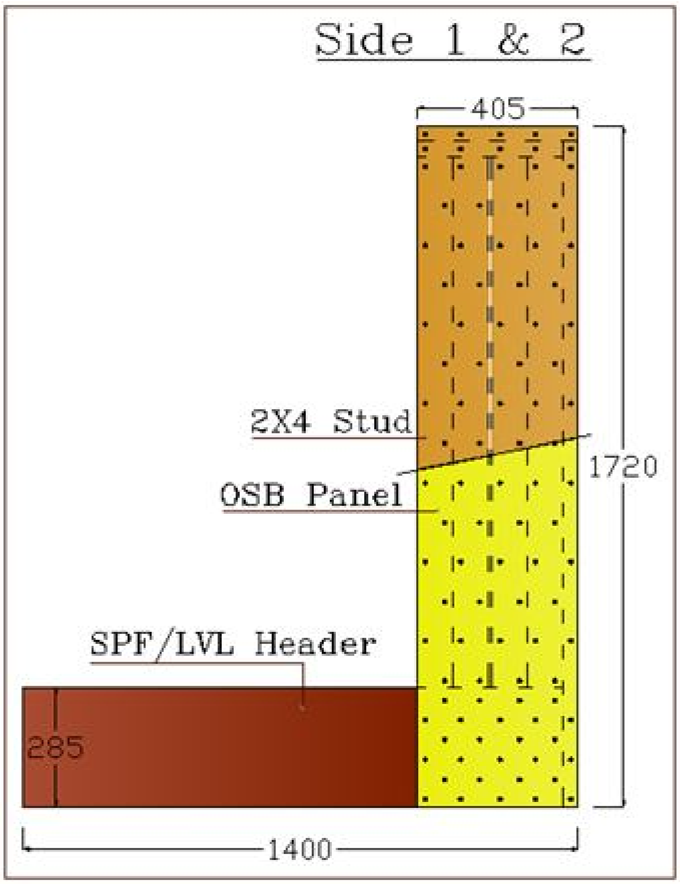


Figure 3.1: Typical MIDPLY corner joint

The wall framing was constructed with 38 mm x 89 mm (nominal 2x4) stud grade Spruce-Pine-Fir lumber. Nine studs were used in each narrow wall segment. 12.5 mm thick oriented strand board (OSB) with a span rating of 2R32 was used as sheathing panels. A 12 mm gap was provided between the middle OSB sheathings and the bottom plate to allow for free rotation during the cyclic loading. Figure 3.2 (a) and (b) show the construction details for the middle OSB panel and a cross section of MIDPLY corner joint, respectively.

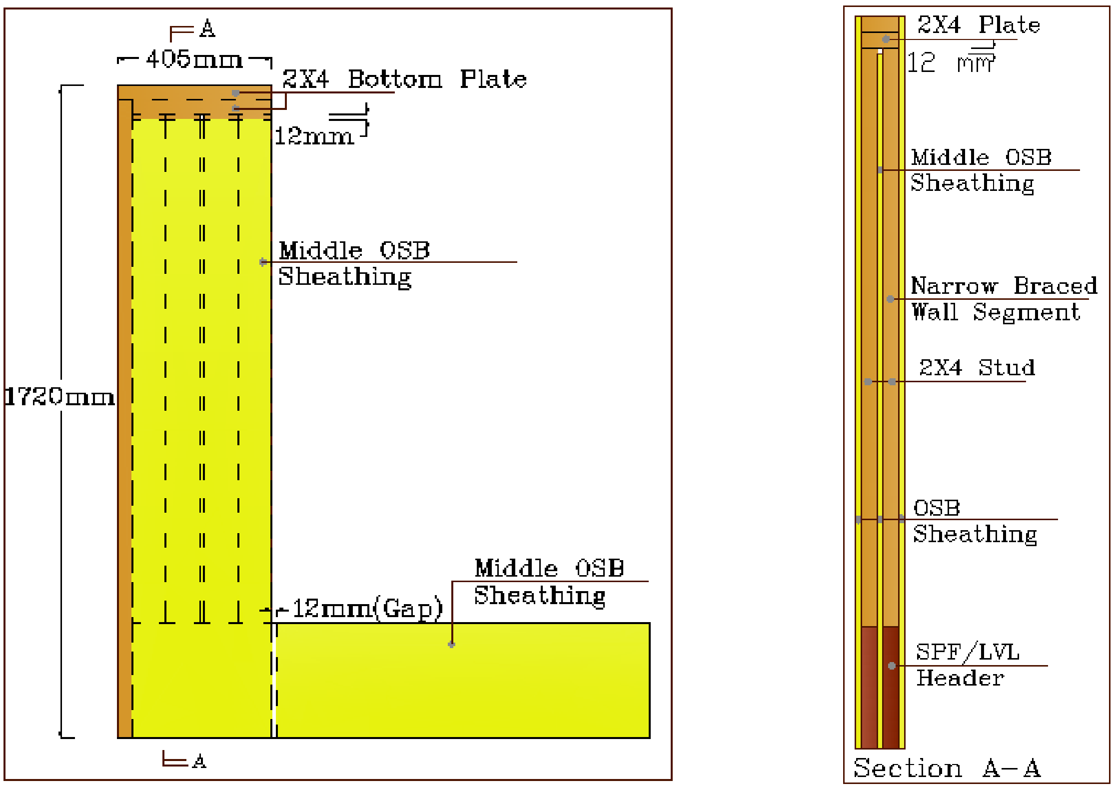


(a) (b)

Figure 3. 2: (a) Orientation of the middle OSB sheathing

(b) Cross section of MIDPLY corner joint

The sheathing was attached to the studs using 16d common nails (4.06 mm in diameter and 90 mm in length). For configurations C1 to C3 the nailing schedule used was two rows of nails spaced @100 mm on each side of the studs, and a grid pattern of nails spaced @50 mm on the header. For configurations C4 to C11 the nailing schedule used was two rows of nails spaced @200 mm on each face of stud, and a grid pattern of nails spaced @50 mm on the header. All nails were power driven using a pneumatic nailing gun. Six wood screws with 5.12 mm diameter and 88 mm long were used to connect end stud with header. Figure 3 shows the nailing pattern of the MIDPLY corner joint specimens.

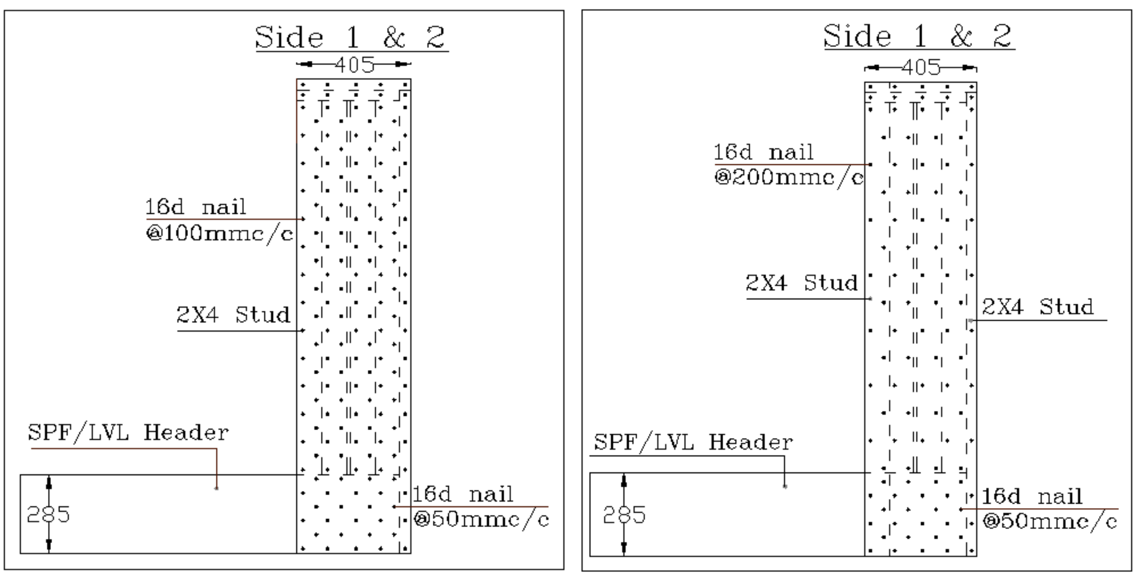


(a) Face nail pattern (C1 to C3)

(b) Face nail pattern (C4 to C11)

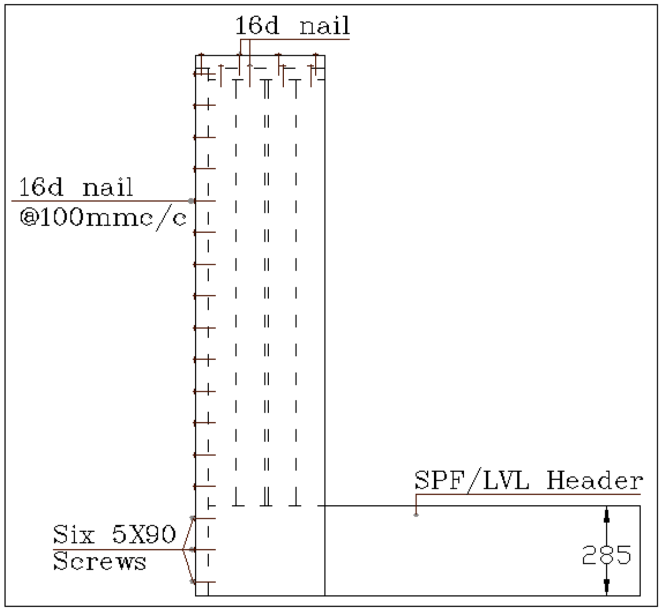


(c) Side nail pattern

Figure 3.3: Nailing pattern of MIDPLY corner joint specimens

Simpson Strong Tie LSTA 21 (1000 lb / 4.45 kN capacity) metal straps were used to connect the header and studs in order to provide vertical continuity and moment resistance. The average moisture content of the test specimens was regularly monitored and at the time of testing, the lumber moisture content was 16.5%. The moisture content never exceeded 19% during storage and prior to testing.

### 3.1.2 Test Set-up

Figures 3.4 and 3.5 show the schematic and laboratory test set-up of the MIDPLY portal frame corner joints. A 12.7 mm thick metal plate, connected to the actuator, was used to apply monotonic or cyclic load at the top of the specimen. The plate was fastened to the wood plates of the assembly using four Ø12.5 mm lag screws. The SPF/LVL header was fastened to a metal base with steel brackets. The base was anchored to the concrete floor with metal tie rods to resist vertical and horizontal movement. Lateral guides made of 100X100 mm HSS members were provided to ensure a consistent unidirectional movement of the corner joint assembly. Two cable displacement transducers, which were placed 270 mm from the top of the wall and 600 mm from the base of the header, were used to measure the lateral displacement. A vertical cable displacement transducer was placed at the bottom of the exterior stud to measure the uplift of joint assembly from foundation. Another cable transducer was placed at the top of header to measure the relative rotation of the narrow wall segment with the header beam.

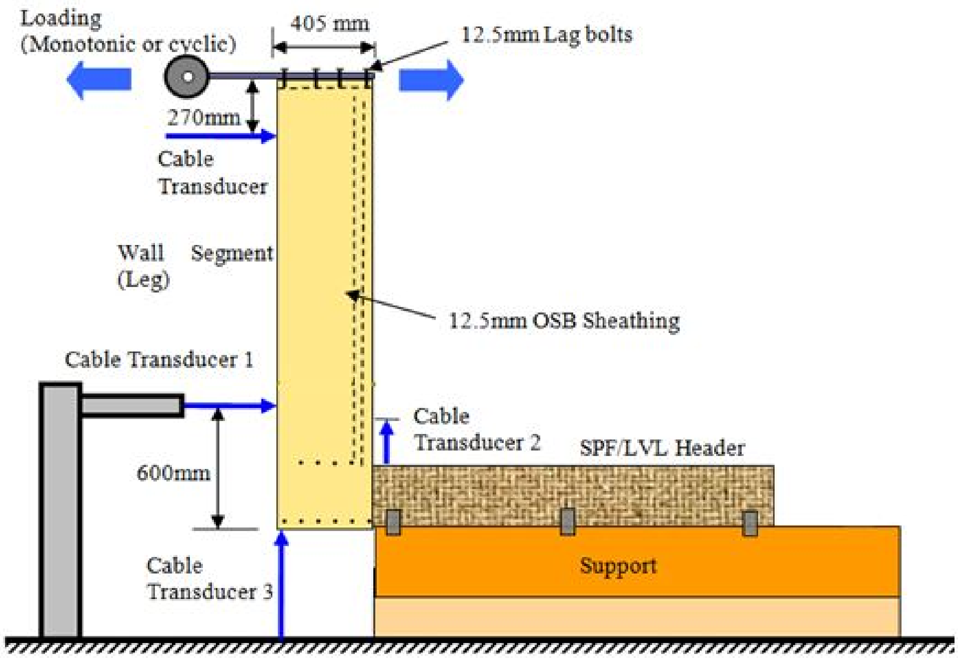


Figure 3.4: Schematic of the test set-up

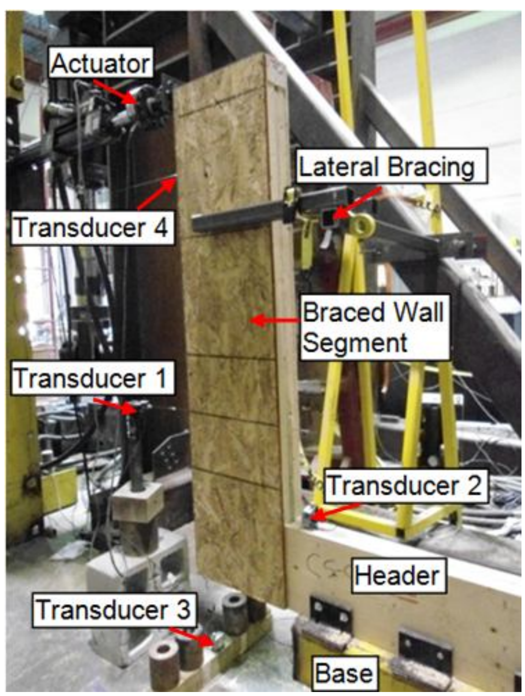


Figure 3.5: Test set-up with MIDPLY portal frame corner specimen installed

### 3.1.3 Load Protocol

The reversed cyclic loading tests were conducted following the ASTM E2126-08 CUREE protocol [3.3], as shown in Figure 3.6. The loading protocol is described in details below:

- 6 cycles at each displacement level of 5% of the reference ultimate displacement;
- Single full cycle consists of 1 cycle at each displacement level of 7.5% and 10% and corresponding 6 cycles at each displacement level of 5.6% and 7.5% of the reference ultimate displacement;
- Single full cycle consists of 1 cycle at each displacement level of 20% and 30% and corresponding 3 cycles at each displacement level of 15% and 23% of the reference ultimate displacement;
- Single full cycle consists of 1 cycle at each displacement level of 40%, 70%, 100%, 150% and 200% and corresponding 2 cycles at each displacement level of 30%, 53%, 75%, 113% and 150% of the reference ultimate displacement.

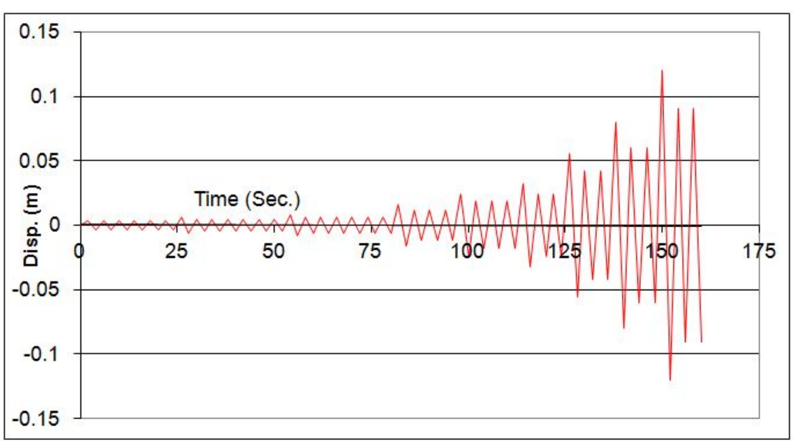


Figure 3.6: CUREE reversed cyclic load protocol for the cyclic tests [3.3]

The cyclic tests were conducted at a frequency of 0.25 Hz and the data acquisition was set to capture the output at a frequency of 10 Hz. The reference displacement used to develop the CUREE load protocol for the cyclic loading was obtained from the monotonic test. Based on the monotonic tests, the reference ultimate displacement was taken as 60 mm (2.36 inch) at the top of the wall segment. The monotonic test was done with a speed of testing equal to 8 mm/min while the frequency of data acquisition was set to 10 Hz. Table 3.1 shows the displacement limit for each cycle of CUREE load protocol for the reversed cyclic tests.

Table 3.1: Displacement limit for each cycle of CUREE reversed cyclic load

| Ref. Dis. (mm) = 60 | | | |
|---|---|---|---|
| Cycles (Times) | % Ref. Dis. | Positive mm | Negative mm |
| | 0.0 | 0.00 | 0.00 |
| 6 | 5.0 | 3.00 | -3.00 |
| 1 | 7.5 | 4.50 | -4.50 |
| 6 | 5.6 | 3.36 | -3.36 |
| 1 | 10.0 | 6.00 | -6.00 |
| 6 | 7.5 | 4.50 | -4.50 |
| 1 | 20.0 | 12.00 | -12.00 |
| 3 | 15.0 | 9.00 | -9.00 |
| 1 | 30.0 | 18.00 | -18.00 |
| 3 | 23.0 | 13.80 | -13.80 |
| 1 | 40.0 | 24.00 | -24.00 |
| 2 | 30.0 | 18.00 | -18.00 |
| 1 | 70.0 | 42.00 | -42.00 |
| 2 | 53.0 | 31.80 | -31.80 |
| 1 | 100.0 | 60.00 | -60.00 |
| 2 | 75.0 | 45.00 | -45.00 |
| 1 | 150.0 | 90.00 | -90.00 |
| 2 | 113.0 | 67.80 | -67.80 |
| 1 | 200.0 | 120.00 | -120.00 |
| 2 | 150.0 | 90.00 | -90.00 |

### 3.1.4 Test Matrix

The test configurations of the corner joints are shown in Figure 3.7. Only configuration C1 was tested both for cyclic and monotonic loading. Although configuration C10 with the LVL header was tested once, all other configurations with SPF header were tested twice for cyclic loading to ensure some level of repeatability in the results. The test matrix for all corner configurations is given in Table 3.2 below.

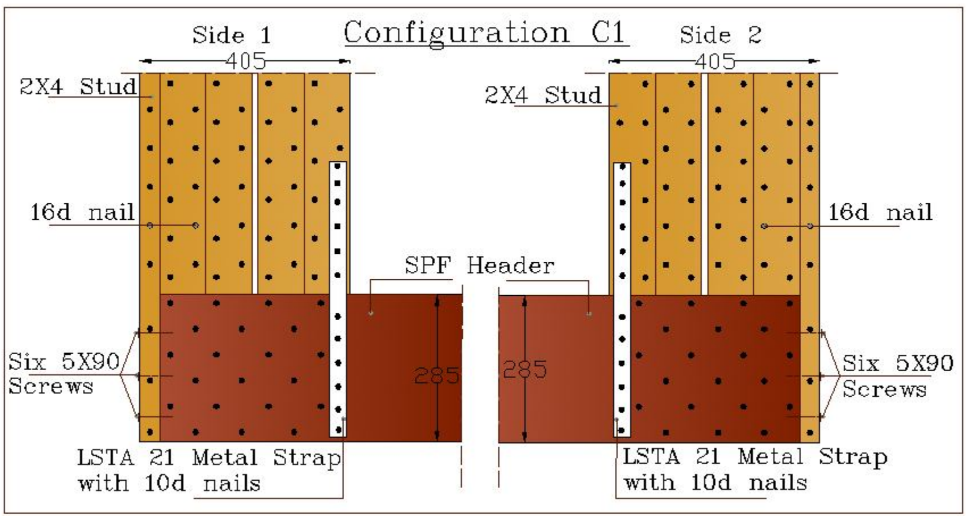


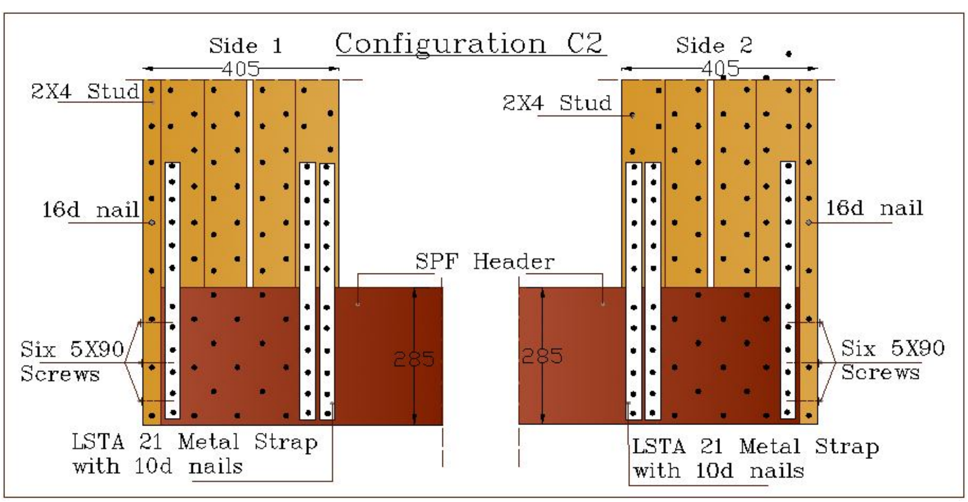

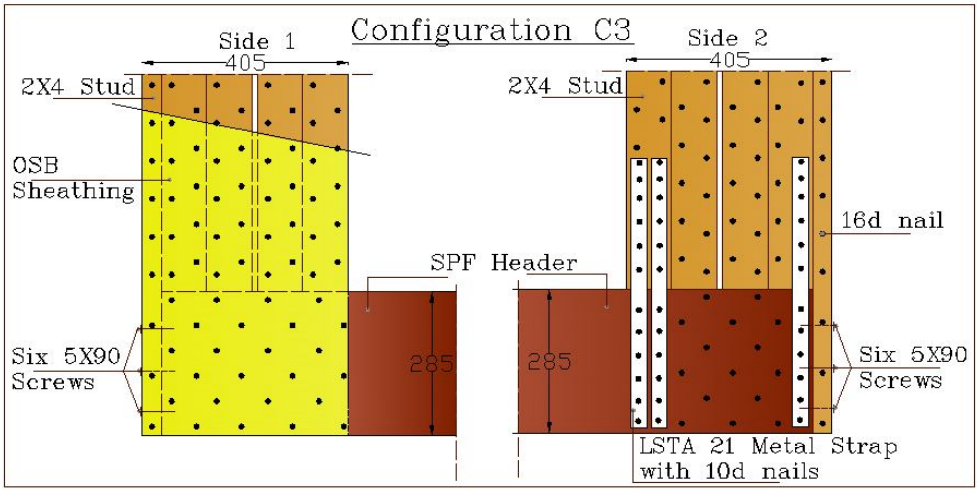
Configuration C3
Side 1
405
Side 2
405
2X4 Stud
2X4 Stud
OSB
Sheathing
16d nail
SPF Header
285
285
Six 5X90
Screws
Six 5X90
Screws
LSTA 21 Metal Strap
with 10d nails

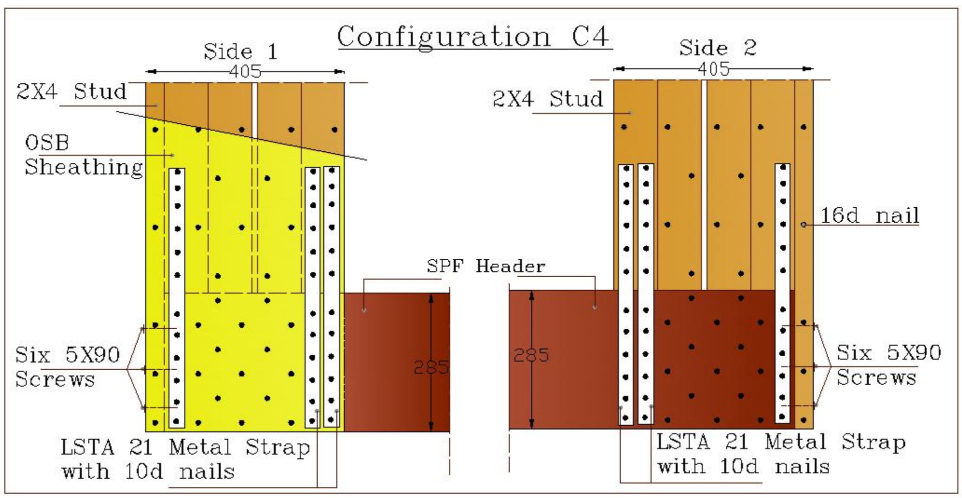
Configuration C4
Side 1
405
Side 2
405
2X4 Stud
2X4 Stud
OSB
Sheathing
16d nail
SPF Header
285
285
Six 5X90
Screws
Six 5X90
Screws
LSTA 21 Metal Strap
with 10d nails
LSTA 21 Metal Strap
with 10d nails

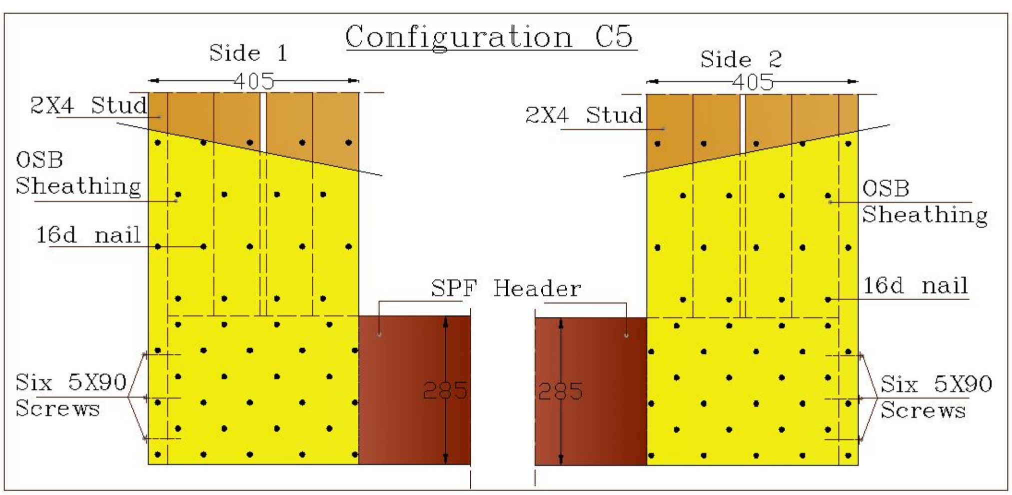
Configuration C5
Side 1
405
Side 2
405
2X4 Stud
2X4 Stud
OSB
Sheathing
OSB
Sheathing
16d nail
16d nail
SPF Header
285
285
Six 5X90
Screws
Six 5X90
Screws

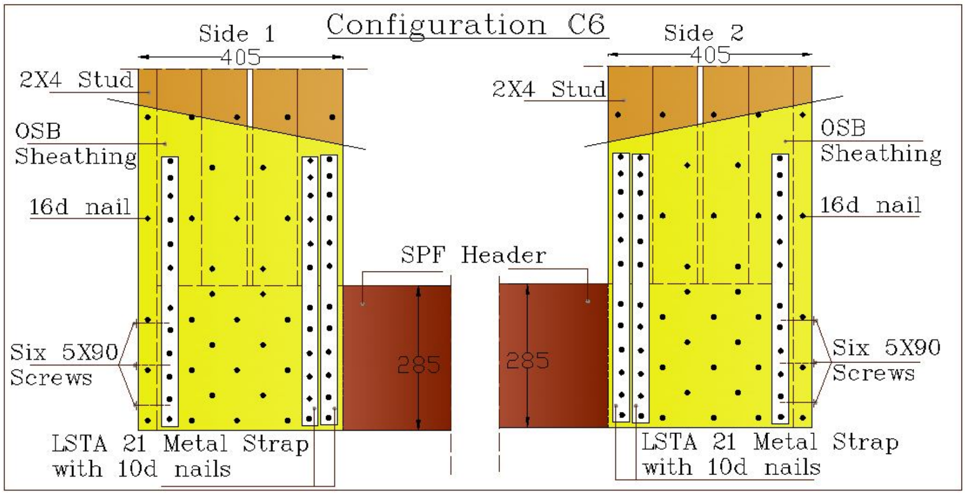
Configuration C6
Side 1
405
2X4 Stud
OSB
Sheathing
16d nail
Six 5X90
Screws
LSTA 21 Metal Strap
with 10d nails
SPF Header
285
285
Side 2
405
2X4 Stud
OSB
Sheathing
16d nail
Six 5X90
Screws
LSTA 21 Metal Strap
with 10d nails

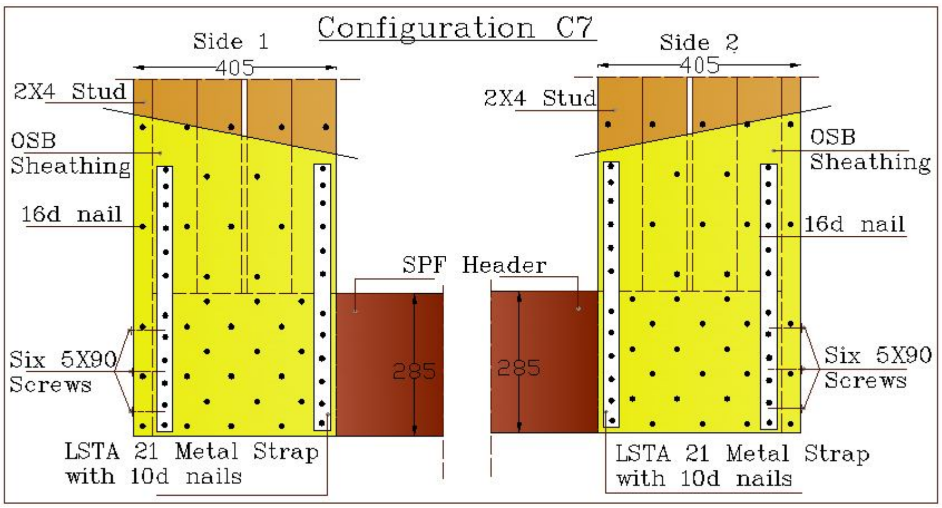
Configuration C7
Side 1
405
2X4 Stud
OSB
Sheathing
16d nail
Six 5X90
Screws
LSTA 21 Metal Strap
with 10d nails
SPF Header
285
285
Side 2
405
2X4 Stud
OSB
Sheathing
16d nail
Six 5X90
Screws
LSTA 21 Metal Strap
with 10d nails

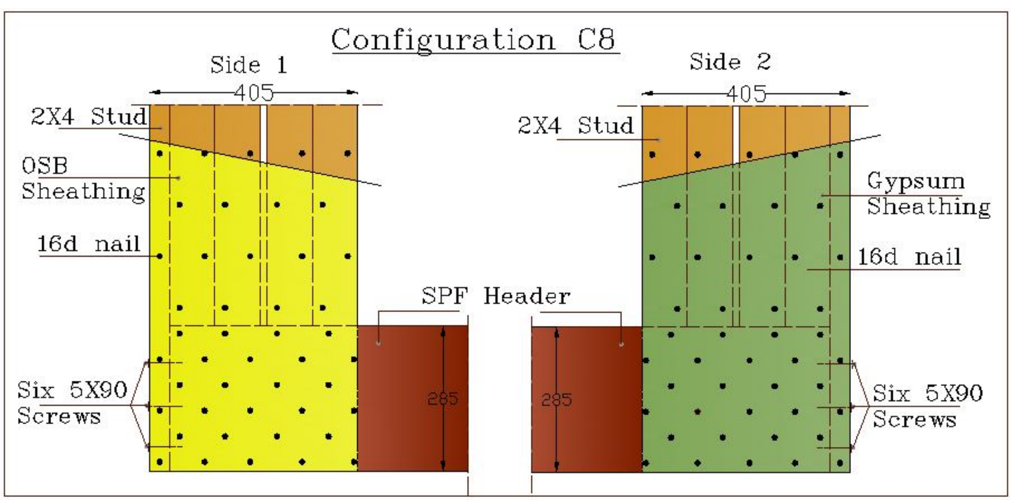
Configuration C8
Side 1
405
2X4 Stud
OSB
Sheathing
16d nail
Six 5X90
Screws
SPF Header
285
285
Side 2
405
2X4 Stud
Gypsum
Sheathing
16d nail
Six 5X90
Screws

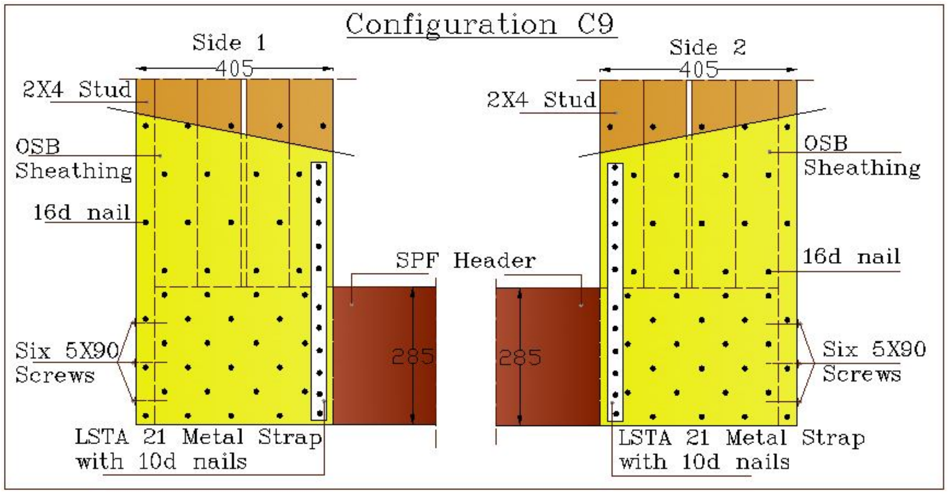


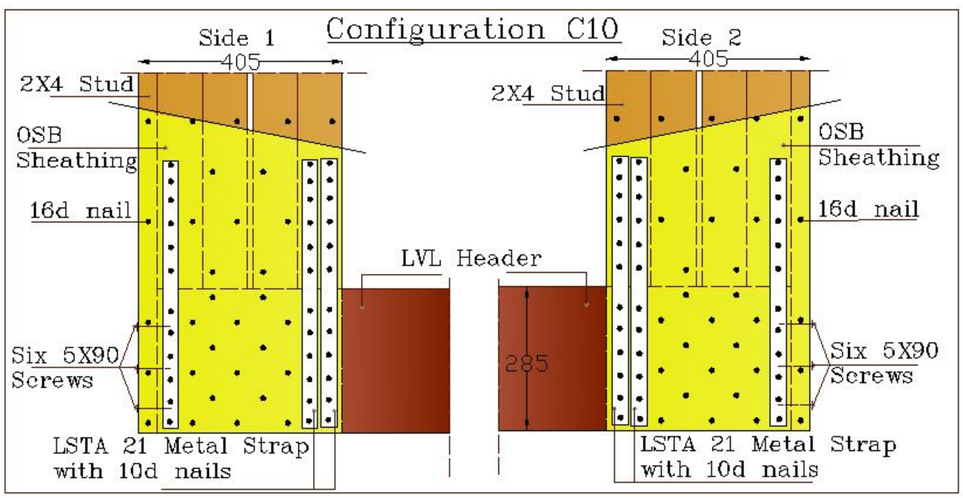


`

Figure 3.7: MIDPLY corner joint configurations (dimensions are in mm)

Table 3.2: Test Matrix of MIDPLY corner joint configurations

| Specimen No. | Exterior Sheathing details | Config. Details | Metal Strap Details |
|---|---|---|---|
| C1-M-1&2 | No exterior sheathing | C1 | Single metal strap on interior stud on both sides. |
| C1-C-1&2 | No exterior sheathing | C1 | Single metal strap on interior stud on both sides. |
| C2-C-1&2 | No exterior sheathing | C2 | Double metal straps on interior jack stud on both sides.<br>Single metal strap on exterior jack stud on both sides. |
| C3-C-1&2 | 1/2" OSB @ one side | C3 | Double metal straps on interior jack stud on unsheathed side.<br>Single metal strap on exterior jack stud on unsheathed side. |
| C4-C-1&2 | 1/2" OSB @ one side | C4 | Double metal straps on interior jack stud on both sides.<br>Single metal strap on exterior jack stud on both sides. |
| C5-C-1&2 | 1/2" OSB @ both sides | C5 | Without metal straps |
| C6-C-1&2 | 1/2" OSB @ both sides | C6 | Double metal straps on interior jack stud on both sides.<br>Single metal strap on exterior jack stud on both sides. |
| C7-C-1&2 | 1/2" OSB @ both sides | C7 | Single metal straps on interior jack stud on both sides.<br>Single metal strap on exterior jack stud on both sides. |
| C8-C-1&2 | 1/2" OSB @ one side & 1/2" GWP @ other side | C8 | Without metal straps |
| C9-C-1&2 | 1/2" OSB @ both sides | C9 | Single metal straps on interior jack stud on both sides. |
| C10-C-1 | 1/2" OSB @ both sides | C10 | Double metal straps on interior jack stud on both sides.<br>Single metal strap on exterior jack stud on both sides. |

## 3.2 Corner Joint Tests with FRP

Since the capacity of the connection between the header beam and the narrow wall segment plays a key role in the overall lateral load carrying capacity of the portal frame bracing system, Fiber Reinforced Polymer (FRP) was used to provide additional tensile strength to the corner joint. FRP was chosen as an alternative to metal straps due to its superior tensile strength. The FRP membrane was applied on top of exterior sheathing. To minimize the risk of delamination, a horizontal FRP layer was applied at mid height of the narrow wall segment in a direction perpendicular to the FRP that was used to resist the tension force, as shown in figure 3.8.

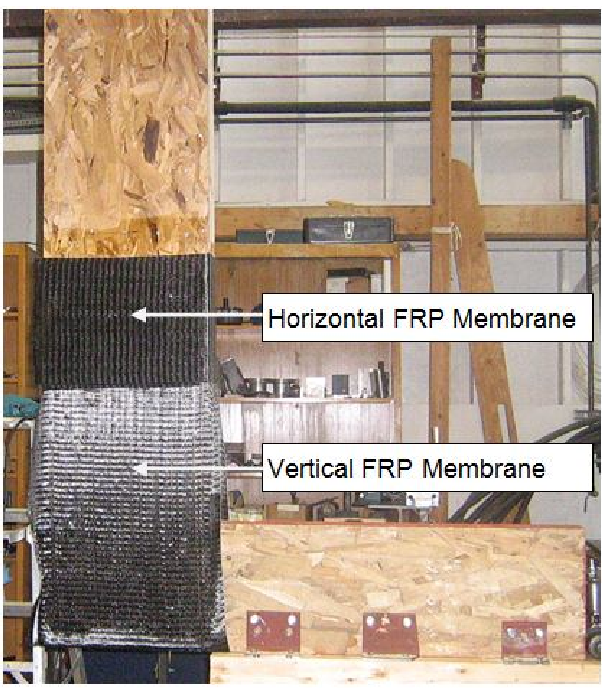


Figure 3.8: FRP layout on exterior OSB sheathing of corner joint

### 3.2.1 Specimen Details

The corner joint configuration with FRP consisted of 1760 mm high and 405 mm wide wall segments connected to two nominal 2x12 Laminated Strand Lumber (LSL) header. The standard narrow wall segment was constructed of 2x4 SPF No. 2 & better studs sheathed with Oriented Strand Boards (OSB). The sheathing to lumber connection consisted of 3.3 mm in diameter and 63.5 mm in length 8d common nails with a nailing schedule of 75 mm o.c. The sheathing was nailed to the LSL header using a nail spacing grid of 75 mm o.c. Six 5.12 mm x 88 mm wood screws were used to connect exterior stud with header. A single top plate was used at the corner between the LSL and narrow stud walls. The FRP membrane was applied vertically on the top of the exterior OSB panel. Tyfo SCH-41S-1 reinforcing fabric with Tyfo S Epoxy was used [3.4]. Tyfo SCH-41S-1 is a custom weave, unidirectional carbon fabric with glass crosses. Carbon fibres are orientated in the length direction and glass fibres are orientated at width direction. Figure 3.9 shows the elevation and cross section of the standard corner joint used in this test.

Figure 3.10 shows the test configuration of corner joint with FRP as well as the reference test configuration that the FRP test was compared with.

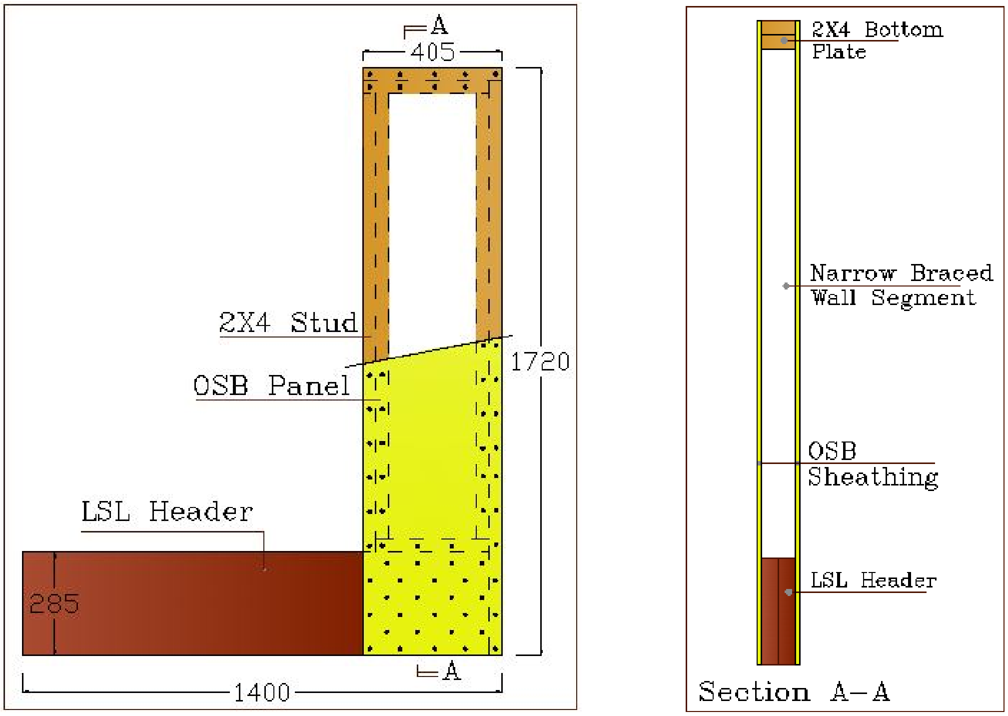


(a) (b)

Figure 3.9: (a) Elevation and (b) cross section of standard portal frame corner joint (dimensions are in mm)

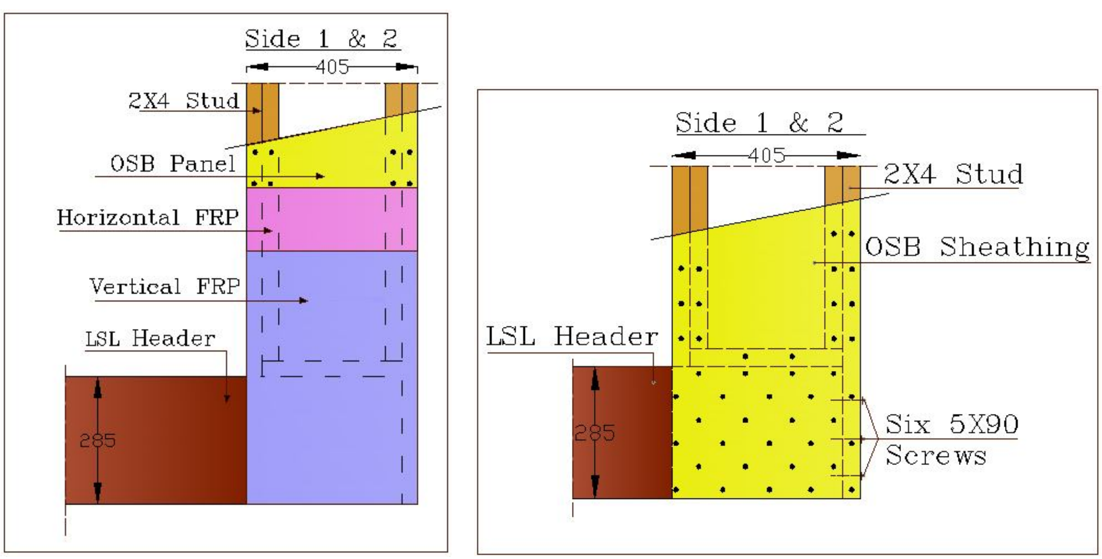


Configuration FRP-1 Configuration C1

Figure 3.10: Test configurations of corner joints (dimensions are in mm)

## 3.3 Nail Connection Tests

Prior to the corner joint testing a simplified finite element model was developed to estimate the characteristics of the corner joints. This was a useful exercise to predict the capacities and stiffnesses of the various test configurations. Input to the model was mainly based on values taken from the literature [3.5]. By comparing the test results to the model, the necessity to perform material component tests on the connections was evident. Nail connection tests were therefore performed to identify the mechanical properties of sheathing to header connection used in the corner joint tests.

Both single shear nail connection for exterior OSB and double shear nail connection for middle OSB sheathing were tested. The load deformation curves of the connection tests are used as input in the development of the numerical model for corner joint and full-scale portal frame. The following describes the details of nail connection tests.

### 3.3.1 Single Shear Nail Connection Test

A 300 mm long and 50 mm wide sheathing panel was connected with 300 mm long SPF header using a single nail with a diameter of 4.06 mm and length of 90 mm. This nail is identical to the one used in the corner joint tests connecting the exterior sheathing to the header. Three specimens were tested for single shear nail connection test.

The preparation of specimens, test setup and test protocols were done according to ASTM D1761 (ASTM 2006) [3.6]. Monotonic loading at a rate of 2.54 mm (0.1”) per minute was used to test the specimens and the frequency of data acquisition was set to 20 Hz. Figure 3.11 shows the test assembly as per ASTM D1761 and Figure 3.12 shows the specimen details and test setup.

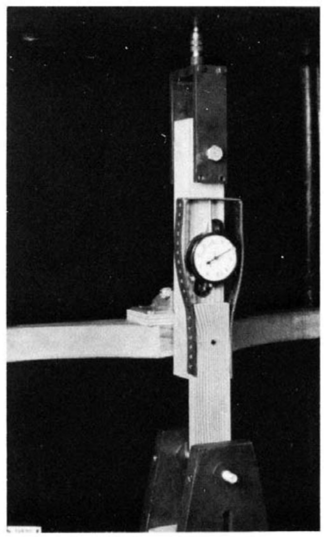

Figure 3.11: Assembly for Lateral Resistance Test of Nail [ASTM 2006]

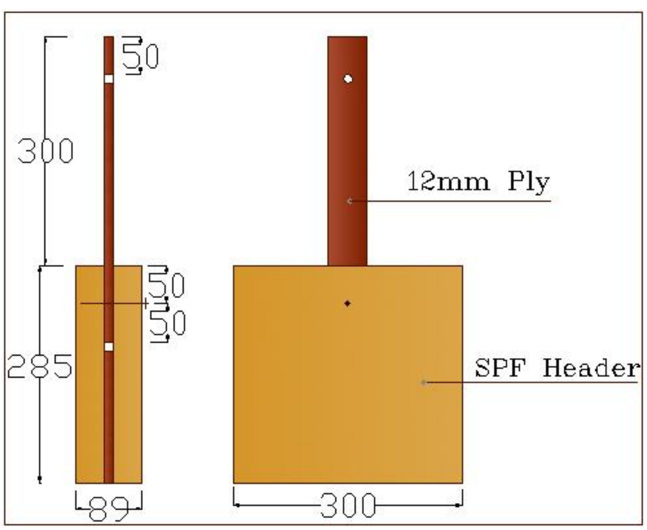


(a) (b)

Figure 3.12: (a) Specimen details and (b) actual test setup of single shear nail connection joint.

### 3.3.2 Double Shear Nail Connection Test

In this test, the sheathing was sandwiched between 2 plies of SPF header. 90mm long nails with 4.06 mm diameter connected the three members simulating the same conditions as in the corner joint specimen tests. The ASTM D1761 protocol [3.6] was followed to conduct the test. Monotonic loading rate was fixed to 2.54 mm (0.1”) per mm and data acquisition was set to 20 Hz. Figure 3.13 shows the specimen details and actual test setup of double shear nail connection test.

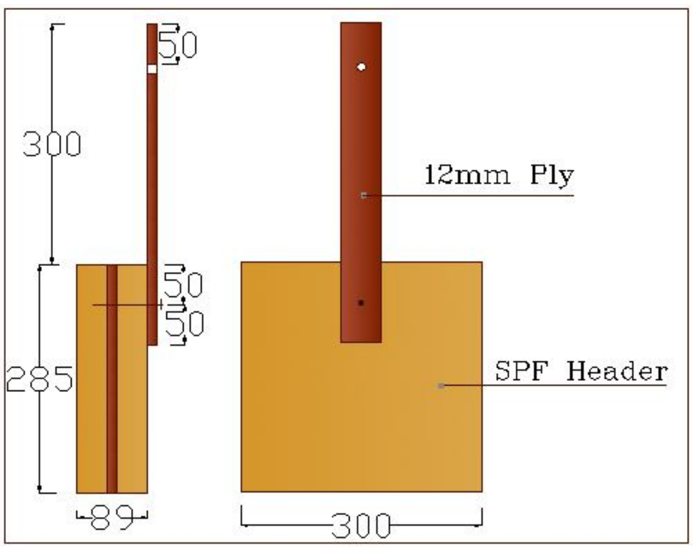



(a) (b)

Figure 3.13: (a) Specimen details and (b) actual test setup of double shear nail connection joint.

# CHAPTER 4

## Results and Discussion

### 4.1 Results and Discussion on the MIDPLY Corner Joint Tests

The analysis of the initial stiffness for each test specimen was carried out in accordance with the Equivalent Energy Elastic-Plastic (EEEP) curve in the ASTM Standard E2126 [4.1]. The EEEP curve is reproduced in Figure 4.1 where $P_{peak}$ is the maximum load. To compare the performance of the various corner joint assemblies, the peak load, initial stiffness, maximum moment and the corresponding rotation and the rotational stiffness were extracted from the test data. Summary of the test results analysis can be found in Table 4.1. The details of test configurations, test setup and procedures are described in Chapter 3.

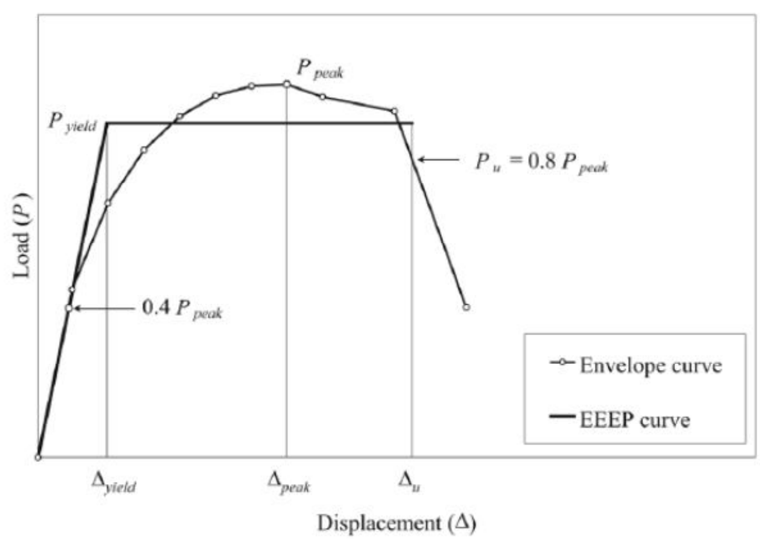


Figure 4.1: Determining of the response properties based on the EEEP curve according to ASTM E2126

Table 4.1: Experimental results for the MIDPLY corner joint tests

| Specimen | Max. Load kN | Displacement @ Max. Load mm | Initial Stiffness kN/mm | Max. Moment kN-m | Rotation @ Max. Moment Rad. | Rotational Stiffness kN-m / Rad |
|---|---|---|---|---|---|---|
| C1-M-1 | 5.39 | 21.3 | 0.273 | 8.51 | 0.0466 | 197 |
| C1-M-2 | 5.35 | 13.0 | 0.680 | 8.45 | 0.0283 | 491 |
| Avg. C1-M | 5.37 | 17.1 | 0.476 | 8.48 | 0.0374 | 344 |
| Ratio Max./Min. | 1.01 | 1.64 | 2.490 | 1.01 | 1.64 | 2.49 |
| | | | | | | |
| C1-C-1 | 6.06 | 15.7 | 0.442 | 9.57 | 0.0343 | 319 |
| C1-C-2 | 4.29 | 12.0 | 0.456 | 6.78 | 0.0262 | 329 |
| Avg. C1-C | 5.18 | 13.8 | 0.449 | 8.17 | 0.0302 | 324 |
| Ratio Max./Min. | 1.41 | 1.31 | 1.034 | 1.41 | 1.31 | 1.03 |
| | | | | | | |
| C2-C-1 | 8.92 | 25.7 | 0.502 | 14.07 | 0.0562 | 363 |
| C2-C-2 | 8.24 | 25.2 | 0.484 | 13.00 | 0.0550 | 350 |
| Avg. C2-C | 8.58 | 25.4 | 0.493 | 13.53 | 0.0556 | 356 |
| Ratio Max./Min. | 1.08 | 1.02 | 1.037 | 1.08 | 1.02 | 1.04 |
| | | | | | | |
| C3-C-1 | 9.23 | 20.9 | 0.574 | 14.57 | 0.0457 | 414 |
| C3-C-2 | 8.27 | 19.5 | 0.592 | 13.05 | 0.0426 | 427 |
| Avg. C3-C | 8.75 | 20.2 | 0.583 | 13.81 | 0.0442 | 421 |
| Ratio Max./Min. | 1.12 | 1.07 | 1.031 | 1.12 | 1.07 | 1.03 |
| | | | | | | |
| C4-C-1 | 9.08 | 20.4 | 0.619 | 14.33 | 0.0445 | 447 |
| C4-C-2 | 8.96 | 28.1 | 0.531 | 14.14 | 0.0614 | 384 |
| Avg. C4-C | 9.02 | 24.2 | 0.575 | 14.24 | 0.0529 | 415 |
| Ratio Max./Min. | 1.01 | 1.38 | 1.165 | 1.01 | 1.38 | 1.16 |
| | | | | | | |
| C5-C-1 | 11.48 | 25.6 | 0.675 | 18.12 | 0.0560 | 488 |
| C5-C-2 | 9.85 | 25.1 | 0.985 | 15.55 | 0.0548 | 711 |
| Avg. C5-C | 10.67 | 25.4 | 0.830 | 16.83 | 0.0554 | 599 |
| Ratio Max./Min. | 1.17 | 1.02 | 1.458 | 1.17 | 1.02 | 1.46 |

Table 4.1: Experimental results for the MIDPLY corner joint tests *cont.*

| | | | | | | |
|---|---|---|---|---|---|---|
| **C6-C-1** | **11.64** | **24.1** | **0.616** | **18.36** | **0.0527** | **445** |
| **C6-C-2** | **10.80** | **20.5** | **0.994** | **17.04** | **0.0447** | **718** |
| **Avg. C6-C** | **11.22** | **22.3** | **0.805** | **17.70** | **0.0487** | **581** |
| **Ratio Max./Min.** | **1.08** | **1.18** | **1.61** | **1.08** | **1.18** | **1.61** |
| | | | | | | |
| **C7-C-1** | **10.57** | **20.3** | **0.815** | **16.68** | **0.0444** | **589** |
| **C7-C-2** | **9.67** | **17.1** | **0.910** | **15.26** | **0.0374** | **657** |
| **Avg. C7-C** | **10.12** | **18.7** | **0.863** | **15.97** | **0.0409** | **623** |
| **Ratio Max./Min.** | **1.09** | **1.19** | **1.12** | **1.09** | **1.19** | **1.12** |
| | | | | | | |
| **C8-C-1** | **6.11** | **18.9** | **0.754** | **9.64** | **0.0414** | **545** |
| **C8-C-2** | **6.53** | **11.7** | **0.802** | **10.30** | **0.0256** | **579** |
| **Avg. C8-C** | **6.32** | **15.3** | **0.778** | **9.97** | **0.0335** | **562** |
| **Ratio Max./Min.** | **1.07** | **1.62** | **1.06** | **1.07** | **1.62** | **1.06** |
| | | | | | | |
| **C9-C-1** | **9.37** | **25.9** | **0.870** | **14.78** | **0.0566** | **628** |
| **C9-C-2** | **10.34** | **19.6** | **0.890** | **16.32** | **0.0427** | **642** |
| **Avg. C9-C** | **9.85** | **22.7** | **0.880** | **15.55** | **0.0497** | **635** |
| **Ratio Max./Min.** | **1.10** | **1.32** | **1.02** | **1.10** | **1.32** | **1.02** |
| | | | | | | |
| **C10-C-1** | **15.14** | **20.4** | **1.009** | **23.77** | **0.0445** | **729** |

The initial stiffness is calculated as the slope of the secant line between 0% and 40% of peak load of the load-displacement curve. The maximum moment is the product of the peak load and moment arm. The moment arm used in the calculation was taken as the distance between the center of the header and vertical wall segment corner to the top of bottom plate connected to the load distribution metal plate (i.e. 1.58m).

The rotational stiffness is calculated by dividing the moment corresponding to 40% of peak loading by the rotational angle at that loading, where the rotational angle is based on the horizontal deflection of the vertical stud as measured using cable transducer 1 (see Figure 3.4 in Chapter 3).

### 4.1.1 Description of Failure Modes and Load-Slip Curves for the MIDPLY Corner Joint Tests

For all corner joint configurations the failure was initiated through the rupture of the middle OSB sheathing panel followed by the rupture of exterior OSB sheathing. Subsequent failure was observed in the metal strap connecting the header beam to the narrow wall segment. Figure 4.2 shows an example of such failure sequence.

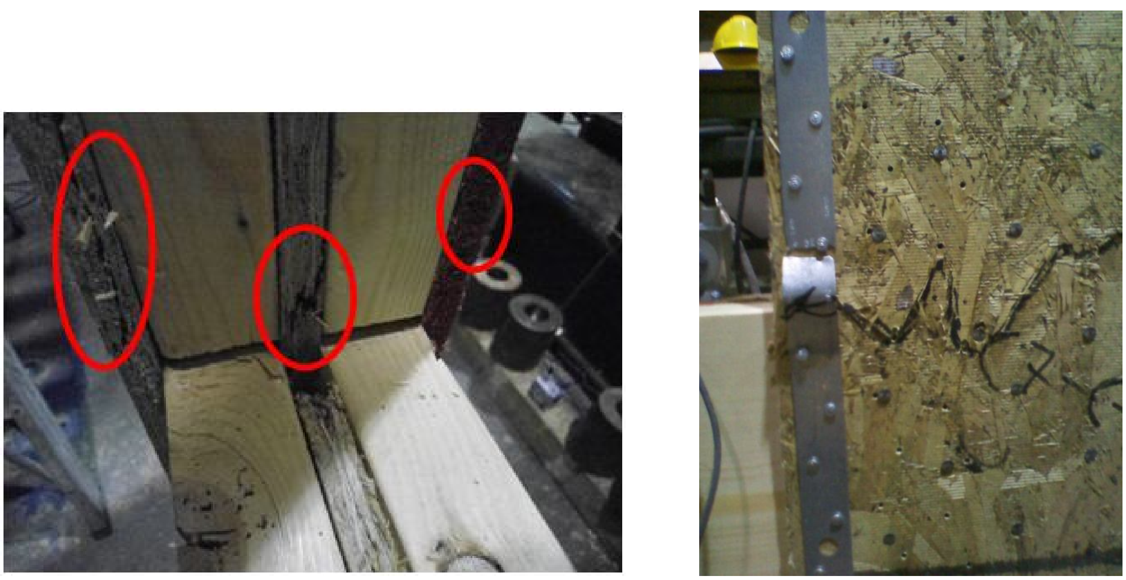

Figure 4.2: Typical failure in sheathing panels for the MIDPLY corner joints.

The consistency in the failure sequence allowed for a better comparison with the finite element model of the corner joint. This is discussed in more details in Chapter 5. Nail pull-out was observed in a limited number of the metal strap connections. This is also observed in light-frame shearwalls and is typically an indication of a ductile failure, where yielding occurs in the steel fastener with some crushing in the wood.

For the test configuration with OSB sheathing on one side and gypsum wallboard (GWB) on the other side (test configuration C8-C), the failure was also initiated with the rupture of middle OSB sheathing panel. As for the exterior panels, the failure started with cracks being developed in the GWB panel followed by the rupture of the exterior OSB panel. This was expected, as the GWB panel is stiffer and more brittle. It would therefore likely attract more force initially, and when it starts cracking the load will be transferred to the other side of the wall, sheathed with the OSB panel.

Figure 4.3 shows typical examples of failure modes observed during testing of the MIDPLY corner joint configurations. Also shown is a typical load-slip hysteresis curve for the MIDPLY corner joint. The graph clearly indicates that due to the engagement of nails and metal straps the behavior of test specimen is ductile. The envelope curve was constructed by taking the maximum load-displacement value for each full cycle (see also Section 3.1.3 in Chapter 3). A full presentation of the failure modes, load-slip hysteresis curves and envelope curves for each corner joint configuration tested is shown in Appendix A.

(a) Middle OSB failure

(b) Exterior OSB sheathing failure

(c) Metal strap failure

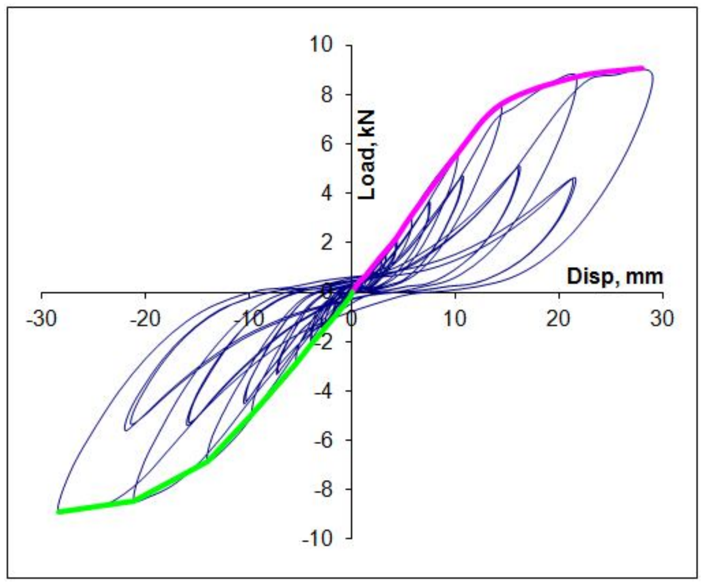


(d) Load-slip hysteresis and backbone curve

Figure 4.3: Typical failure modes and load-slip hysteresis graph of MIDPLY corner joint

### 4.1.2 Maximum Moment Resistance

The maximum moment of each specimen was calculated as the average of the push and pull moment capacities where “push” and “pull” refers the in-plane movement of narrow wall segment towards and away from the header due to applied cyclic loading. As shown in Table 4.1, the difference between the peak loads (same applies to maximum moment) for each of the two test specimens is very small. On average the maximum-to-minimum ratio was 1.11. In Figure 4.4 below, the average values of the maximum moment capacities for each configuration were compared.

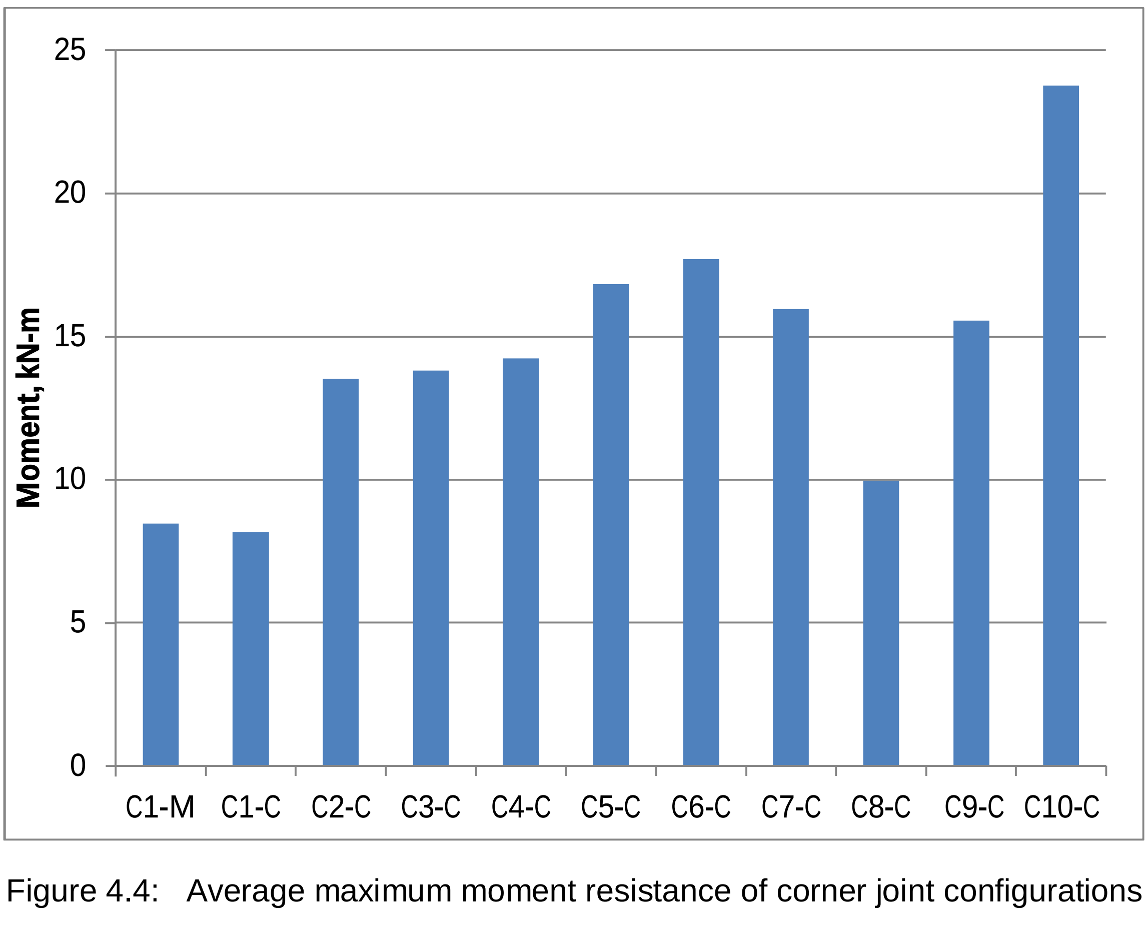


Figure 4.4: Average maximum moment resistance of corner joint configurations

The results indicate that no significant differences were found when comparing assemblies subjected to monotonic loading with those tested under cyclic loading (comparing C1-M and C1-C). This is also shown in Figure 4.5 below.

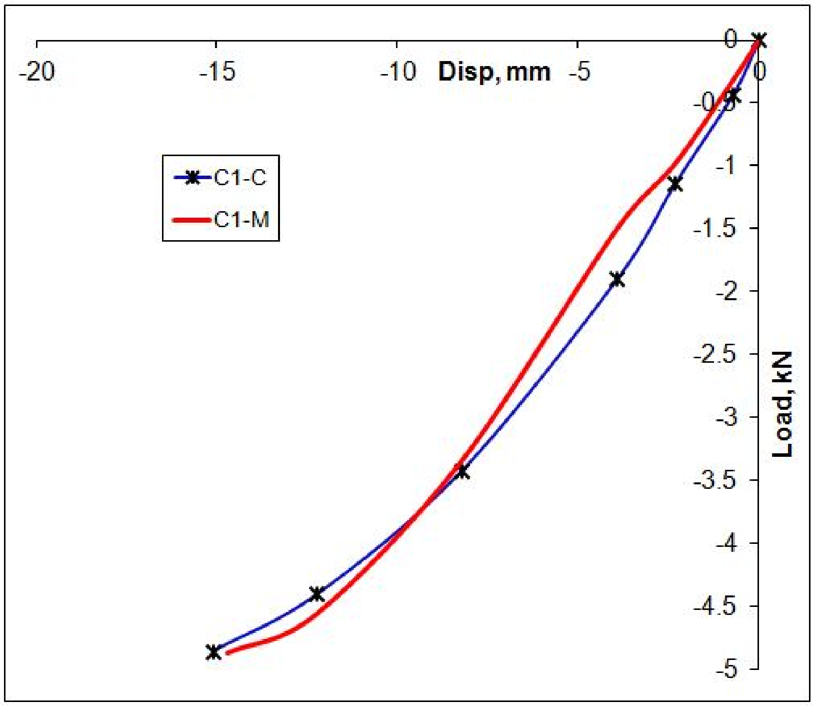


Figure 4.5: Load-slip curve for monotonic (C1-M) and cyclic (C1-C) loading for corner joint configuration C1-C

Figure 4.4 also shows that in general the maximum moment resistance increased with the addition of the metal straps and exterior sheathings. Configuration C2-C, with three metal straps on each face and no exterior sheathing, had 66% more moment resisting capacity than configuration C1-C with a single metal strap on each face. The reader is encouraged to see Figure 3.7 in Chapter 3 for a clearer idea on the distribution of the metal strap on each face. Substituting the three metal straps on one side of configuration C2-C with an OSB sheathing panel (C3-C) resulted in that the lateral load carrying capacity remained virtually unchanged. Adding three metal straps on top of the sheathed side (C4-C) caused only a minor (3%) improvement compared with the C3-C configuration. This observation was also consistent for the double-sided sheathing configurations. For example, where single metal strap was added on top of the sheathing on both faces (configuration C7-C and C9-C) and compared with the configuration with sheathing and three metals straps (C6-C) and the configuration with sheathing and two metals straps (C7-C), the difference in capacity was only between 11% and 3%, respectively. One explanation for this is that the presence of the metal straps ensures that the load was transferred in the straps in tension rather than through the nails connecting the sheathing to the framing. In other words, the effects from the exterior sheathing and the straps are not additive.

It was observed from the test results that all the configurations with double-sided sheathing (C5-C, C6-C, C7-C, C9-C) had higher capacity than those with single-sided sheathing (C3-C, C4-C). For example, configuration C6-C had 24% higher capacity compared with configuration of C4-C, which had similar detailing but sheathing on one side only.

A significant increase in the moment capacity of 34% was achieved by replacing the SPF header (C6-C) with the LVL header (C10-C). The increase could be attributed partly to the fact that the LVL header has higher density than SPF, providing a higher capacity to the connection with the straps as well as with the OSB sheathing. The other reason could be the higher bending capacity of the LVL header.

As predicted, the configuration with the Gypsum Wallboard (GWB) on one side (C8-C) did not meet the performance level of the configuration with OSB panels on both sides (C5-C). The moment capacity of C8-C was 41% lower than that of configuration C5-C. The drop in capacity was excepted as GWB is a weaker material compared to OSB.

### 4.1.3 Rotational Stiffness

It is evident from figure 4.6 that the rotational stiffness increases with the addition of metal straps and exterior sheathing to the assemblies. The figure also shows that adding a layer of exterior OSB sheathing to one side (configurations C3-C and C4-C) increased the rotational stiffness compared to corner joint configurations with no exterior OSB sheathing (configurations C1-C and C2-C). Also adding the exterior OSB sheathing to both sides (C5-C, C6-C, C7-C, C9-C) introduced a higher rotational stiffness than corner joint configurations with single sided exterior OSB sheathing (C3-C, C4-C).

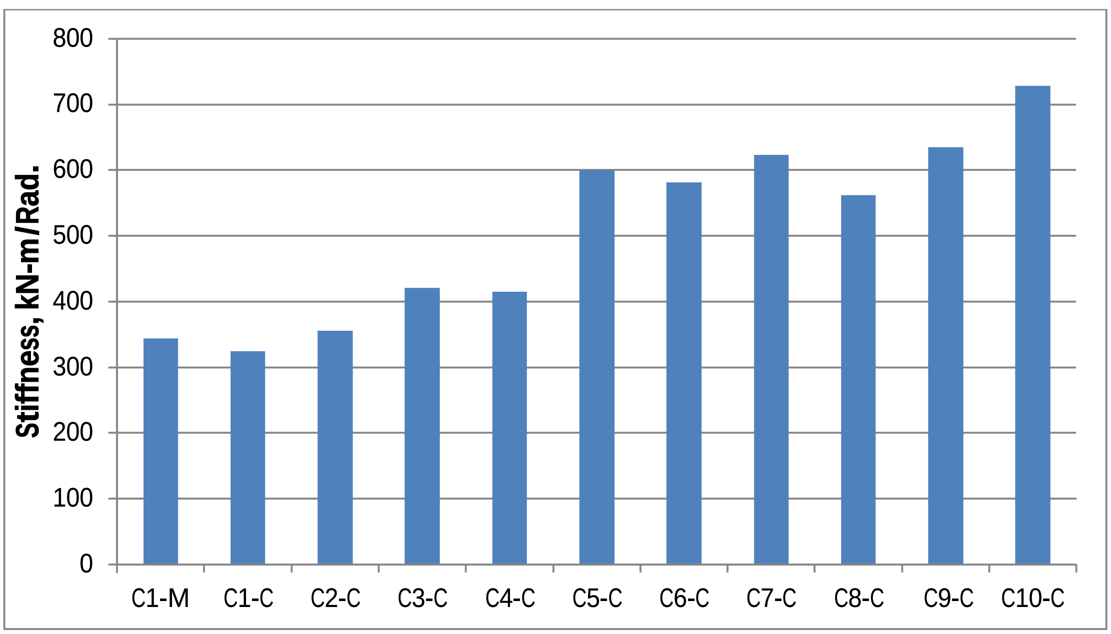


Figure 4.6: Average maximum rotational stiffness of corner joint configurations

The configuration without exterior sheathing and three metal straps on each face (C2-C) had only 10% higher rotational stiffness than the test assembly with only a single metal strap on each face and no exterior sheathing (C1-C). The fact that the contribution of the metal straps to stiffness was not more pronounced than observed in the testing was expected. Metal straps contribute significantly to the overall strength due to their high tensile strength; however their rotational stiffness is very small and would therefore have little contribution to the overall stiffness of the frame.

For configuration with sheathing on both sides (C6-C), the rotational stiffness increased by 63% compared to configuration C2-C with no exterior sheathing. This means the sheathing had a significant impact on the stiffness properties of corner joint.

Replacing SPF header (C6) with LVL header (C10) increased the rotational stiffness by 25% for otherwise similar configurations. This is again due to the high bending stiffness of the LVL header.

.

## 4.2 Results and Discussion on the Corner Joint Tests with FRP

The procedure used to analyze the test results of corner joints with FRP was similar to that used for the MIDPLY corner joints by utilizing the Equivalent Energy Elastic-Plastic (EEEP) curves [4.1]. The maximum lateral capacity, maximum moment as well as the rotational stiffness were calculated to compare the performance of the corner joint assemblies with and without the application of FRP. The details of specimens and test configurations are described in Chapter 3. For the moment resistance calculations, the distance between the center of the header and vertical narrow wall segment corner to the top of bottom plate connected to the load distribution metal plate (i.e. 1.58 m) was taken as the moment arm. Transducer 1 (Figure 3.4 in Chapter 3) was used to measure the deflection of the vertical stud to calculate the rotation angle. A summary of the analysis results and load displacement envelope curves for corner joint with and without FRP are given in Table 4.2 and Figure 4.7.

Table 4.2: Experimental results of portal frame corner joints

| | | | Max. Load | Max. Moment | Rotation @ Max. Moment | Rotational Stiffness |
|---|---|---|---|---|---|---|
| **Specimen** | **Corner Joint Type** | **Header** | **kN** | **kN-m** | **Rad.** | **kN-m / Rad.** |
| **C1** | **Standard** | **LSL** | **9.26** | **15.0** | **0.0471** | **610** |
| **FRP-1** | **Standard** | **LSL** | **14.26** | **23.0** | **0.0793** | **540** |
| **% Increase** | | | **54.0** | **54.0** | **68.4** | **-11.5** |

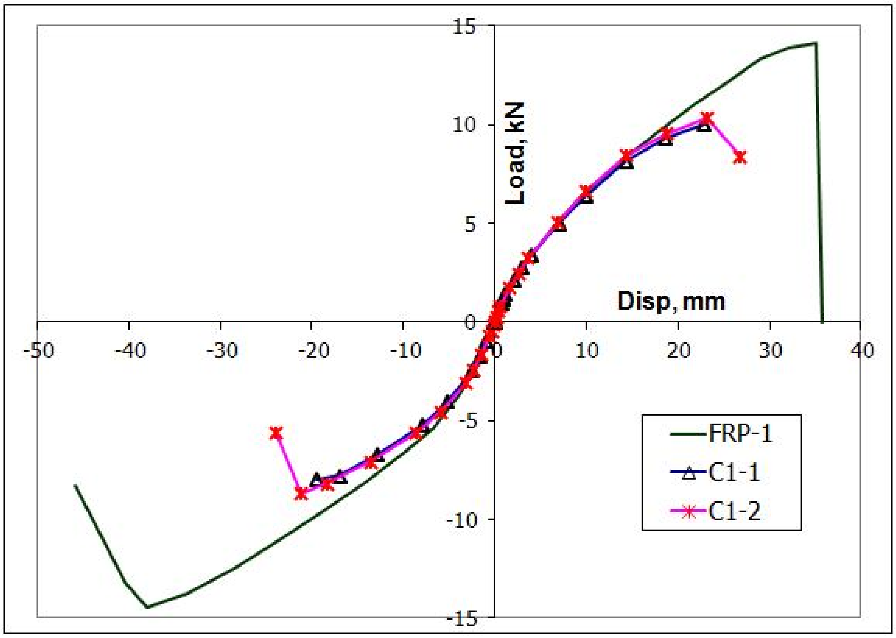


Figure 4.7: Envelope curve comparison of corner joint configurations with and without FRP.

### 4.2.1 Description of failure Modes and Load-Slip Curves for Corner Joint Tests with FRP

For specimens where FRP was used to upgrade the standard wall configuration, the FRP membrane started to tear at both corners of the narrow wall segment and propagated towards the centre. No failure of exterior OSB was observed. Figure 4.8 shows the failure mode and load slip hysteresis curve.

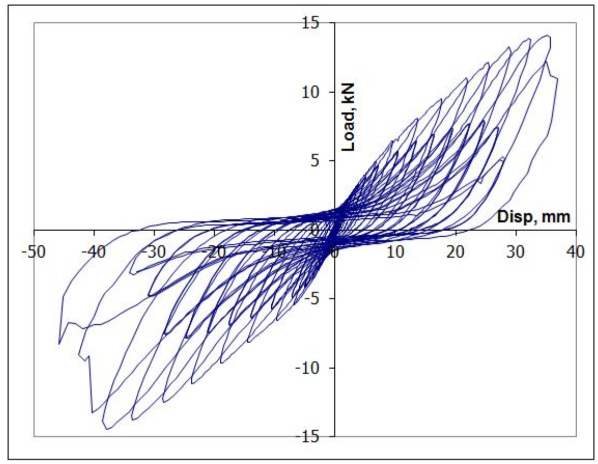


(a) (b)

Figure 4.8: (a) Failure mode of FRP membrane and (b) Load displacement curve of corner joint with FRP

### 4.2.2 Maximum Moment Resistance and Rotational Stiffness

The maximum moment resistance was calculated as the average of maximum push and pull moment of each specimen. Table 4.2 shows that the configuration with the FRP membrane had 54% more moment resisting capacity compared to the standard configuration with no FRP.

Also, it appears that the addition of the FRP membrane had no significant effect on the stiffness properties of the corner joint. Given the variability found between similar configurations (see Table 4.1); it is inconclusive based on the limited data available to evaluate the effect of the FRP on stiffness.

# CHAPTER 5

## Numerical Modeling

### 5.1 FE Model Inputs

All framing members were modeled as beam elements. An average value for the modulus of elasticity based on the lumber species and grade was taken from the Canadian design code CSA 086 (CSA 2009) [5.1]. The local axis of the studs were turned 90-degree when the MIDPLY model was developed. The OSB sheathing was defined as an orthotropic shell element, where the out-of-plane movements were restricted. The tensile properties and modulus of elasticity for the OSB panel was taken from material tests on similar members by Chen and Ni [5.2] and the compressive properties were taken from a study by Zhu et al. [5.3]. The values are reproduced in Table 5.1 (a) and (b).

Table 5.1 (a): Average results of tension tests for OSB panel [5.2]

| Parallel to surface strand orientation MPa | | | | Perpendicular to surface strand orientation MPa | | | |
|---|---|---|---|---|---|---|---|
| MOE | MOR | G | *v* | MOE | MOR | G | *v* |
| 5390 | 12.2 | 1360 | 8.3 | 3360 | 8.9 | 1400 | 8.2 |

Note: MOE is the modulus of elasticity of the panel in tension, MOR is the ultimate tensile stress of the panel, G is the through-thickness modulus of rigidity of panel and v is the ultimate shear stress of panel.

Table 5.1 (b): Average results of compression tests for OSB panel [5.3]

| Parallel to surface strand orientation MPa | Perpendicular to surface strand orientation MPa |
|---|---|
| 14.1 | 12.62 |

Nails were defined as non-linear link element. Hold-down connectors were assigned as linear tension link element. Linear elastic behavior was assumed for the framing members and the header. Table 5.2 shows the input properties of all the elements used in the FE model.

Table 5.2: Input data of elemental properties for Finite Element model.

| Construction Member | Finite Element | Material Property |
|---|---|---|
| Framing | Beam element | E = 9000 MPa |
| Sheathing | Shell element | Table 5.1 |
| Sheathing-to-framing nail connection | Link element | Test data shown in Figure 5.2 |
| Framing-to-framing metal strap connection | Link element | Test data shown in Figure 5.3 |
| Framing members in contact | Link element | U = 40 kN/mm (open = 0 mm) [5.2] |
| Hold-down | Link element | U = 5 kN/mm [5.2] |

Note: U – spring stiffness, E – the modulus of elasticity

The sheathing-to-framing and framing-to-framing nail connections were modeled using a 3D link element, where component 2 (U2) and 3 (U3) represented the nail's shear resistance parallel and perpendicular to the grain of the framing member, respectively, as shown in Figure 5.1. Component 1 represents the withdrawal resistance of the nail.

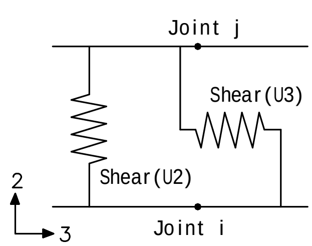


Figure 5.1: Sheathing-to-framing and framing-to-framing connection detail

A detailed description of the component tests used in the test model is reported elsewhere [5.2, 5.4].

Experimental work on nail slip between sheathing and framing elements have shown that there is no significant difference in the nail slip behavior between the parallel and the perpendicular to grain directions (e.g. [5.2]). Therefore, the same load-slip curve as shown in Figure 5.2 was used to represent the sheathing-to-header connection link. Link element properties such as the framing-to-framing connections as well as the nail/screw withdrawal resistance were taken from testing work by FPInnovations [5.4].


Figure 5.2: Load-slip curve of sheathing to SPF framing nail connection

The metal strap was represented as a one-dimensional non-linear tension link element. Different link properties were assigned for SPF framing to SPF header and SPF framing to LSL header connection as shown in Figure 5.3.

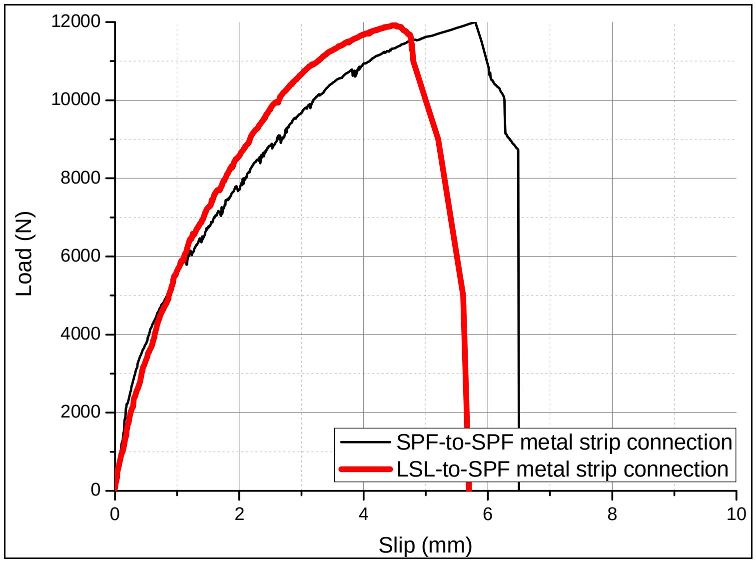


Figure 5.3: Load-slip curves of framing-to-framing strap connection [5.2]

In the model, the OSB sheathing was not directly connected to the SPF header where the metal strap was applied on top of the exterior OSB panel. Out-of-plane deformations due to wall frames, header, and the torsions of wall frames were restricted in the model analysis in order to be consistent with the test conditions.

Displacement was applied incrementally in the displacement-controlled non-linear analysis. In each step the iterations were carried out until convergence. The solution could be stopped due to numerical sensitivity if there was an excess number of a null step, where the solution could not converge in the solution. Iteration convergence tolerance, maximum iterations per step, maximum number of steps and maximum null (zero) steps can be controlled in model as the time required to run the analysis proportionally increased with the increment of steps.

In order to accurately predict the failure mode of the portal frame corner joint it was assumed that metal strap, placed over the exterior OSB, carried the entire load after rupture of the exterior OSB panel. Since SAP2000 cannot remove the component automatically when OSB reaches maximum capacity, splitting of OSB sheathing was assigned manually in the numerical model. It was predicted that ultimate lateral load carrying capacity of the corner joint increased until the rupture of metal strap. Since displacement-controlled was used, the software continued to run the analysis after failure of metal straps until meeting the required null steps.

A 12mm gap in between the middle OSB sheathing panels was also provided in FE model to allow the rotation of middle OSB sheathing as well as simulate the middle OSB sheathing alignment with the actual test specimens.

## 5.2 Verification of the FE Model

### 5.2.1 Validation Against Experimental Tests on MIDPLY Corner Joints

In order to validate the MIDPLY corner joint FE model, comparisons were made between the model predictions and the test results of selected MIDPLY corner joint configurations including some key variables such as different number and alignment of metal straps and OSB sheathing arrangements. Monotonic load was applied in FE model (pulling of the braced wall segment). Figure 5.4 shows the corner details of the MIDPLY portal frame corner joint.

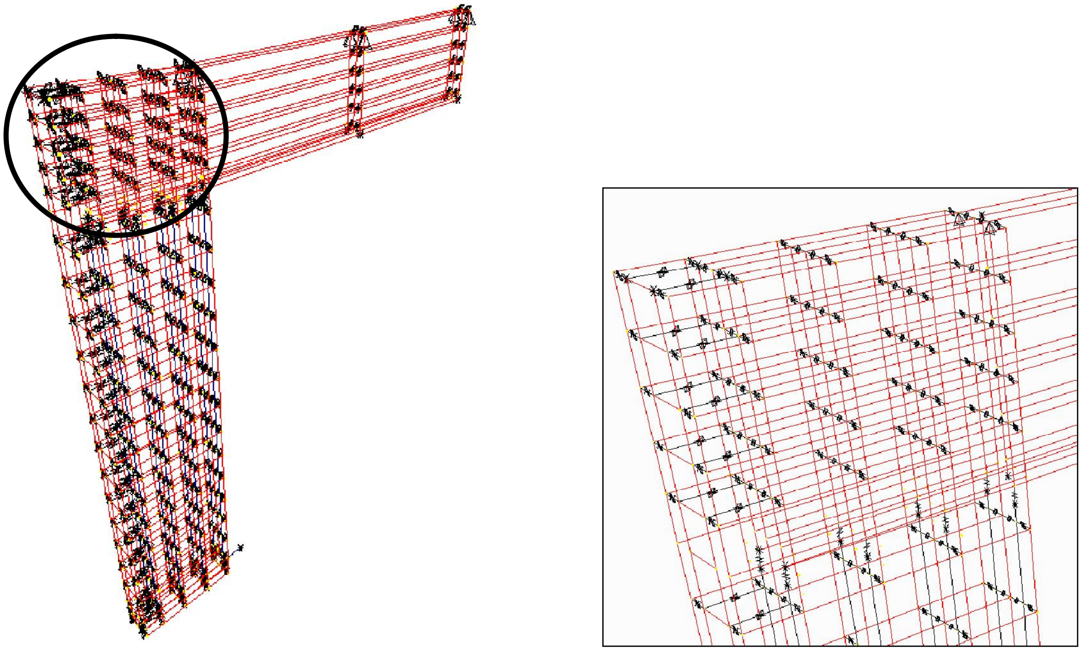

(a) 3D view of FE model of MIDPLY corner joint (b) Corner details of connections

Figure 5.4: FE model of MIDPLY corner joint

Table 5.3 shows the MIDPLY corner joint configurations used to verify the FE model. More details about the configurations are given in Chapter 3. Figure 5.5 shows the comparison of load displacement graphs of the FE model with experimental test result and Table 5.4 summarizes the percentage difference in the maximum load, displacement at maximum load and the initial stiffness between the FE model and the corner joint test results. The values in Table 5.4 differ from those in Table 4.1 because only the one direction (pull) has been presented in this table to compare with the same direction in the model.

Table 5.3: MIDPLY corner joint configurations for Finite Element model

| Specimen No. | Sheathing detail | Config. Details | Header | Metal Strap Details |
|---|---|---|---|---|
| C3-C | 1/2" OSB @ middle and one side | C3 | SPF | Double metal straps on interior jack stud on unsheathed side. Single metal strap on exterior jack stud on unsheathed side. |
| C5-C | 1/2" OSB @ middle and both sides | C5 | SPF | Without metal straps |
| C6-C | 1/2" OSB @ middle and both sides | C6 | SPF | Double metal straps on interior jack stud on both sides. Single metal strap on exterior jack stud on both sides. |
| C7-C | 1/2" OSB @ middle and both sides | C7 | SPF | Single metal straps on interior jack stud on both sides. Single metal strap on exterior jack stud on both sides. |
| C9-C | 1/2" OSB @ middle and both sides | C9 | SPF | Single metal straps on interior jack stud on both sides. |

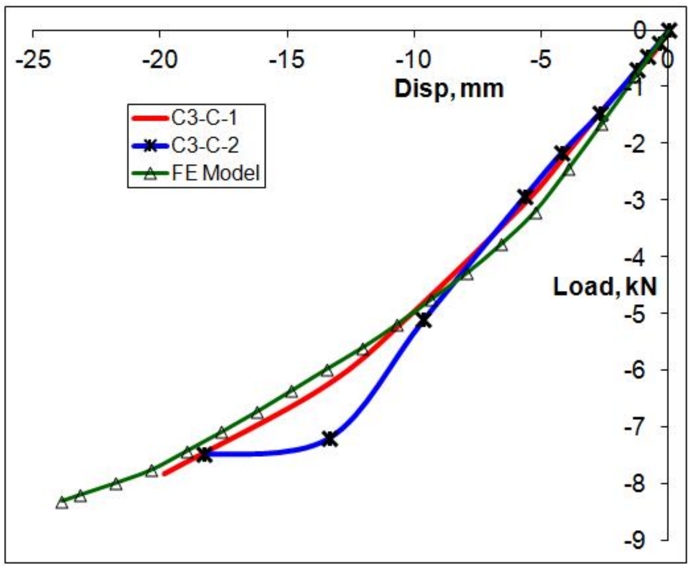


(a)

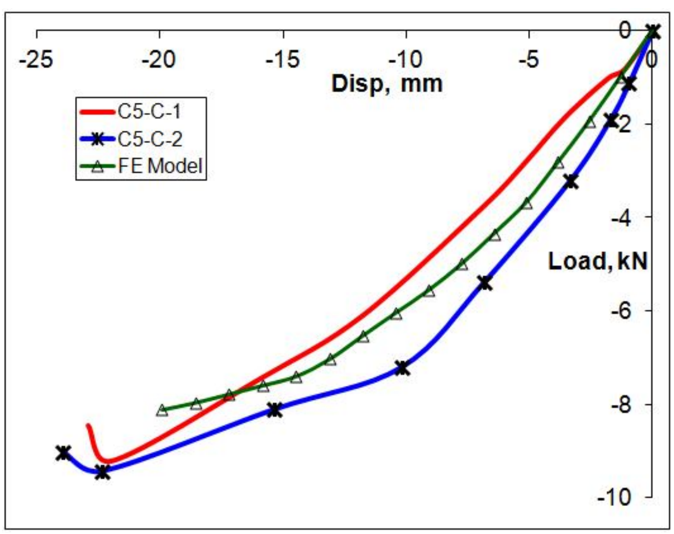


(b)

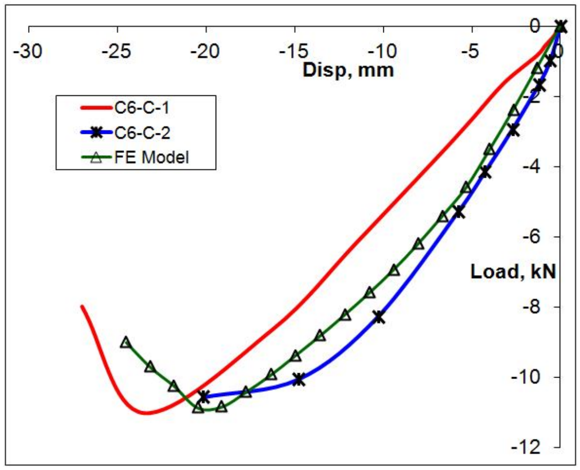


(c)

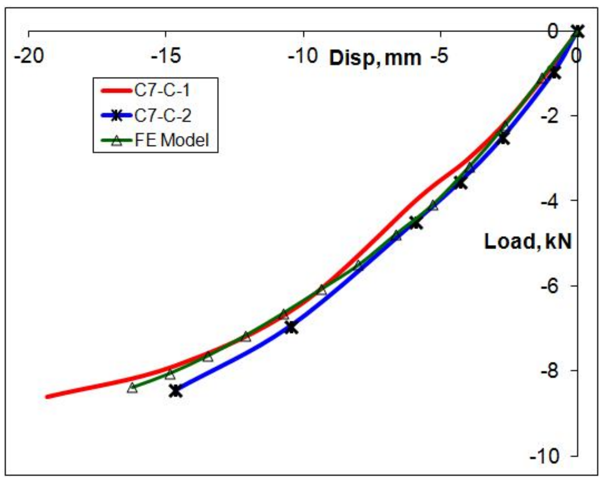


(d)

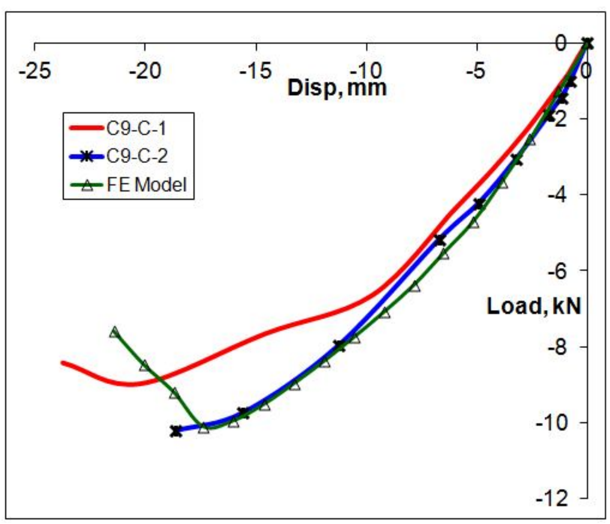


(e)

Figure 5.5: Comparison of the load-displacement responses between experiments and FE modeling

Table 5.4: Comparison between the corner joint test results and FE model

| Specimen | Test Type | Header | Max. Load kN | Disp. @ Max. Load mm | Initial Stiffness kN/mm | Max. Moment kN-m |
|---|---|---|---|---|---|---|
| C3-C | Experiment | SPF | 7.66 | 19.0 | 0.528 | 12.1 |
| C3 | FE model | SPF | 8.30 | 23.9 | 0.604 | 13.1 |
| **% variation** | | | **8.4** | **25.3** | **14.3** | **8.4** |
| C5-C | Experiment | SPF | 9.32 | 22.1 | 0.742 | 14.7 |
| C5 | FE model | SPF | 8.12 | 19.9 | 0.738 | 12.8 |
| **% variation** | | | **-12.9** | **-9.9** | **-0.6** | **-12.9** |
| C6-C | Experiment | SPF | 10.79 | 21.9 | 0.746 | 17.0 |
| C6 | FE model | SPF | 10.87 | 20.5 | 0.870 | 17.2 |
| **% variation** | | | **0.8** | **-6.3** | **16.6** | **0.8** |
| C7-C | Experiment | SPF | 8.54 | 17.0 | 0.775 | 13.5 |
| C7 | FE model | SPF | 8.39 | 16.3 | 0.799 | 13.2 |
| **% variation** | | | **-1.7** | **-4.4** | **3.1** | **-1.7** |
| C9-C | Experiment | SPF | 9.60 | 19.5 | 0.835 | 15.2 |
| C9 | FE model | SPF | 10.11 | 17.4 | 0.940 | 15.9 |
| **% variation** | | | **5.3** | **-10.7** | **12.6** | **5.3** |

Figure 5.5 shows that the Finite Element model is capable of predicting the structural behavior of corner joint in a reasonable manner. Load displacement curves of the FE models are in close agreement with the experimental tests. Table 5.4 shows that the FE model closely predicted the ultimate lateral capacity for all the configurations. On average, the maximum load was predicted within 6%, and in the worst case the difference between the test results and the predicted model value was 12.9%. The displacement at maximum load was predicted within 10% (maximum difference was 25.3% for configuration C3). The prediction of the initial stiffness was reasonably good. It is unusual to be able to predict the initial stiffness with better accuracy than this given the contributions of phenomena such as friction, initial slip of the fastening joints etc.

## 5.2.2 Validation Against Experimental Tests on Standard Corner Joints

Since experimental data on corner joints with different configurations were available from [5.4], a FE model using techniques similar to the one described in this Chapter, but modified with the appropriate member and connection inputs, was developed. Table 5.5 shows the test matrix of corner joint configurations from [5.4].

Table 5.5: Test matrix of FPInnovations [5.4] corner joint configurations

| Wall No. | Sheathing details | Header | Metal strap details |
|---|---|---|---|
| C1-C-1&2 | ½" OSB – One side | LSL | - Single metal strap on unsheathed side (interior stud) |
| C3-1&2 | ½" OSB – One side | LSL | - Double straps on interior jack studs of both sides<br>-Single strap on exterior jack stud on unsheathed side<br>- Strap nailed over OSB sheathing |
| C4-SS-1&2 | ½" OSB - One side | LSL | - Double straps on interior jack studs of both sides<br>-A single strap on exterior stud on both sides<br>- Strap nailed over OSB sheathing |
| C4-SL-1&2 | ½" OSB - One side | LSL | - Double straps on interior jack studs of both sides<br>-A single strap on exterior stud on both sides<br>- Strap nailed to lumber studs not OSB |
| C5-1&2 | ½" OSB - Both sides | LSL | - Without metal straps |
| C6-SS-1&2 | ½" OSB – Both sides | LSL | - Double straps on interior jack studs of both sides<br>-A single strap on exterior stud on both sides<br>- Strap nailed over OSB sheathing |

SS: Metal strap nailed over OSB sheathing
SL: Metal strap nailed over lumber (i.e. nailed between sheathing and lumber studs/LSL header)

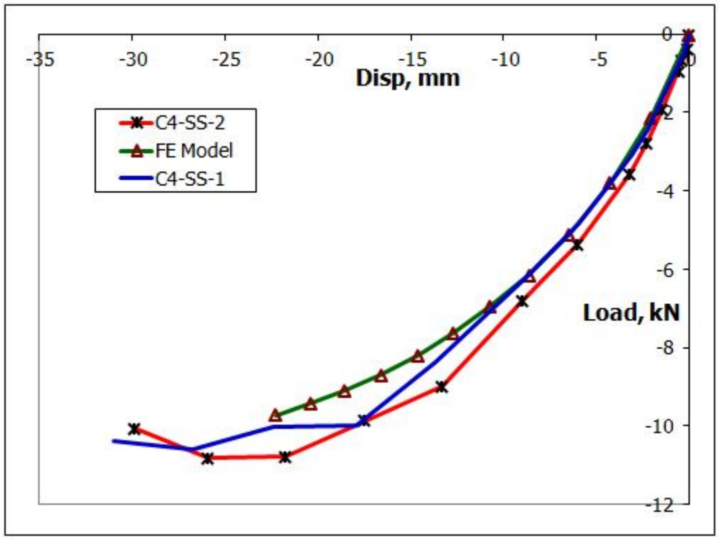


Figure 5.6: Validation of standard corner joint FE model with test results

Figure 5.6 shows an example of the comparison made between the standard corner joint FE model prediction and the test results. A full presentation of the comparison for the other configurations is shown in Appendix B.

The comparison shows that the standard corner joint FE model can reasonably predict the behavior of corner joint i.e. maximum lateral load resisting capacity and initial stiffness. This standard joint corner joint FE model was later used to develop full-scale standard portal frame FE model.

### 5.2.3. FE Model of Corner Joint with FRP

From the corner joint test and failure mode it was observed and measured that only small portion (about 25 mm) of FRP membrane was active in taking the tensile stress induced by the lateral load. Figure 5.7 shows that corner joint configurations with FRP followed exactly the same path as the corner joint with metal straps, which indicates that FRP membrane acted like high strength metal straps compared to the metal straps used for portal frame corner joints. Thus the FRP membrane was defined in the FE model as a single non-linear circular cable element and placed near the interior stud to carry all the tensile force induced by the lateral load.

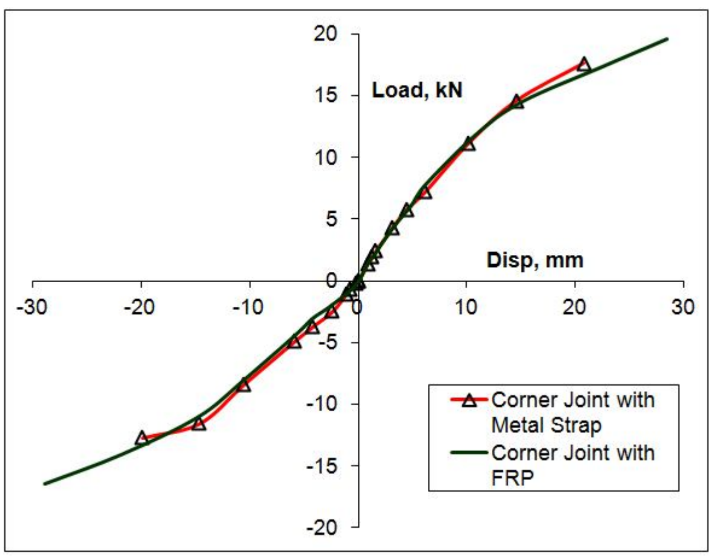


Figure 5.7: Comparison of configuration with FRP versus metal strap

The diameter of the assigned FRP cable was calculated from the equivalent area of FRP membrane as observed and measured after the corner joint experiment. Figure 5.8 shows the FE model of standard corner joint with FRP.

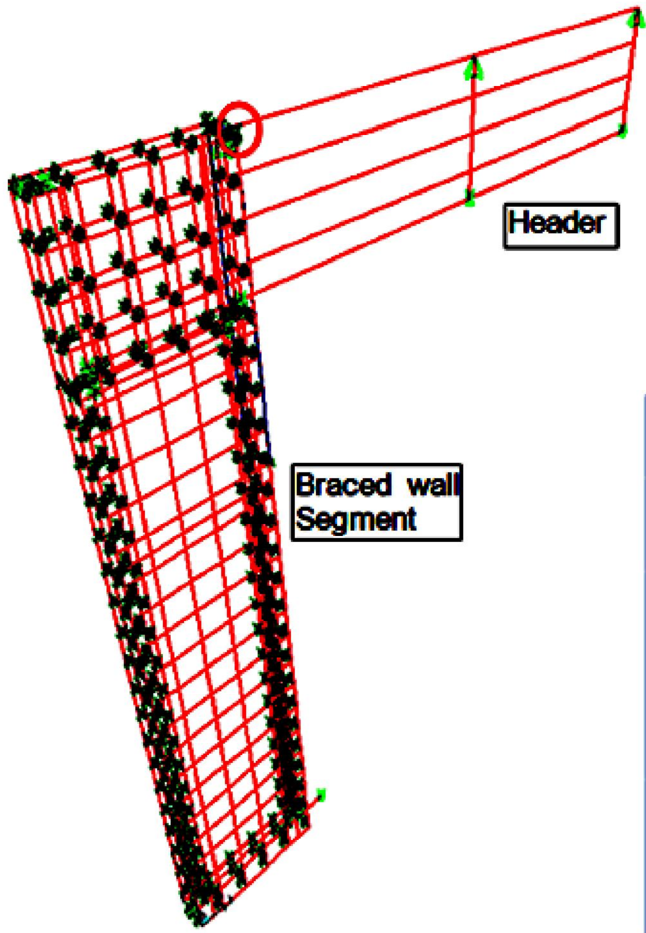


(a) Numerical model of corner joint

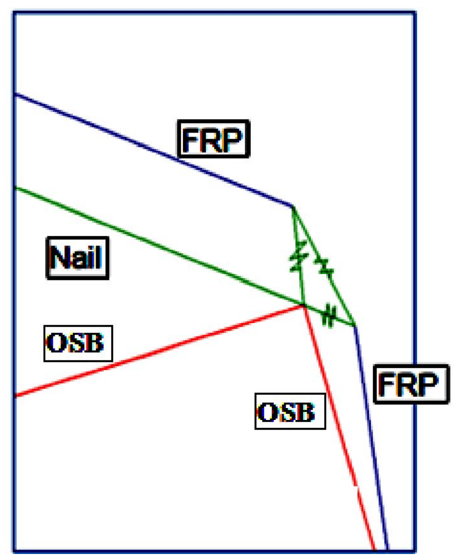


(b) Enlarged view of highlighted corner

Figure 5.8: FE model of corner joint with FRP

The FRP properties used in the FE model was based on the manufacturer's specifications [5.5]. One-dimensional compression contact element was used to represent epoxy interface to connect FRP with exterior OSB. To connect the FRP around the bottom plate with the one used along the narrow wall segment, a one-dimensional linear tension link element with the same tensile properties of the circular FRP cable was used. Figure 5.8 (b) shows the connection detail of FRP at the top header corner of corner joint.

Figure 5.9 shows the results from the FE model compared with test results of standard corner joint with FRP.

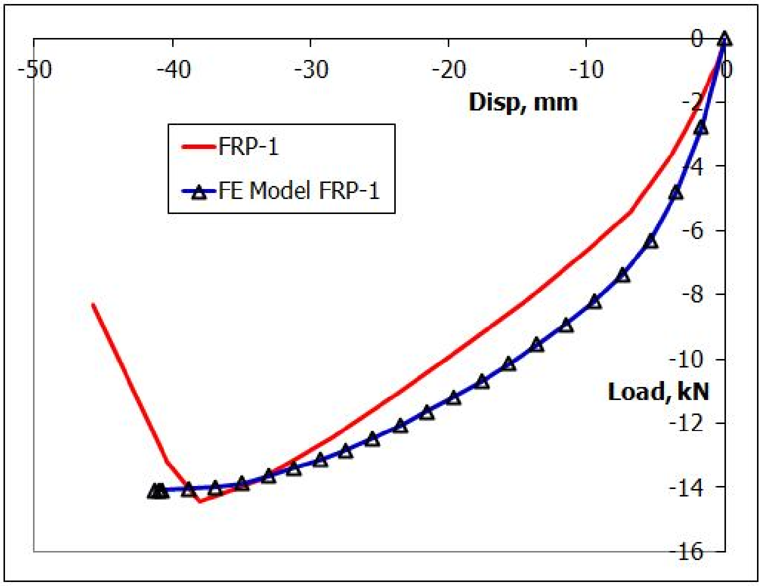


Figure 5.9: Comparison of FE model with FRP corner joint

Table 5.6 shows the percentage difference for the maximum load and the initial stiffness between the FE model and the corner joint test.

Table 5.6: Result variation of FE model and corner joint with FRP

| | | | **Max. Load** | **Initial Stiffness** |
|---|---|---|---|---|
| **Specimen** | **Corner Joint Type** | **Header** | **kN** | **kN/mm** |
| **FRP-1** | **Standard** | **LSL** | **14.26** | **0.726** |
| **FE Model-1** | **Standard** | **LSL** | **14.08** | **1.237** |
| **% Variation** | | | **1.2** | **70.4** |

It is clear from this table that the model was able to reasonably predict the maximum capacity, but the initial stiffness had not been well-predicted. This is not uncommon for light frame wood structures, as initial stiffness is a function of complex mechanisms involving, amongst others, friction, gaps and other redundancy issues, which the model does not take into account. This could considerably affect the load path, stress distribution and ultimately, the assembly stiffness.

### 5.2.4 Validation Against Experimental Tests on Standard Full-Scale Portal Frames

Similar to the standard corner joints, full-scale portal frame tests with realistic end-conditions were available based on work by FPInnovations described in [5.6]. The full-scale tests consist of 3.66 m in length, 2.44 m in height portal frames. The FE model was developed using similar techniques to the one described in this Chapter, but modified to mimic the member and connection input, including the end fixity used in the full-scale portal frame tests. Table 5.7 provides a description of the portal frames tested in full-scale. More details can be found in [5.6]. Wall 1, 2 5 and 9 were used to validate the FE model of full-scale standard portal frame.

Table 5.7: Selected traditional portal frames reproduced by FE model.

| Specimen No. | Sheathing detail | Hold Down | Metal Straps Details |
|---|---|---|---|
| Wall 1 | One Side | No | Single metal straps on interior jack stud on unsheathed side. |
| Wall 2 | One Side | HTT 16# | Single metal straps on interior jack stud on unsheathed side. |
| Wall 5 | One Side | HTT 16# | Double metal straps on interior jack stud on both sides.<br>Single metal strap on exterior jack stud on unsheathed side. |
| Wall 9 | Both Sides | HTT 16# | Double metal straps on interior jack stud on both sides.<br>Single metal straps on exterior jack stud on both sides. |

# Hold-downs are installed at ends of portal frame (no hold-downs at the opening)

Table 5.8 shows the comparison between the full-scale portal frame results and the FE model prediction. Figure 5.10 is a graphical representation of the comparison shown as load-displacement curves. The results confirmed that the FE model could reasonably predict the behavior of full scale standard portal frame.

Table 5.8: Standard portal frame test result and FE model comparison.

| Specimen | Header | Hold Down | Max. Load kN | Disp. @ Max. Load mm | Initial Stiffness kN/mm |
|---|---|---|---|---|---|
| Wall 1 | LSL | No | 10.9 | 55.4 | 0.450 |
| FE Model | LSL | No | 8.0 | 52.0 | 0.337 |
| % Variation | | | 26.7 | 6.2 | 25.0 |
| Wall 2 | LSL | HTT 16[#] | 14.8 | 67.5 | 0.380 |
| FE Model | LSL | HTT 16[#] | 14.4 | 100.0 | 0.373 |
| % Variation | | | 2.2 | -48.1 | 1.9 |
| Wall 5 | LSL | HTT 16[#] | 21.4 | 80.2 | 0.630 |
| FE Model | LSL | HTT 16[#] | 20.1 | 88.0 | 0.460 |
| % Variation | | | 5.8 | -9.7 | 27.0 |
| WALL 9 | LSL | HTT 16[#] | 25.8 | 61.2 | 0.990 |
| FE Model | LSL | HTT 16[#] | 24.8 | 78.0 | 0.589 |
| % Variation | | | 4.2 | -27.4 | 40.5 |

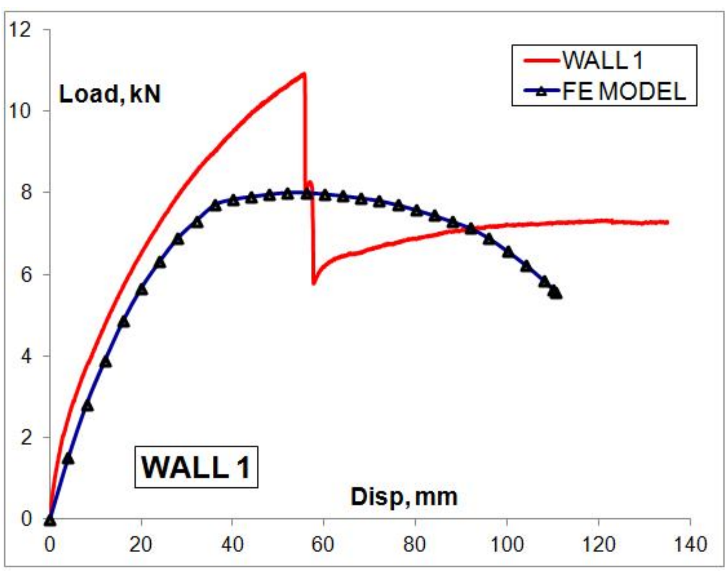


(a)

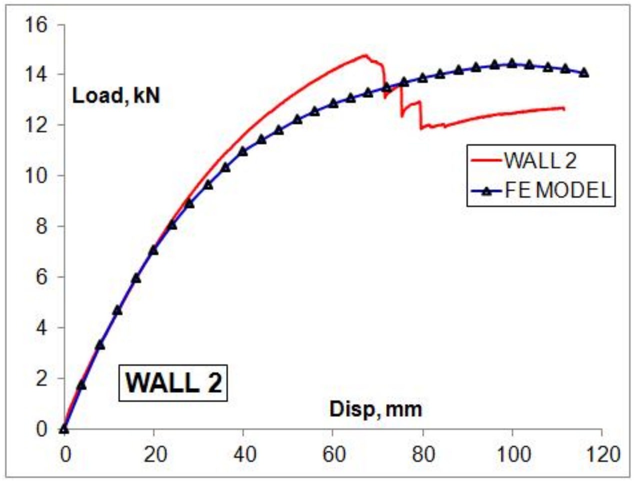


(b)

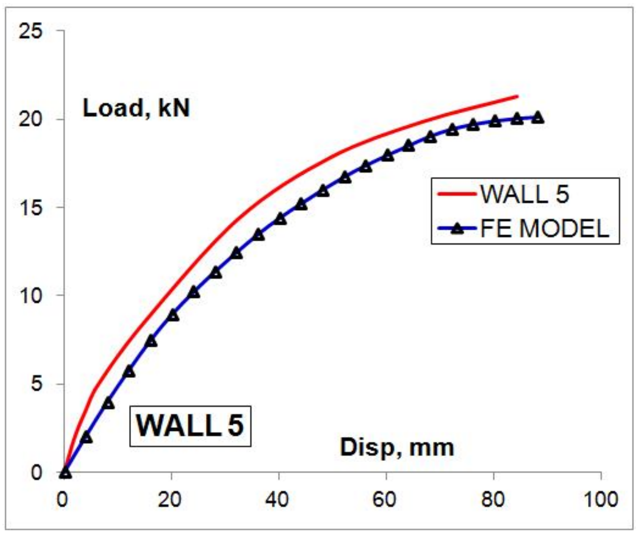


(c)

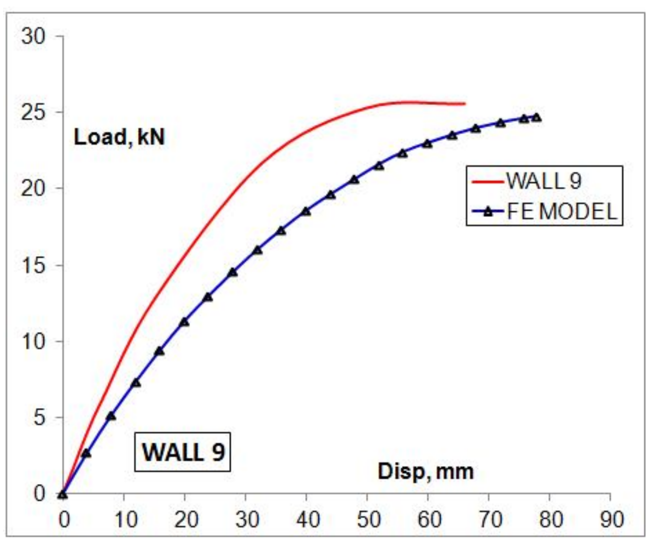


(d)

Figure 5.10: Comparison of standard portal frame test results with FE model

## 5.3 Estimating the Capacity of the Full-Scale Portal Frame Using the MIDPLY Framing Technique

The main goal of developing the FE model was to be able to estimate and predict the behavior of portal frames constructed using the MIDPLY framing techniques. Since it was not feasible to conduct full-scale tests to establish the behavior of such bracing systems, the approach was to make this prediction analytically. The model presented herein is only an estimate and future work should be undertaken to verify the predictions made here. In order to make such analytical predictions, the previous section dealing with corner test verification and full scale portal frame verification was deemed necessary.

A Finite Element model of the MIDPLY portal frame was developed using the same techniques described in section 4.1. The frame was 3.66 m in length and 2.44 m in height. Figure 4.11 shows the FE model of the full-scale MIDPLY portal frame.

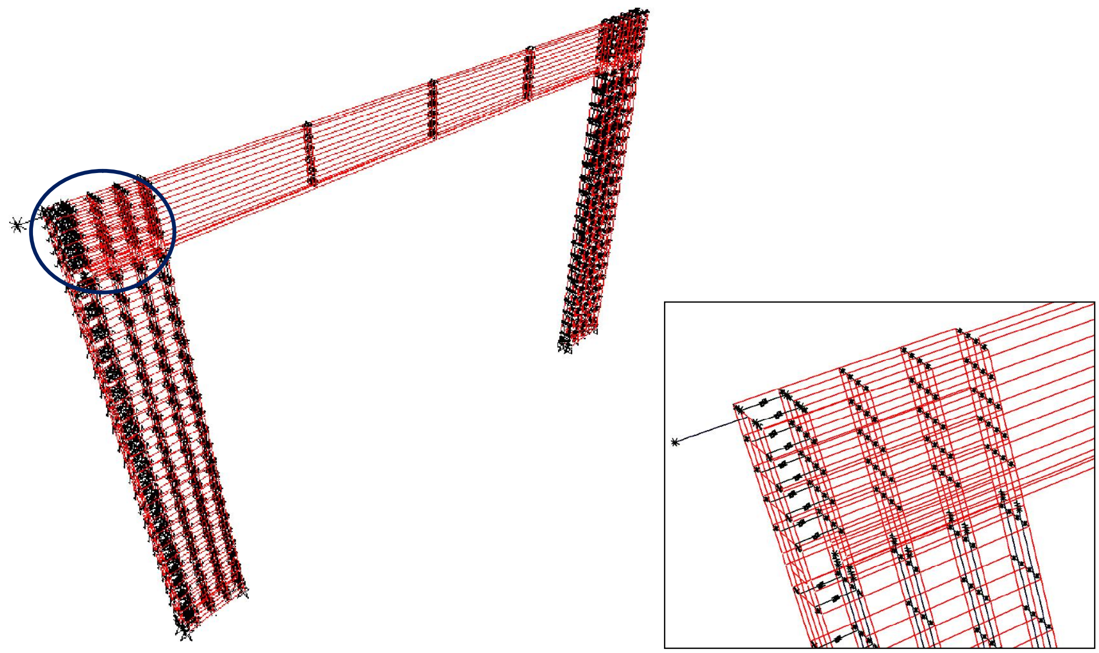

(a) 3D view of MIDPLY portal frame FE model (b) Corner details of connections

Figure 5.11: FE model of MIDPLY corner joint

To compare the performance of developed MIDPLY portal frame with the traditional portal frames tested at FPInnovations [5.4], the models' corner joint configurations and end fixities were mimicking those tested in [5.4]. The expected outcome of this comparison is to establish behavior characteristics for the MIDPLY portal frame bracing system as well as estimate the effect of the framing technique on capacity and stiffness. The test matrix used is shown in Table 5.9. The focus of the comparison was on the capacity, because, as shown earlier, the prediction of the capacity was more reliable than stiffness.

Table 5.9: Traditional portal frame configurations used for comparison with the FE model of MIDPLY portal frame.

| Specimen No. | Sheathing detail | Hold Down | Metal Straps Details |
|---|---|---|---|
| Wall 3 | One Side | HTT 16* | Double metal straps on interior jack stud on unsheathed side. |
| Wall 4 | One Side | HTT 16# | Double metal straps on interior jack stud on unsheathed side. |
| Wall 5 | One Side | HTT 16# | Double metal straps on interior jack stud on both sides.<br>Single metal strap on exterior jack stud on unsheathed side. |
| Wall 6 | One Side | HTT 16* | Double metal straps on interior jack stud on both sides.<br>Single metal straps on exterior jack stud on both sides. |
| Wall 9 | Both Sides | HTT 16# | Double metal straps on interior jack stud on both sides.<br>Single metal straps on exterior jack stud on both sides. |

# Hold-downs are installed at ends of portal frame (no hold-downs at the opening)

* Hold-downs are installed at ends of portal frame and opening

Table 5.10: Comparison of FE analysis results of MIDPLY portal frame with traditional portal frame.

| FE Analysis | Specimen | Max. Load kN |
|---|---|---|
| 1 | Wall 3 | 16.5 |
| | FE MIDPLY wall | 26.6 |
| | % Increase | 61.2 |
| 2 | Wall 4 | 15.7 |
| | FE MIDPLY wall | 26.3 |
| | % Increase | 67.5 |
| 3 | Wall 5 | 21.4 |
| | FE MIDPLY wall | 28.2 |
| | % Increase | 31.8 |
| 4 | WALL 6 | 21.2 |
| | FE MIDPLY wall | 28.9 |
| | % Increase | 36.3 |
| 5 | WALL 9 | 25.8 |
| | FE MIDPLY wall | 30.8 |
| | % Increase | 19.4 |

Based on the data shown in Table 5.10, it is observed that for walls with sheathing on one side only, the MIDPLY portal frame appears to have a significant increase in the lateral load carrying capacity relative to the traditional portal frame. The increase varies between 31 and 67% (comparing 1 and 4 in Table 5.10). It is also noteworthy to mention that the lateral load carrying capacity of the MIDPLY portal frame is not affected by whether the hold-down is installed at the end of the frame or end of the frame as well as the opening (comparing 1 and 2 in Table 5.10). This is also consistent with findings from the full-scale testing project [5.6]. Similar to the full-scale tests, the lateral load carrying capacity of the MIDPLY portal frame increased with the addition of the metal straps on exterior faces (comparing 2 and 4 in Table 5.10).

For walls with sheathing on both sides (FE analysis 5), the increase in the lateral load carrying capacity was less pronounced (only 20%). This is likely due to the fact that the contribution of the narrow wall segment is less when the capacity of the corner joint is increased by the addition of the second sheathing panel. It is however premature to make such conclusion based on the limited data available.

## 5.4 Parametric Study

Four basic full-scale MIDPLY portal frames were selected as the reference frames in this study. The frames were 3.66 m in length and 2.44 m in height, with an LSL header. Frame 1 and 2 had the panels sheathed only on one side of the framing.

Frame 3 and 4 had the panels sheathed on both sides of the framing. For Frame 2 and 4, hold-downs were installed at the ends of MIDPLY portal frames. No hold-downs were used in Frame 1 and 3. Figure 5.12 shows the corner joint details of the reference frame for used in the parametric studies.

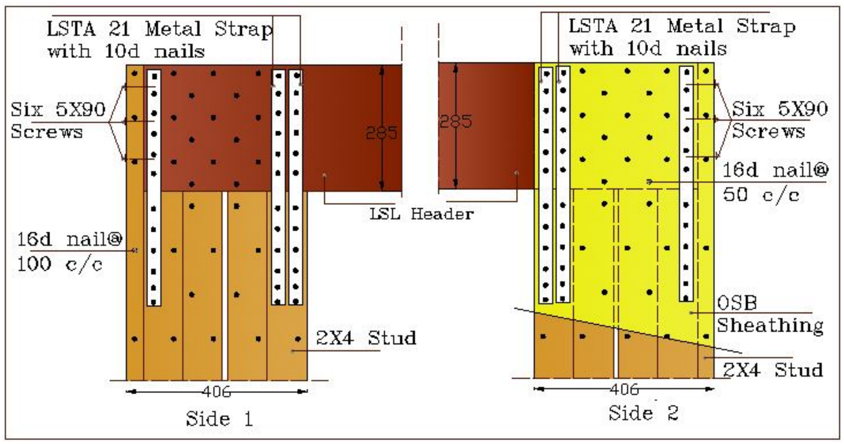


Frame 1 & 2

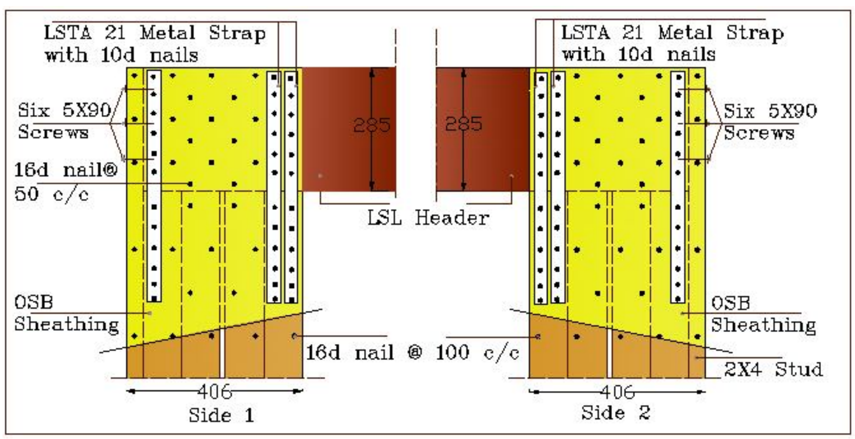


Frame 3 & 4

Figure 5.12: Corner joint details of full-scale portal frame (dimensions in mm)

Three parameters were studied for each wall type. The first parameter was the use of SPF header instead of LSL header in the MIDPLY portal frame. The second parameter studied was the use of high strength metal straps with double the tensile strength of the Simpson Strong Tie LSAT 21 strap used in the testing. The configuration with the high strength strap is referred to as “high strength metal strap frame”. The third parameter was different nailing pattern between the header and braced wall segment and is referred to as “double spaced nail frame”. The nailing schedule investigated was a single row of nails spaced at 200 mm on each face of stud on the wall segment, and a grid pattern of nails spaced @100 mm on the header. This would be compared to a single row of nails spaced at 100 mm on each face of stud on the wall segment and a grid pattern of nails spaced @50 mm on the header in reference frames. All other material properties for the framing members, sheathings, nails and metal straps were kept the same as those used in the corner joint FE model and full-scale MIDPLY portal frame FE model.

### 5.4.1 Discussion and Analysis of Parametric Study

#### 5.4.1.1 SPF Header

The stiffness, ultimate capacities and shear resistances of reference frames with LSL header and the portal frames consisting of SPF header are summarized in Table 5.11. The load-displacement responses of the LSL header and SPF header MIDPLY portal frames are shown in Figure 5.13.

Table 5.11: Analysis summary of LSL and SPF header MIDPLY portal frame

| | | Maxm. Load kN | Initial Stiffness kN/mm |
|---|---|---|---|
| FRAME 1 | LSL HEADER | 11.9 | 0.328 |
| | SPF HEADER | 11.5 | 0.284 |
| | **% INCREASED** | **3.5** | **15.7** |
| FRAME 2 | LSL HEADER | 28.7 | 0.347 |
| | SPF HEADER | 24.3 | 0.300 |
| | **% INCREASED** | **17.7** | **15.9** |
| FRAME 3 | LSL HEADER | 16.4 | 0.374 |
| | SPF HEADER | 15.4 | 0.328 |
| | **% INCREASED** | **6.3** | **14.2** |
| FRAME 4 | LSL HEADER | 30.8 | 0.403 |
| | SPF HEADER | 26.3 | 0.356 |
| | **% INCREASED** | **17.2** | **13.0** |

The FE analysis showed that for all cases the LSL header increased the lateral load carrying capacity of the frames. The increase was up to 17%. However, compared with the corner joint tests, the increase in the full-scale seems less pronounced. Initial stiffness was also increased by 13 to 15% for all of the frames regardless of end fixity and whether single or double sheathing panels were used.

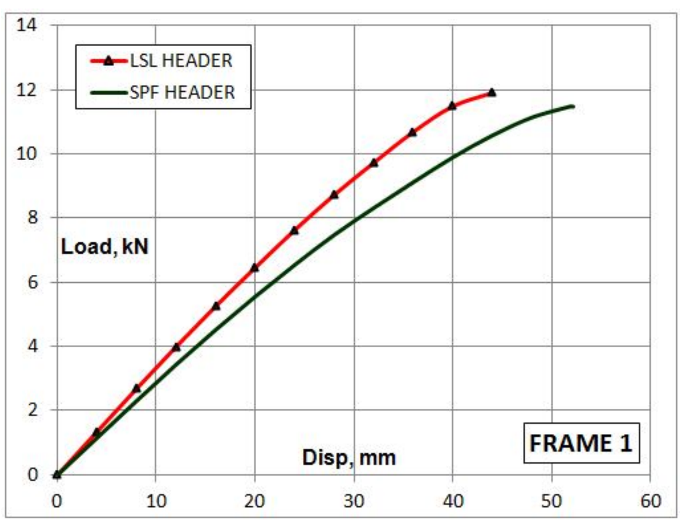

(a)

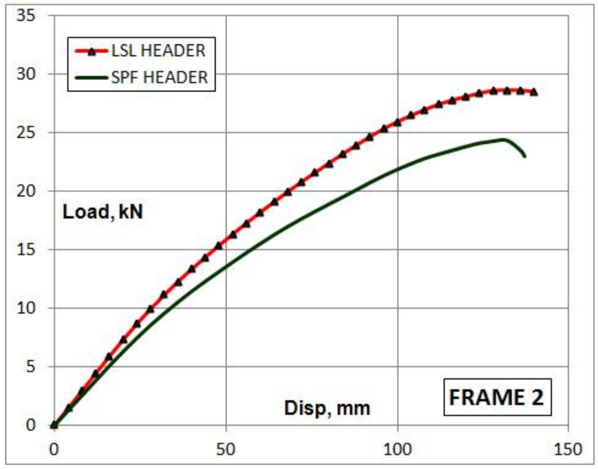


(b)

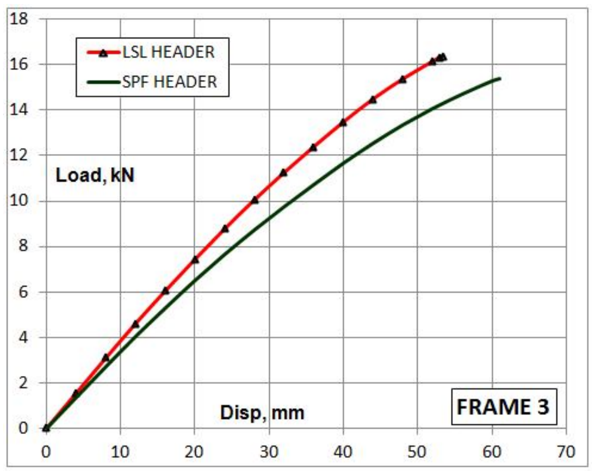


(c)

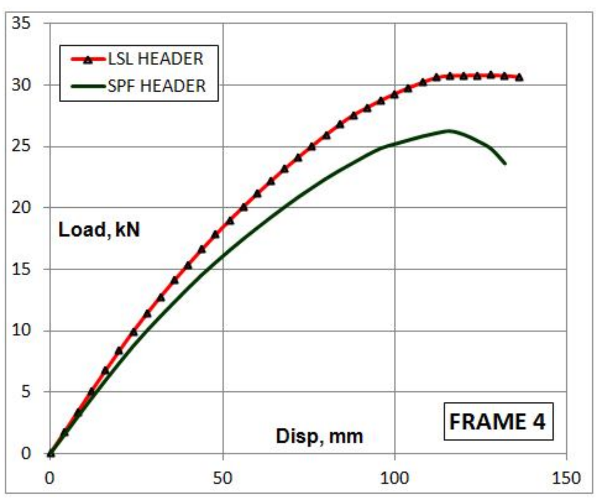


(d)

Figure 5.13: Load displacement curve of MIDPLY portal frame consisting of LVL and SPF header

#### 5.4.1.2 Metal Strap and Nailing Pattern Variation

The ultimate lateral load carrying capacity and stiffness of the reference frames and modified frames are summarized in Table 5.12. The load-displacement responses are shown in Figure 5.14 and 5.15.

Based on the FE analysis results, following observations can be made:

- There was an increase of 6% for single sided and 23% for double sided sheathing for frames with hold-down connections due to the use of high strength metal strap frames. The same increase was not found for the configurations with no hold-down.

Table 5.12: Analysis summary of high strength metal strap and double spaced nail portal frame.

| | | Maxm. Load kN | Initial Stiffness kN/mm |
|---|---|---|---|
| FRAME 1 | REFERENCE FRAME | 11.9 | 0.328 |
| | HIGH STRENGTH METAL STRAP | 12.0 | 0.343 |
| | DOUBLE SPACED NAIL | 11.6 | 0.290 |
| FRAME 2 | REFERENCE FRAME | 28.7 | 0.347 |
| | HIGH STRENGTH METAL STRAP | 30.5 | 0.359 |
| | DOUBLE SPACED NAIL | 23.4 | 0.304 |
| FRAME 3 | REFERENCE FRAME | 16.4 | 0.374 |
| | HIGH STRENGTH METAL STRAP | 16.7 | 0.392 |
| | DOUBLE SPACED NAIL | 15.4 | 0.330 |
| FRAME 4 | REFERENCE FRAME | 30.8 | 0.403 |
| | HIGH STRENGTH METAL STRAP | 37.8 | 0.410 |
| | DOUBLE SPACED NAIL | 28.0 | 0.342 |

- As expected, the high strength metal strap had almost no significant effect on the stiffness of the MIDPLY portal frames (only 1-5% increase).

- Doubling of the nail spacing at header and braced wall segment (double spaced nail frame), had a considerable effect on the lateral capacity of portal frame with hold down. The lateral load carrying capacity decreased by 18% for single sided and 9% for double sided sheathing.

- The initial stiffness reduced by 12-15% for all the configurations with doubling of the nail spacing at the header and braced wall segment as compared to reference frame.

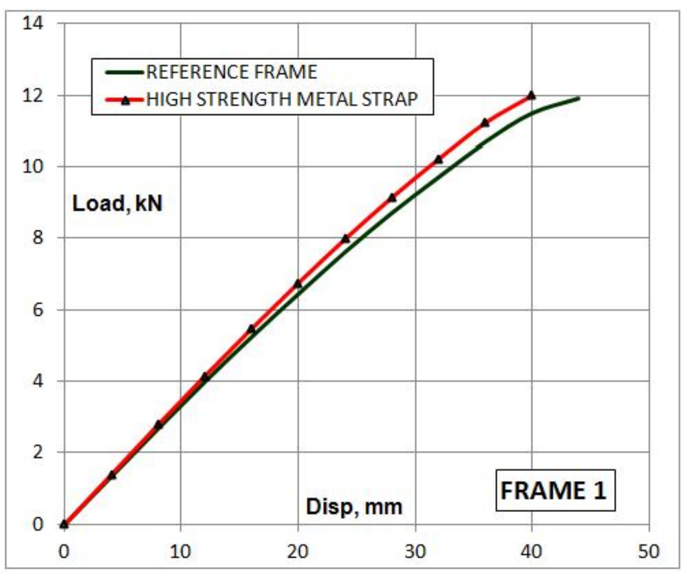


(a)

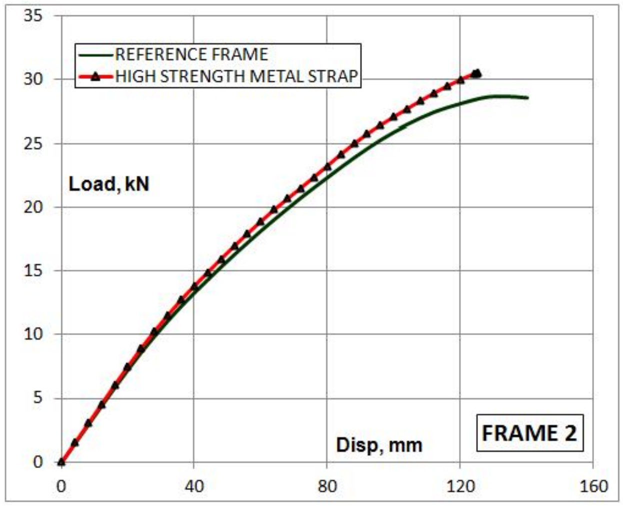


(b)

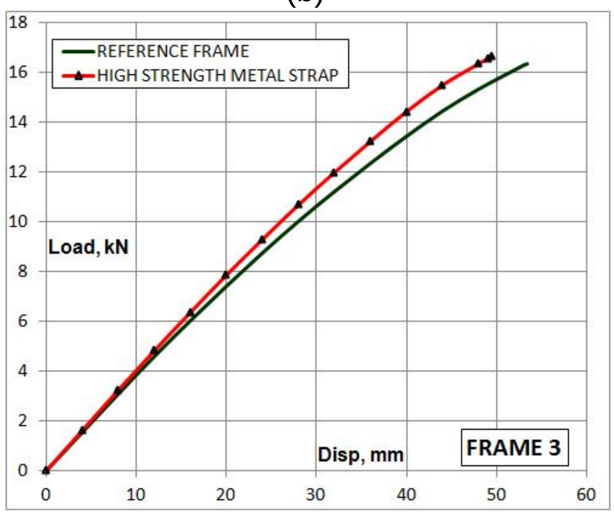


(c)

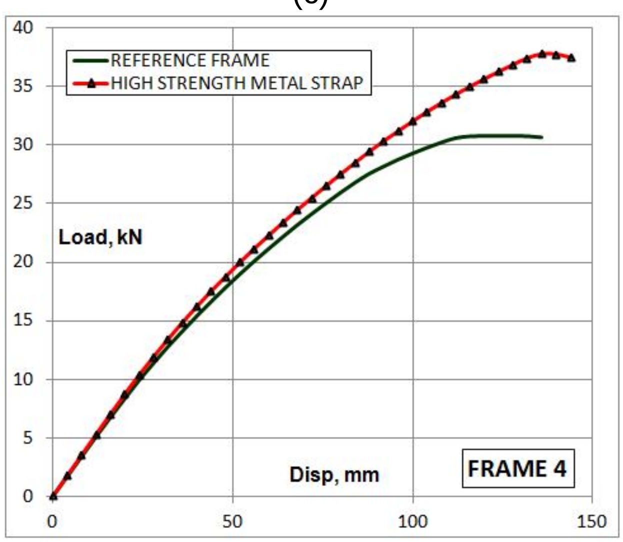


(d)

Figure 5.14: Load-displacement responses of the reference frames and high strength metal strap frames

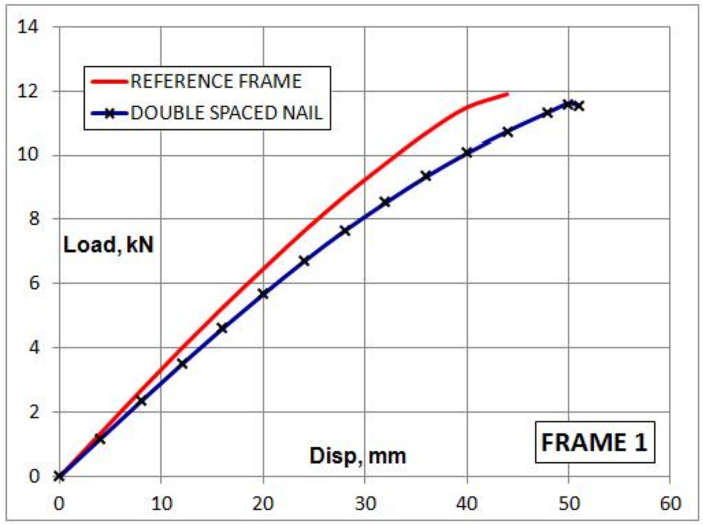

REFERENCE FRAME
DOUBLE SPACED NAIL
Load, kN
Disp, mm
FRAME 1
0
2
4
6
8
10
12
14
0
10
20
30
40
50
60


(a)

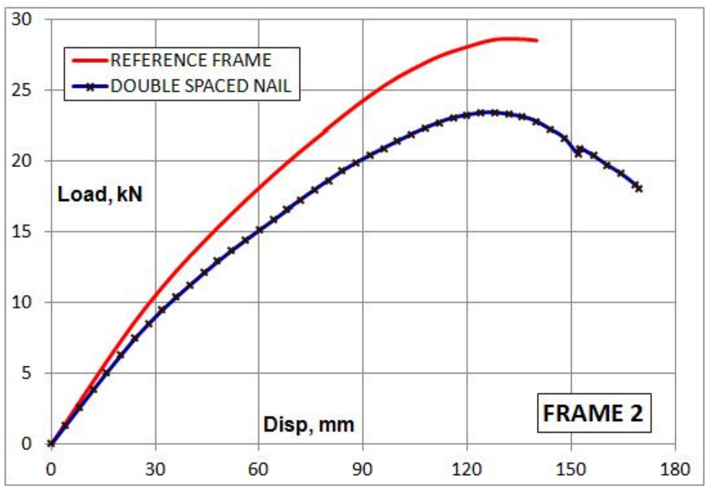

REFERENCE FRAME
DOUBLE SPACED NAIL
Load, kN
Disp, mm
FRAME 2
0
5
10
15
20
25
30
0
30
60
90
120
150
180


(b)

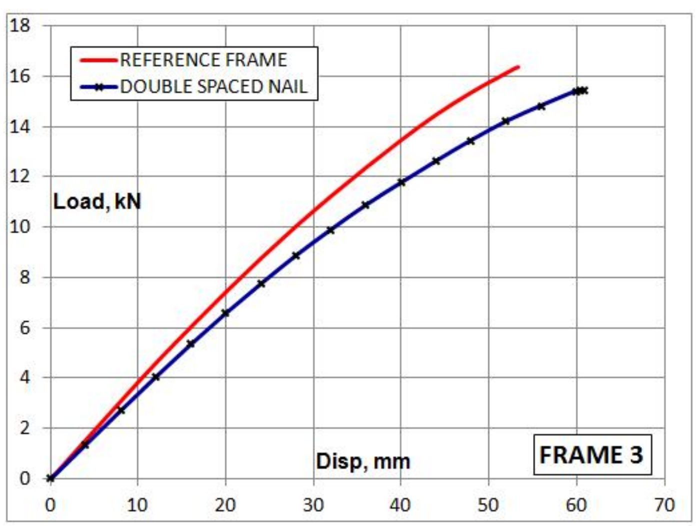

REFERENCE FRAME
DOUBLE SPACED NAIL
Load, kN
Disp, mm
FRAME 3
0
2
4
6
8
10
12
14
16
18
0
10
20
30
40
50
60
70


(c)

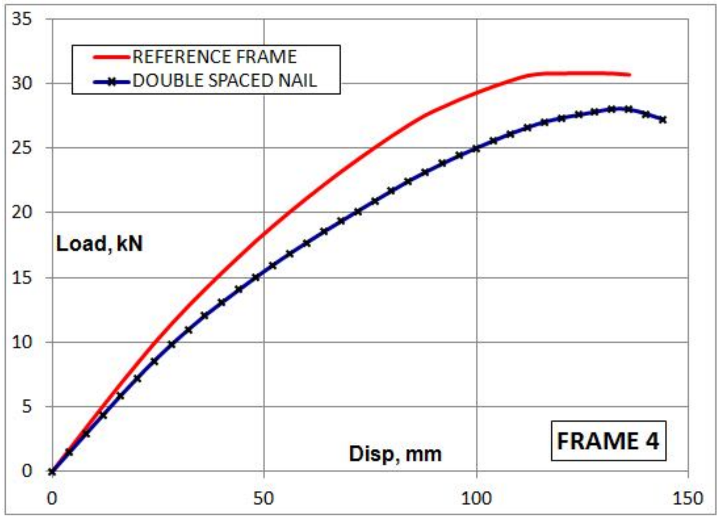


(d)

Figure 5.15: Load-displacement responses of the reference frames and double spaced nail frames

# CHAPTER 6

# Conclusion

## 6.1 Summary of Literature Review

The literature review showed that only limited studies had been conducted on wood portal frame bracing systems, where the focus had been limited to configurations used in prescriptively designed structures. Previous work established an understanding of the failure modes of portal frames and proved that it was feasible to create portal frame systems with capacities comparable to light-frame braced wall systems.

## 6.2 Behavior of MIDPLY Portal Frames

The current study established the sequence of failures for the MIDPLY portal frame system. It was shown that the failure in the joint configurations was always initiated through the rupture of the middle OSB sheathing panel followed by the rupture of exterior OSB sheathing. Subsequent failure was observed in the metal strap connecting the header beam to the narrow wall segment. Nail pull-out was only observed in a limited number of the metal strap connections. Tests with gypsum wallboard confirmed that failure is initiated in the stiffer, more brittle elements.

It can be concluded from the corner joint tests that, in general, the maximum moment resistance increases with the addition of the metal straps or exterior sheathings. A significant increase in capacity was observed when either the metal strap or the exterior sheathing was added. Combining the two, by adding the metal straps on top of the sheathing resulted only in a minor improvement in the performance. It was also shown that all double-sided sheathing increased the lateral capacity compared to those with single-sided sheathing. The test results also showed a significant increase in the moment capacity by replacing the SPF header with the LVL header. The increase is likely due to LVL header's higher density and bending capacity.

The rotational stiffness was shown to increase significantly with the addition of exterior sheathing to the assemblies. The increase due to the addition of metal straps was limited. Also, using a header with a higher bending capacity (e.g. LVL) increased the rotational stiffness.

The addition of the FRP to the standard wall configuration resulted in a significant increase in the moment capacity. However, the addition of the FRP membrane had no significant effect on the stiffness properties of the corner joint.

## 6.3 Finite Element Modeling

Observations and measurements made on the portal frame tests are limited and often difficult to generalize. This is why finite element modeling is an essential companion approach to testing. The first step was to validate the finite element models created. The validation was done at the following stages:

- Model of MIDPLY portal frame corner joints
- Model of Standard wall portal frame joints with and without FRP
- Model of full-scale Standard wall portal frame systems

In general, the Finite Element model was capable of predicting the behavior of corner joints in a reasonable manner. The FE model closely predicted the ultimate lateral capacity for all the configurations. On average, the maximum load was predicted within 6% for the MIDPLY corner configurations. The prediction of the initial stiffness was also reasonably good and within 10% of the measured values. The uncertainty in predicting the stiffness is expected since it is difficult to measure experimentally or to predict, with nonlinearities always present at early stages of loading.

Similar to the corner joints, full-scale portal frames with realistic end-conditions were modeled. The results here also confirmed that the FE model could reasonably predict the behavior of full scale standard portal frame.

The FE model used to estimate the behavior of the full-scale portal frame constructed using the MIDPLY framing techniques showed a significant increase in the lateral load carrying capacity when compared with the traditional portal frame, especially for the case with sheathing on one side. It is also noteworthy to mention that the lateral load carrying capacity of the MIDPLY portal frame was not affected by whether the hold-down was installed at the end of the frame or at the end of the frame as well as the opening. It was predicted using the full-scale FE model that the lateral load carrying capacity of the MIDPLY portal frame would increase with the addition of the metal straps on exterior faces. This is consistent with observations made on corner and full-scale tests on standard wall portal frames.

## 6.4 Parametric Study

A parametric study was conducted to investigate the effect of the header on the MIDPLY portal frame, the effect of varying the strength of the metal straps, the effect of the nailing pattern.

The results showed that for all cases, the LSL header increased the lateral load carrying capacity and the initial stiffness of the frames relative to the SPF header.

The study also showed that there was an increase in the capacity due to the use of high strength metal straps. However, the high strength metal strap had almost no significant effect on the stiffness of the MIDPLY portal frames.

Doubling of the nail spacing at header and braced wall segment had a considerable effect on the lateral capacity of portal frame with hold down. Also, the initial stiffness was reduced for all the configurations with the doubling of the nail spacing at the header and braced wall segment in comparison with the reference frame.

## 6.5 Future Works

Even though the current research study helped establish failure modes and behavior of portal frames, the author foresees that more work is needed in order to establish a comprehensive understanding of this bracing system. The most obvious next step would be to verify the full-scale MIDPLY model by conducting tests on MIDPLY portal frame systems including end conditions. These results could also be compared with the corner tests to investigate if a potential relationship exists between the corner scale and the full scale tests. This would allow for simpler and cheaper test to be conducted with emphasis on corner scale tests and only few full-scale tests.

In order to incorporate the portal frame bracing systems with other lateral load resisting systems in light-frame wood structures, full-scale experimental or analytical work should be undertaken where the portal frames are combined with wood shearwalls or other bracing systems.

Even though the lateral load carrying capacity was improved by using the MIDPLY construction system, there is a potential to investigate portal frame or moment connection frame systems with an even higher anticipated capacity. Examples of such systems are: Cross-laminated Timber (CLT) frames, Glulam frames, and frames using truss construction in the header and the narrow wall segment.

Finally, FRP was investigated in a very cursory manner. A more in-depth investigation of the effect of FRP on the capacity and stiffness or the corner joint in a portal frame system is warranted.

# APPENDIX A

## Failure Modes and Load-Slip Curves for the MIDPLY Corner Joint Tests

### Configuration C1-M

(a) Metal strap failure left face

(b) Metal strap failure right face

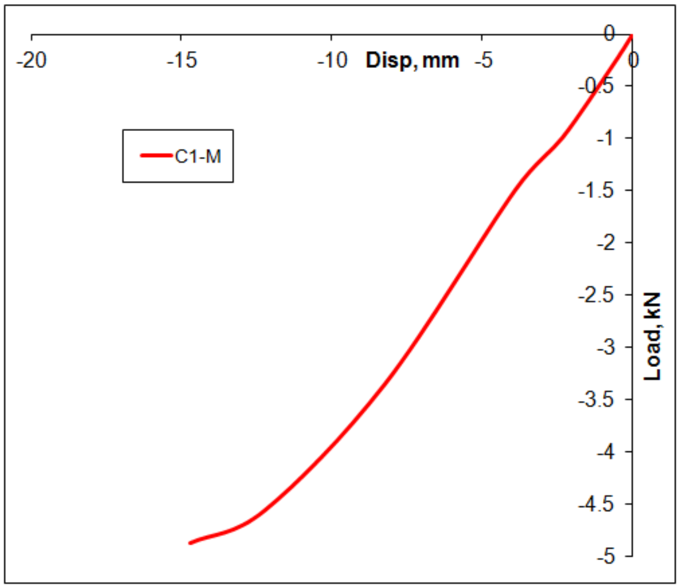


(c) Envelope curve of C1-M

Figure A1: Failure modes and load-slip curve for corner joint C1-M

## Configuration C1-C

(a) Middle OSB failure and
Metal strap failure left face


(b) Metal strap failure right face

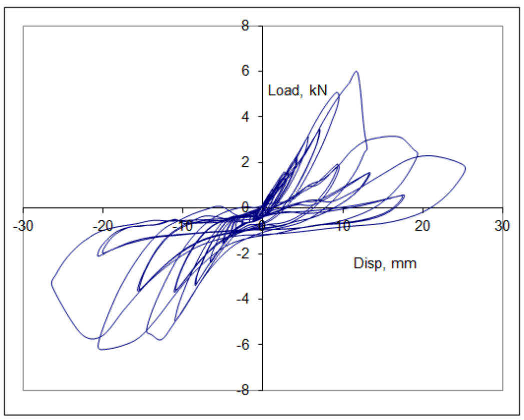


(c) Load-slip response of C1-C-1

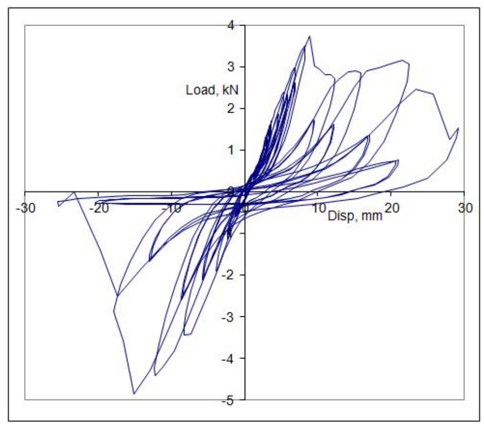


(d) Load-slip response of C1-C-2

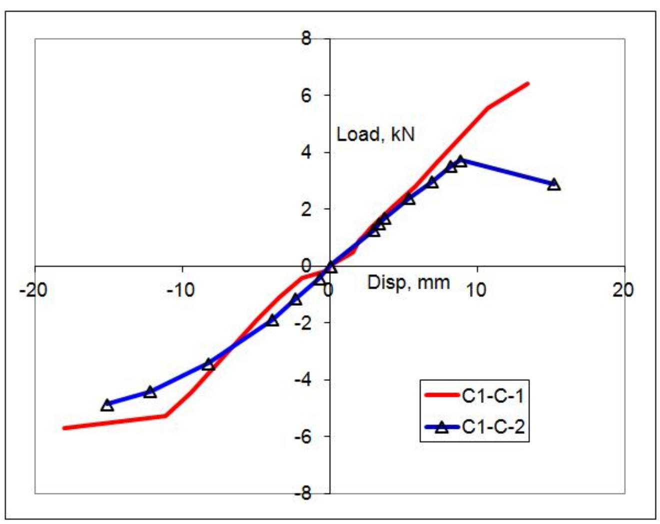


(e) Envelope curve of C1-C

Figure A2: Failure modes and load-slip curve for corner joint C1-C

## Configuration C2-C


(a) Metal strap failure left face


(b) Metal strap failure right face

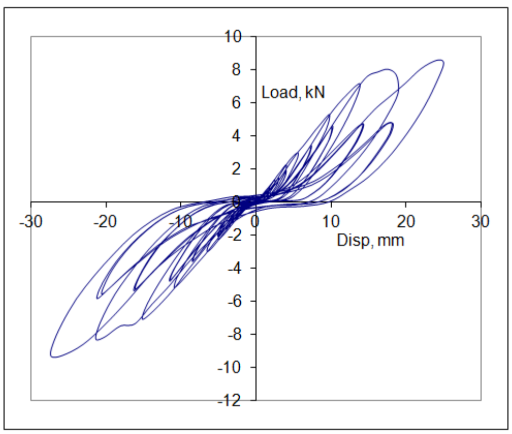


(c) Load-slip response of C2-C-1

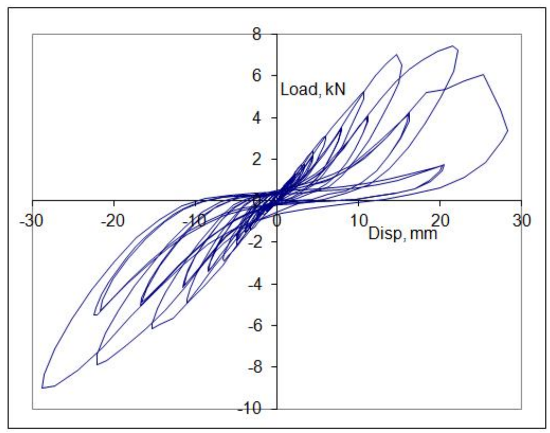


(d) Load-slip response of C2-C-2

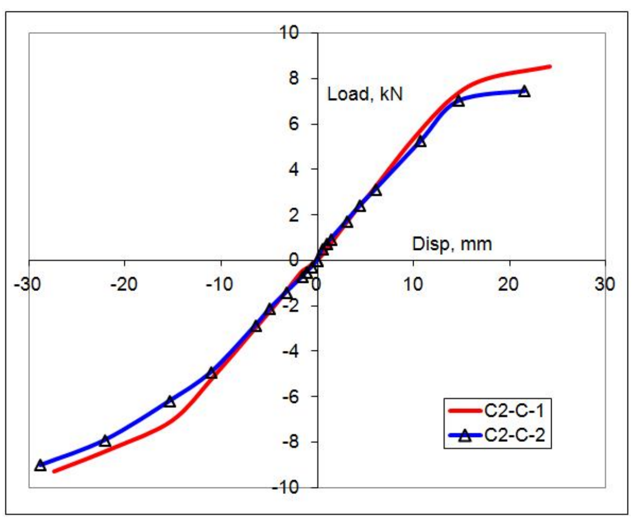


(e) Envelope curve of C2-C

Figure A3: Failure modes and load-slip curve of corner joint C2-C

## Configuration C3-C

(a) Rupture of OSB  left face

(b) Metal strap failure right face

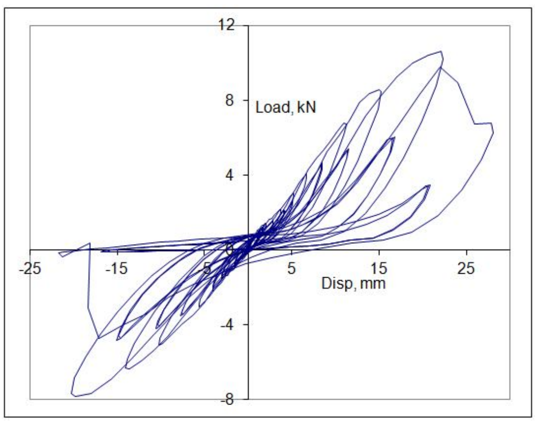


(c) Load slip response of C3-C-1

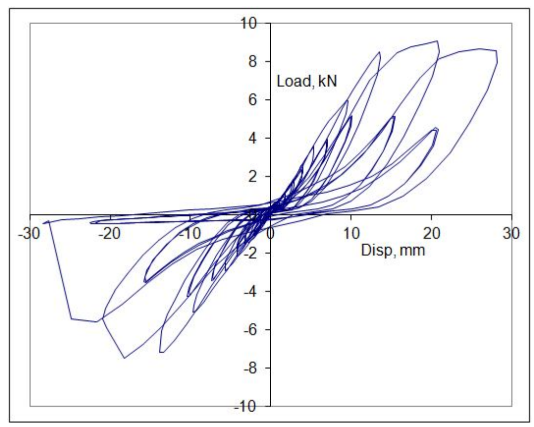


(d) Load slip response of C3-C-2

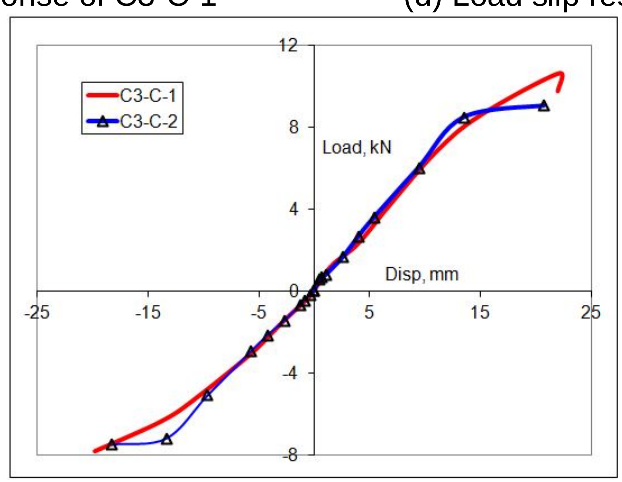


(e) Envelope curve of C3-C

Figure A4: Failure modes and load-slip curve of corner joint C3-C

## Configuration C4-C

(a) Rupture of OSB left face

(b) Metal strap failure right face

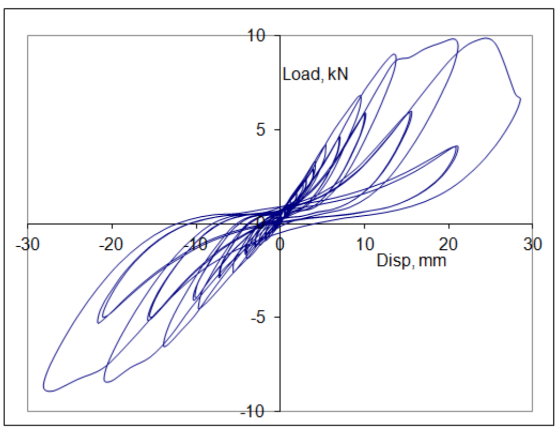


(d) Load-slip response of C4-C-1

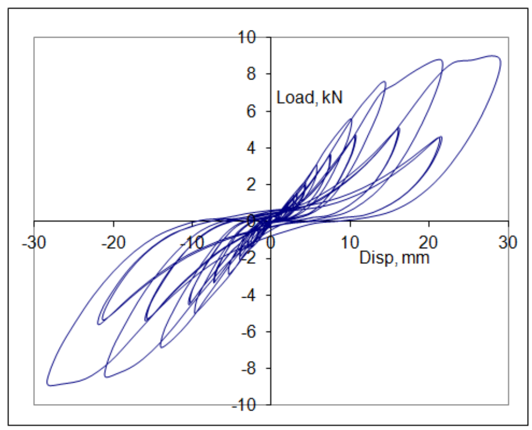


(d) Load-slip response of C4-C-2

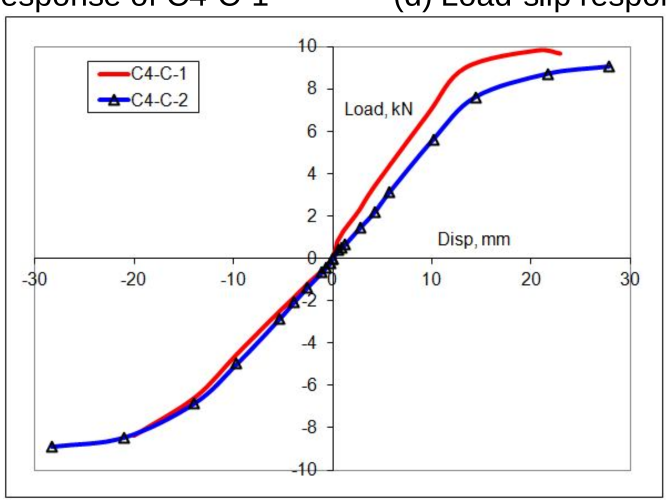


(e) Envelope curve of C4-C

Figure A5: Failure modes and load-slip curve of corner joint C4-C

## Configuration C5-C


(a) Rupture of OSB left face

(b) Rupture of OSB right face

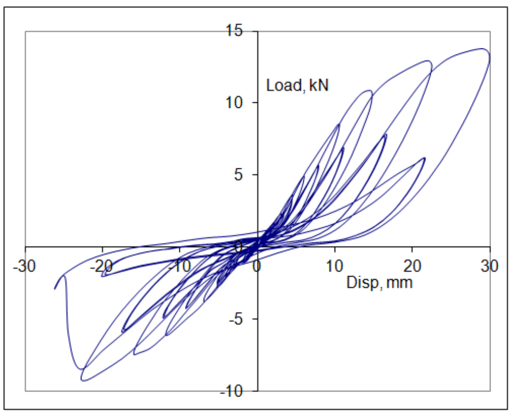


(c) Load slip response of C5-C-1

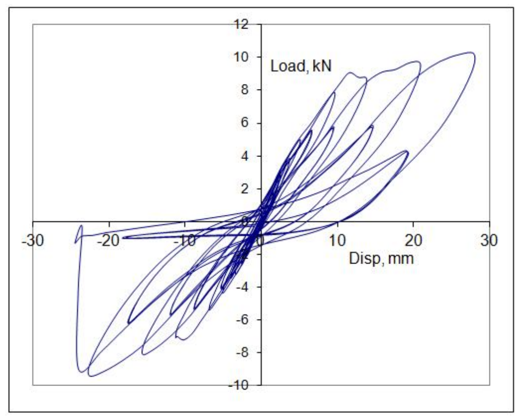


(d) Load slip response of C5-C-2

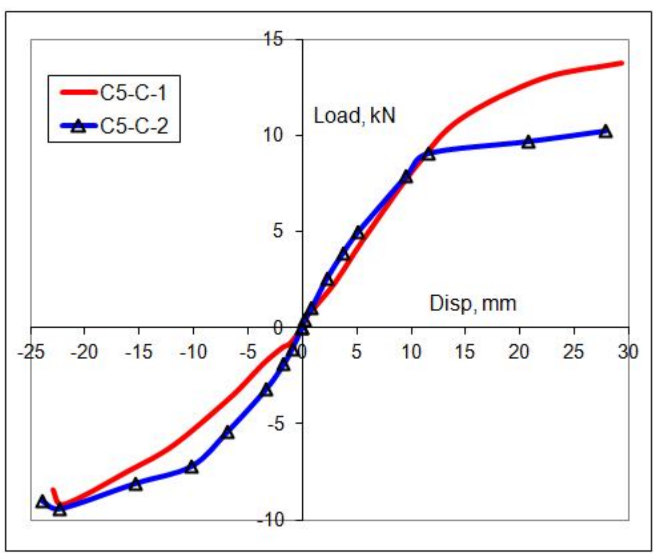


(e) Envelope curve of C5-C

Figure A6: Failure modes and load-slip curve of corner joint C5-C

## Configuration C6-C

(a) SPF header breaks

(b) SPF header breaks

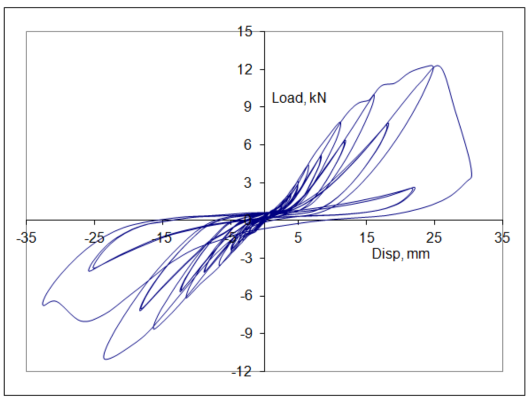


(c) Load slip response of C6-C-1

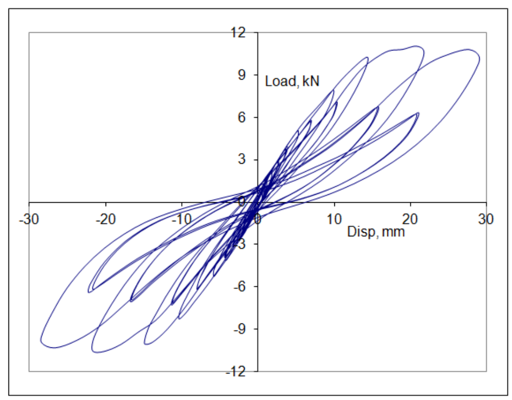


(d) Load slip response of C6-C-2

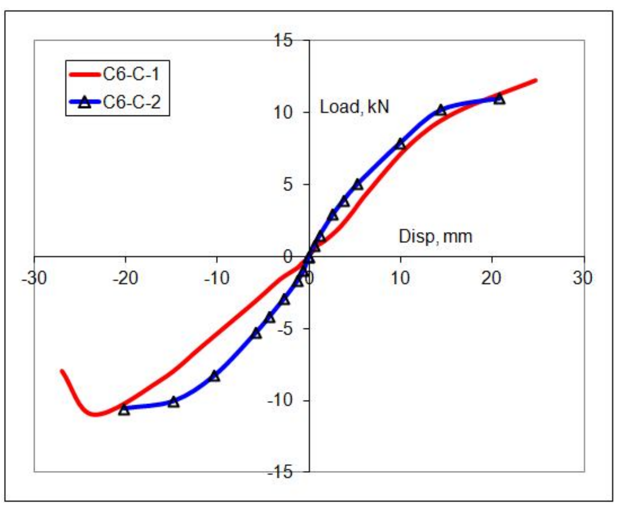


(e) Envelope curve of C6-C

Figure A7: Failure modes and load-slip curve for corner joint C6-C

## Configuration C7-C

(a) Metal strap and OSB failure left face

(b) Metal strap and OSB failure right face

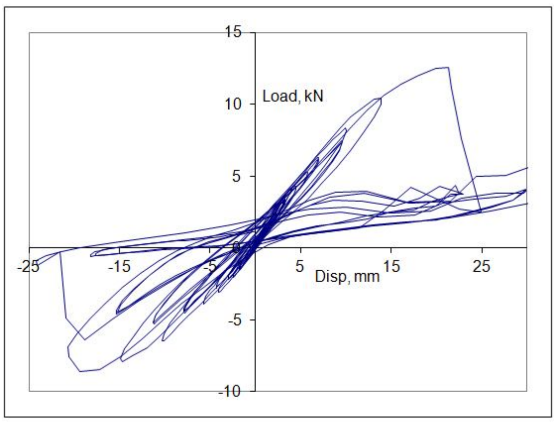


(c) Load slip response of C7-C-1

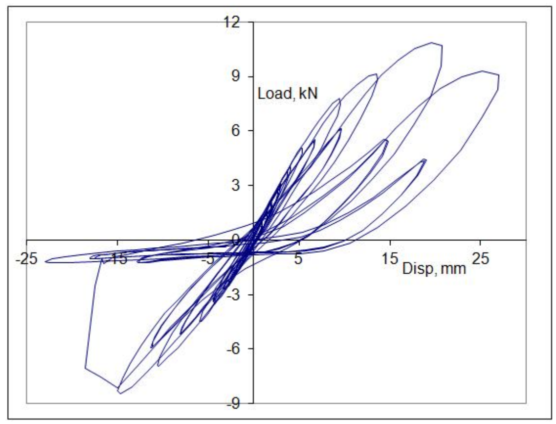


(d) Load slip response of C7-C-2

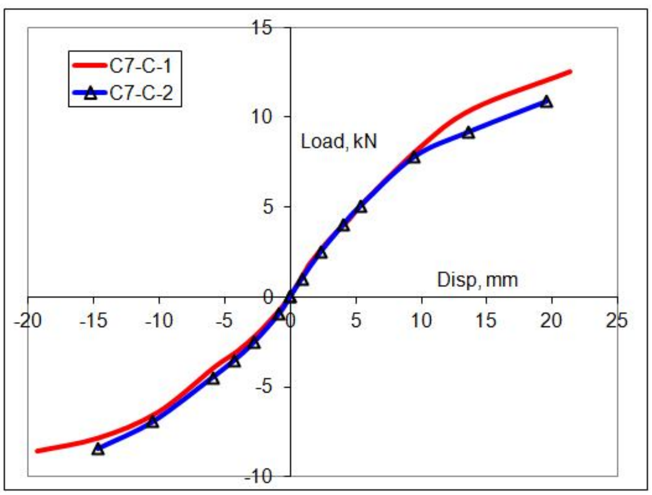


(e) Envelope curve of C7-C

Figure A8: Failure modes and load-slip curve for corner joint C7-C

## Configuration C8-C

(a) OSB failure left face

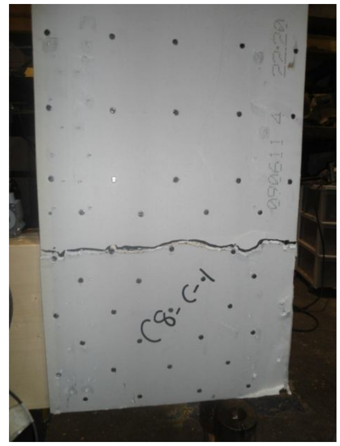


(b) GWP failure right face

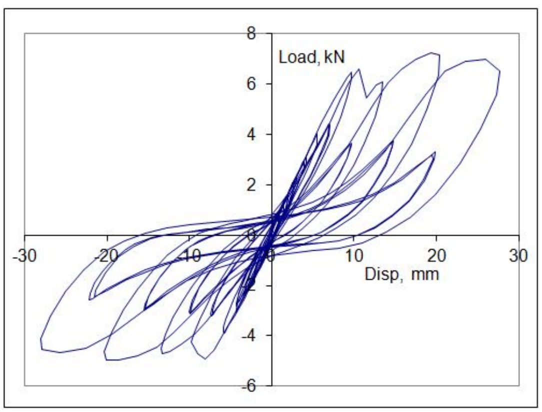


(c) Load slip response of C8-C-1

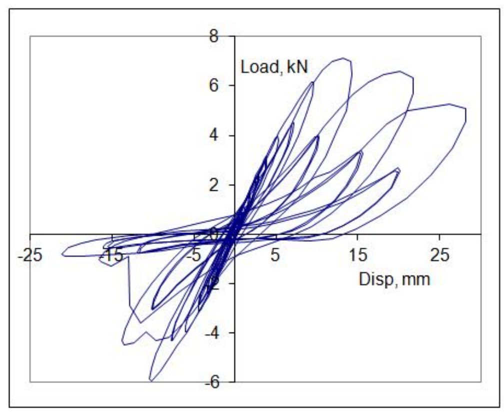


(d) Load slip response of C8-C-2

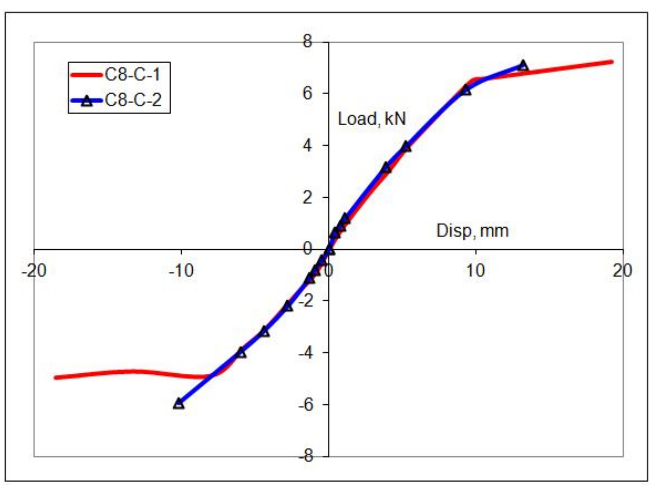


(e) Envelope curve of C8-C

Figure A9: Failure modes and load-slip curve for corner joint C8-C

## Configuration C9-C

(a) OSB and metal strap failure left face

(b) OSB and metal strap failure right face

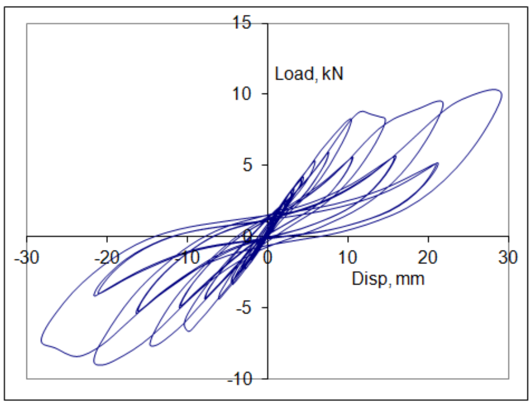


(c) Load slip response of C9-C-1

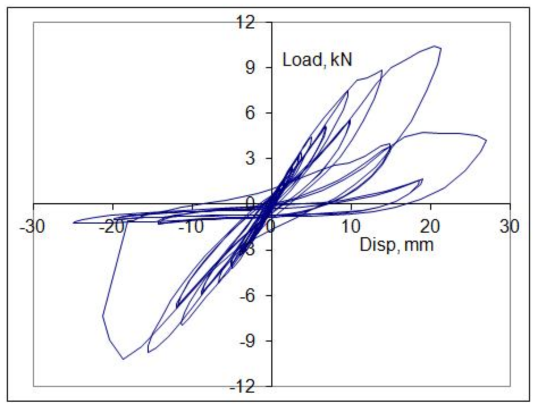


(d) Load slip response of C9-C-2

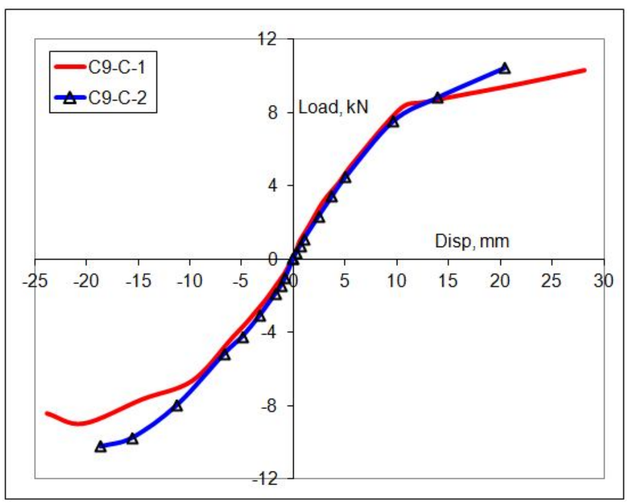


(e) Envelope curve of C9-C

Figure A10: Failure modes and load-slip curve for corner joint C9-C

## Configuration C10-C

(a) OSB and metal strap failure left face

(b) OSB and metal strap failure right face

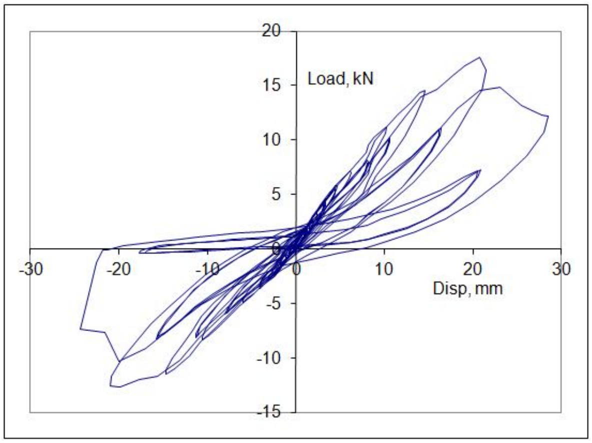


(d) Load displacement response of C10-C-1

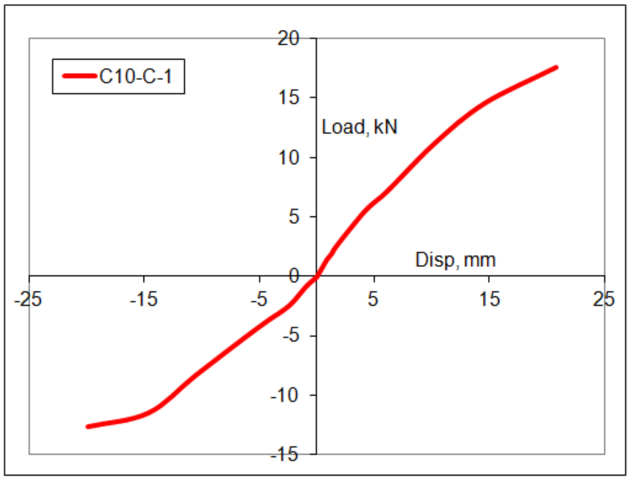


(e) Envelope curve of C10-C

Figure A11: Failure modes and load-slip curve for corner joint C10-C

# APPENDIX B

Validation of standard corner joint FE model with test results

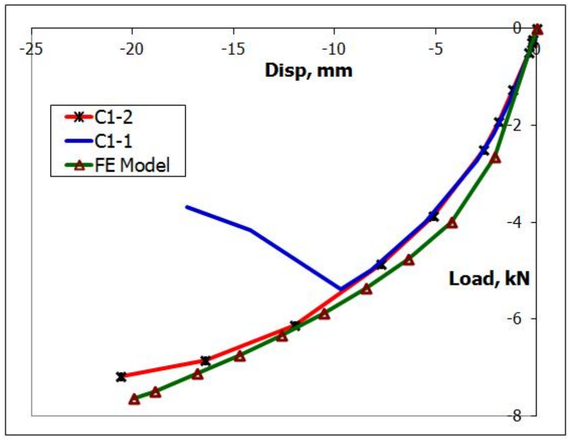


(a)

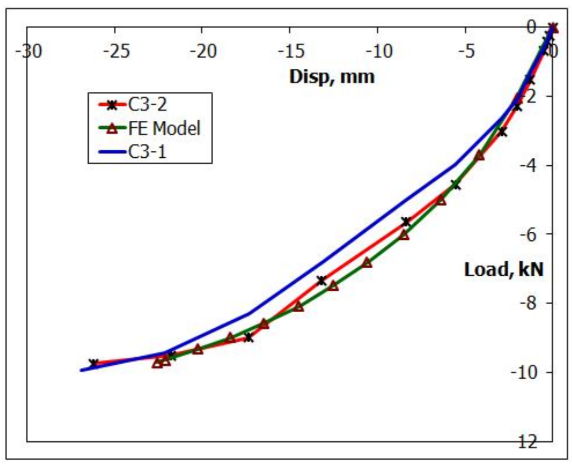


(b)

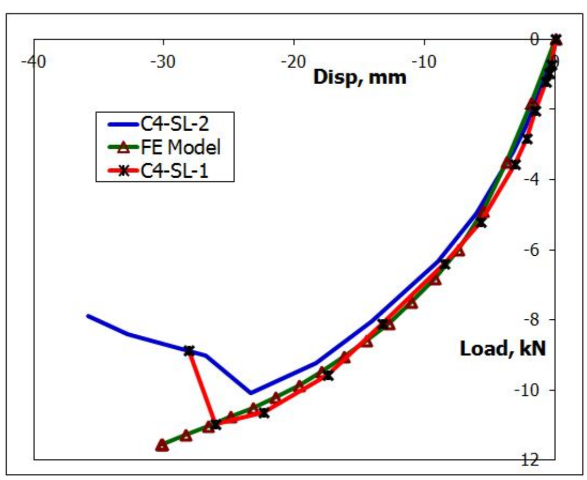


(c)

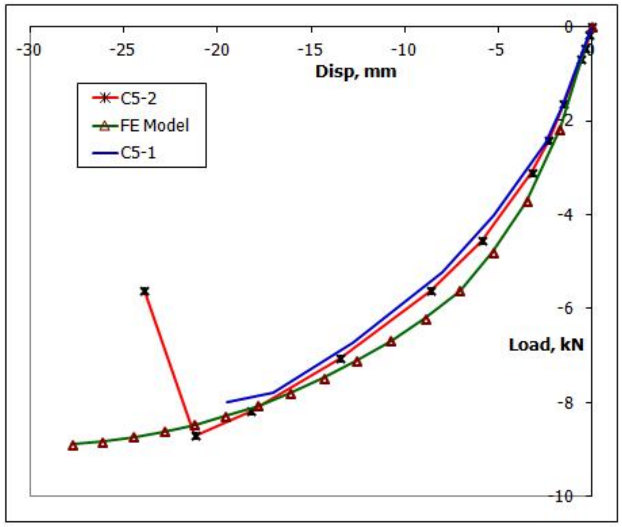


(d)

Figure B1: Comparison of standard corner joint FE model prediction with test results

# REFERENCES

## CHAPTER 1

[1.1] APA. 2009. Introduction to wall bracing. *APA report Form F430*. The Engineered Wood Association, Tacoma, WA.

[1.2] APA. 2010. A portal frame with hold downs for engineered applications. *APA report Form TT-100D*. The Engineered Wood Association, Tacoma, WA.

[1.3] APA. 2008. Portal frame bracing without hold-down devices. *APA report Form J740*. The Engineered Wood Association, Tacoma, WA.

[1.4] Al Mamun, Doudak, Ni, Mohammad. 2011. Alternative Bracing Systems in Light-Wood Frame Buildings. *CSCE General Conference*, June 14-17 2011, Ottawa, Canada. GC-101

[1.5] Varoglu E., Karacabeyli E., Stiemer S., Ni C., 2006 midply wood shear wall system: Concept and performance in static and cyclic testing. *ASCE Journal of Structural Engineering*, Vol. 132, No. 9, 2006, pp. 1417-1425.

[1.6] Ni C., Follesa M., Popovski M., Karacabeyli E., 2008. Assessment of seismic design parameters for midply wood shear wall system. *Proceedings of the 10th World Conference on Timber Engineering 2008*, Miyazaki, Japan.

[1.7] Karacabeyli E., Stiemer S., Ni C. 2004. MIDPLY shear wall system. *Structural Engineering Odyssey Proceedings of Structures Congress 2001*. ASCE Conf. Proc. Doi: 10.1061/40558(2001)177

[1.8] Buyukozturk O., Hearing B. 1998. Failure behavior of precracked concrete beams retrofitted with FRP. *Journal of Composites for Construction. ASCE*. Vol. 2, No. 3, August 1998. ISSN 1090-0268/98/0003-0138-0144.

[1.9] Mirmiran M., Shahawy M., Samaan M., Echary H., Mastrapa J., Pico O. 1998. Effect of column parameters on FRP-confined concrete. *Journal of Composites for Construction*. ASCE. Vol. 2, No. 4, November 1998. ISSN 1090-0268/98/0004-0175-0185.

[1.10] Eric D. Cassidy; William G. Davids, Habib J. Dagher, Douglas J. Gardner, 2006. Performance of Wood Shear Walls Sheathed with FRP-Reinforced OSB Panels. *Journal of Structural Engineering, ASCE*. Vol. 132, No. 1, January 1, 2006. ISSN 0733-9445/2006/1-153–163

[1.11] SAP 2000. Static and dynamic finite element analysis of structures, Advanced 14.1.0. *Computers and Structures Inc*. 1995 University Avenue, Berkeley, Canada. www.csiberkeley.com

## CHAPTER 2

[2.1] APA. 2008. Portal frame bracing without hold-down devices. *APA report Form J740.* The Engineered Wood Association, Tacoma, WA

[2.2] APA. 2009. Introduction to wall bracing. *APA report Form F430B*. The Engineered Wood Association, Tacoma, WA.

[2.3] APA. 2010. A portal frame with hold downs for engineered applications. *APA report Form TT-100D.* The Engineered Wood Association, Tacoma, WA.

[2.4] APA. 2007. 3-D Testing With 6:1 Aspect Ratio Portal Frame Wall Bracing. *APA report Form 3D-004*. The Engineered Wood Association, Tacoma, WA.

[2.5] Martin Z, Skaggs T, Keith E, Yeh B. 2007. Cyclic Response of Narrow Wall Bracing Design. *APA Report prepared for Dolan Committee on Wall Bracing.*

[2.6] Al Mamun, Doudak, Ni, Mohammad. 2011. Alternative Bracing Systems in Light-Wood Frame Buildings. *CSCE General Conference*, June 14-17 2011, Ottawa, Canada. GC-101

[2.7] NAHB Research Center, Inc. 1998. The performance of perforated Shear walls with narrow wall segments, reduced base restraint, and alternative framing methods. *Contract H-21065CA*

[2.8] Ni C., Popovski M., Karacabeyli E., Varoglu E., Stiemer S. 2007. Midply wood shear wall system:concept, performance and code implementation*, Proceedings of Meeting 40 of CIB-W18*. paper 40-15-3, Bled, Slovenia.

[2.9] Varoglu E., Karacabeyli E., Stiemer S., Ni C., Buitelaar M., Lungu D. 2007. MIDPLY wood shear wall system: performance in dynamic testing, *ASCE Journal of Structural Engineering*, Vol.133, No. 7, 2007, pp. 1035-1042

[2.10] Varoglu E., Karacabeyli E., Stiemer S., Ni C., 2006. MIDPLY wood shear wall system: Concept and performance in static and cyclic testing, *ASCE Journal of Structural Engineering.* Vol. 132, No. 9, 2006, pp. 1417-1425.

[2.11] Ni C., Follesa M., Popovski M., Karacabeyli E., 2008. Assessment of Seismic Design Parameters for Midply Wood Shear Wall System. *Proceedings of the 10th conference World Conference on Timber Engineering*. Miyazaki Japan.

[2.12] SAP 2000 Advanced 14.1.0. *Computers and Structures Inc.* 1995 University Avenue, Berkeley, California USA 94704. www.csiberkeley.com

[2.13] Doudak G., Mcclure G., Smith I. 2006. Modelling the Structural Response of Wood Light-frame Structures. *Proceedings of the 9th World Conference on Timber Engineering.* August 6-10, 2006. Portland, OR, USA

[2.14] Mohammed Noory, Ian Smith, Andi Asiz. 2010. Tests and numerical models for shear-walls with various layers. *Proceedings of the 11th World Conference on Timber Engineering.* June 20-24, 2010. Trentino, Italy.

[2.15] Simsir C.C., Jain A. Nonlinear analysis of wood frame shear walls. *Proceedings of the 14$^{th}$ World Conference on Earthquake Engineering*. October 12-17, 2008, Beijing, China

[2.16] Hongyong Mi. 2004. Behavior of unblocked wood shear walls. *M.Sc.Thesis*. The University of New Brunswick

[2.17] Ni C., Chen S., 2010. Evaluation of racking performance of wood portal frames with different wall configurations and construction details. *Proceedings of the International Association for Shell and Spatial Structures (IASS) Symposium*. November 8-12 2010, Shanghai, China.

[2.18] Colin Nigel Clarke. 2009. MIDPLY shear walls use in non-residential buildings. *M.A.Sc. thesis*. The University of British Columbia. February 2009.

## CHAPTER 3


[3.1] Varoglu E., Karacabeyli E., Stiemer S., Ni C., 2006. MIDPLY wood shear wall system: Concept and performance in static and cyclic testing. *ASCE Journal of Structural Engineering*, Vol. 132, No. 9, 2006, pp. 1417-1425.

[3.2] Karacabeyli E., Stiemer S., Ni C., 2004. MIDPLY Shear Wall System. Structural Engineering Odyssey Proceedings of Structures Congress 2001. *ASCE conference proceedings*. Doi: 10.1061/40558(2001)177

[3.3] ASTM 2009. American Society for Testing and Materials (ASTM) Standard E2126-09. Standard Test Method for Cyclic (Reversed) Load Test for Shear Resistance of Walls for Buildings. *Annual Book of ASTM Standards*. ASTM, West Conshohocken, PA, USA

[3.4] Tyfo SCH-41S-1 Composite using Tyfo S Epoxy. *FYFE Co. LLC*

[3.5] Ni C., Mohammad M., 2011. Evaluation of Lateral Load Prescriptive Details of Small Wood Buildings. *FPInnovations Project No. 2010002842*

[3.6] ASTM. 2006. Standard Test Methods for Mechanical Fasteners in Wood. ASTM D1761. *Annual Book of ASTM Standards.* American Society for Testing and Materials, West Conshohocken, PA, U.S.

## CHAPTER 4

[4.1] ASTM 2009. American Society for Testing and Materials (ASTM) Standard E2126-09. Standard Test Method for Cyclic (Reversed) Load Test for Shear Resistance of Walls for Buildings. *Annual Book of ASTM Standards*. ASTM, West Conshohocken, PA, USA

## CHAPTER 5


[5.1] CSA. 2009. Engineering Design in Wood. CSA O86-09, Canadian Standards Association, Toronto, Ontario, Canada.

[5.2] Ni C., Chen S., 2010. Evaluation of racking performance of wood portal frames with different wall configurations and construction details. *Proceedings of the International Association for Shell and Spatial Structures (IASS) Symposium*. November 8-12 2010, Shanghai, China.

[5.3] Zhu, EC., Guan, ZW., Rodd, PD., Rope, DJ. 2005. Finite element modeling of OSB webbed timber I-beams with interactions between openings. *Advances in Engineering Software*, 36: 797-805.

[5.4] Ni C., Mohammad M., 2011. Evaluation of Lateral Load Prescriptive Details of Small Wood Buildings. *FPInnovations Project No. 2010002842.*

[5.5] Tyfo SCH-41S-1 Composite using Tyfo S Epoxy. *FYFE Co. LLC.*

[5.6] Al Mamun, Doudak, Ni, Mohammad. 2011. Alternative Bracing Systemsin Light-Wood Frame Buildings. *CSCE General Conference*, June 14-17 2011, Ottawa, Canada. GC-101

[5.7] C.Ni, K.B. Shim, and E. Karacabeyli. Performance of braced walls under various boundary conditions. *Proceedings of World Conference on Timber Engineering*, Lake Garzar, Italy, 2010.